Laura Giustarini

Dem Fachbereich VI
(Raum- und Umweltwissenschaften)
der Universität Trier
zur Verleihung des akademischen Grades
Doktor der Naturwissenschaften (Dr. rer. nat.)
genehmigte Dissertation

Integrating remote sensing information from SAR sensors and hydraulic modelling

Betreuender:
Prof. Dr. Thomas Udelhoven
Department of Remote Sensing and Geoinformatics
University of Trier

Berichterstattende:
Dr. Andreas Krein
Department of Hydrology - University of Trier
Prof. Dr. Paul Bates
School of Geographical Sciences - University of Bristol

Trier, 2015

Egli muta il deserto in lago
e la terra arida in fonti d'acqua.
Salmo 107:35

CONTENTS

ACKNOWLEDGEMENTS

First and foremost, thanks to the Lord, the loving God, for His showers of blessings throughout my life and for the opportunity of discovering a reflection of His beauty in science.

I would like to thank my husband, Giovanni, the love of my life and also my biggest fan. I am very much thankful for his love, understanding, prayers and continuing support. I thank God for enlightening my life with his presence.

I would like to express my deep and sincere gratitude to my research advisors, Prof. Dr. Thomas Udelhoven, Dr. Andreas Krein and Prof. Dr. Paul Bates, for giving me the opportunity to complete this thesis. I am extremely grateful for their enthusiasm and help. I would like to thank Prof. Dr. Paul Bates also for the period he offered me as a visiting scientist at Bristol University: it was an invaluable opportunity to carry out research in a highly dynamic environment.

A special thank goes to Dr. Patrick Matgen. His kindness, motivation and sincerity have deeply inspired me. He has taught me the methodology to carry out and present research work as clearly as possible. It is a great privilege and honor to work under his guidance.

I would like to express my gratitude to Tommaso Moramarco, for his genuine support at the very beginning of my career. I would also like to thank him for his friendship. My thank goes also to Florisa Melone.

I would like to specially thank all my colleagues and supervisors, all those I met along my carrier, from IRPI-CNR in Italy, to CRP Gabriel Lippmann and LIST in Luxembourg, passing from the University of Bristol in the UK.

I am extremely grateful to my parents for their love, prayers, caring and sacrifices for educating and preparing me for my future. A big thank goes to my brother and his girlfriend. A very heartfelt thanks also to my parents, brother and sister in-law, for their love and constant encouragement.

Finally, my thanks go to all the friends who have supported me to complete the research work, directly or indirectly, even though their names are not listed here.

I would have never thought research was for me, let alone completing a PhD, but God's plans are always higher and greater.

SUMMARY

Floods are hydrological extremes that have enormous environmental, social and economic consequences and it is expected that climate change effects will increase their impacts in the future.

Yet we still lack reliable technological solutions that enable us to accurately and consistently monitor inundations. Reliable observation data integrated into hydraulic models are needed to help us monitoring, predicting and projecting the responses of hydro-systems to varying boundary conditions. However, required data for setting-up, driving, calibrating and evaluating models and offering decision support are often inexistent or too crude and unreliable. With Earth Observation (EO) entering a new era, the increasing availability of free, open and reliable global satellite data and high quality measurement from airborne platforms is expected to trigger a step change in the quality and usefulness of such data. As a consequence, the operational assimilation of such data into high resolution modelling of hydrological processes can be envisaged for the first time.

In this framework, the overall objective of this thesis was a contribution to the implementation of an end-to-end processing chain that integrates remote sensing information into hydraulic models. Specifically, the aim was to improve water elevation and discharge simulations by assimilating microwave remote sensing-derived flood information into hydraulic models. This work highlighted the complementarity of remote sensing-derived inundation maps and hydraulic modelling, with a specific focus on flood mapping in urban areas, where risks to people and the economic impacts are most critical.

The first component of the proposed end-to-end processing chain is represented by a flood mapping algorithm which is used to process satellite data and convert them into hydraulic information. A fully automated flood mapping algorithm was here developed to enable the automated, objective, and reliable flood extent extraction from Synthetic Aperture Radar images, providing accurate results in both rural and urban regions. The method operates with minimum data requirements and it is efficient in terms of computational time, a characteristic that is fundamental for near real time applications. The output of this algorithm is a binary flooded/non-flooded map that represents an invaluable near real-time overview of flood extent and its impact on population and infrastructure.

Given that there is no perfect procedure, the map obtained with the developed algorithm is still subject to uncertainties, introduced by the flood mapping algorithm itself. However, the additional component of uncertainty that is inherent in the image itself should also be taken into account. In this work, particular attention was given to image uncertainty deriving from speckle and its effect on the final flood map. From an original satellite image, by bootstrapping the image pixels, several synthetic images were generated and provided as input to the developed flood

mapping algorithm. From the analysis performed on the mapping products, it was concluded that speckle uncertainty could be considered as a negligible component of the total uncertainty.

The final step of the proposed end-to-end processing chain is the actual integration of remote sensing information into hydraulic models. This was performed through data assimilation, using a Particle Filter. Real event water elevations, obtained from two subsequent satellite observations, were assimilated into a properly adapted version of the Particle Filter, modified to work with non-Gaussian distribution of observations. To deal with model structure error and, at the same time, possibly biased observations, a global and a local weight variant of the Particle Filter were tested. The variant to be preferred depends on the level of confidence that is attributed to the observations or to the model. This study also highlighted the complementarity of remote sensing derived and in-situ data sets.

To sum up, it can be concluded that an accurate binary flood map, as the one that can be obtained in a completely unsupervised way from the developed flood mapping algorithm, represents an invaluable product for several end users. However, deriving additional hydraulic information, such as water elevations, from this binary map is a way of enhancing the value of the product itself. The additional data so derived can be assimilated, as tested in this study, into hydraulic models that will fill the gaps where EO, for technical reasons, cannot provide information. Moreover, these updated models will enable a more accurate and reliable short- to medium-range prediction of flooded areas.

1. INTRODUCTION

1.1. Facing flood risk

Flood is defined by the European Union (EU) Floods Directive (2007) as a covering by water of land not normally covered by water.

Hydrological extremes such as floods have enormous environmental, social and economic consequences and it is expected that climate change effects, combined with concentration of population and economic development in many of the world's largest port cities and deltaic locations, will increase their impacts in the future. The majority of major cities are located on floodplains, meaning that a significant part of human populations are vulnerable to floods and associated waterborne diseases and pollution. Almost one billion people are estimated to be exposed to flooding with an annual probability above 0.01 (Jongman et al., 2012). Financial losses due to flooding are expected to increase from ~US$6 billion per annum in 2005 to ~US$52 billion per annum by 2050, due to socio-economic change alone (Hallegatte et al., 2013).

In recent years, insurance companies face the problem of a substantial increase of flood claims. SwissRe's latest report "Flood – an underestimated risk" states that floods nowadays rival earthquakes and hurricanes in terms of economic losses. According to Torsten Jeworrek of MunichRe (2013), the frequency of flood events in Germany and central Europe has increased by a factor of two since 1980. In 2013, around 45% of the insured losses derived from inland flooding. One particular concern of the insurance industry is the mapping of so-called 'hot spot' areas. These are clusters of industries relevant to global supply chains that are located within flood prone regions. Experience shows that interruption of such international supply-chains due to flooding causes extreme economic loss. In order to improve their services, insurance companies thus require detailed global and national disaster impact databases, to better identify areas vulnerable to flood losses.

The migration of people towards cities located on river floodplains and coastal deltas is expected to increase flood risk over the coming decades (Jongman et al., 2012; Hirabayashi et al., 2013; Vörösmarty et al., 2000). In parallel, the observed and predicted altered precipitation and evapotranspiration distributions caused by climatic change are further increasing the threats posed on water security around the world. The more and more frequent occurrence of water excess periods also has a strong impact on food production and the availability of other natural resources at global scale.

With more lives predicted to be touched by climate change-induced flooding, it is of utmost importance to mitigate the impact of floods and, at the same time, to keep water resources secure.

One of the main objectives of the European Union (EU) Floods Directive (2007) concerns the mitigation of the impact of floods. For this, consistent and accurate short- to medium-range flood forecasts are essential to allow stakeholders in flood management to better react to crises. According to the World Health Organization (2015), a fast and reliable assessment of the situation helps to anticipate critical needs such as search and rescue, medical assistance, evacuation and managing displacement of people and goods. This reduces the risk of exposure to waterborne diseases in the short term and maintains food security conditions over the long term (as crops and livestock are likely to be lost), while avoiding at the interruption of critical supply chains that are known to cause extreme financial losses to industry. To fulfil this mission, Civil Protections need information such as current and forecasted water levels, streamflow and inundation duration, especially in urban areas. Flood extent observations are used by emergency response services to target their limited resources on the most risk prone areas.

However, risk estimations and optimal decision making in emergency situations are hampered by uncertainties inherent to numerical modelling-based flood forecasting.

We still lack precise and reliable technological solutions that enable us to accurately monitor and predict floods, keeping at the same time water resources secure. Reliable observation data integrated into various types of environmental models are needed to help monitoring, predicting and projecting the responses of hydrosystems to varying boundary conditions. They will help answer major questions such as where, when, how often and for how long does water inundates the continental land surface, along with what volume of freshwater is stored, for how long does it reside in a particular place and what adaptation or mitigation strategies are effective to minimize negative impacts. These questions are recognised as some of the grand challenges facing the hydrological and land surface modelling communities over the coming decade and are fundamental to understanding the link between wetlands and our climate (Wood et al., 2011).

Central to understanding inundation dynamics are consistent and accurate estimates of global freshwater discharge and high resolution data on how floodplains and wetlands inundate in response to river discharge dynamics (Wood et al., 2011). For most of the world, the river discharge at which floodplains inundate along river networks (e.g. bank full discharge) is unknown, yet this is fundamental to understanding the non-linear transform between runoff and floodplain inundation. Unfortunately, the data on river discharge and observations of flood inundation frequency, which might be used for bank full discharge estimation, are poor in many regions of the world. For example, the global gauge network is declining and is effectively non-existent for large areas of the planet (Hannah et al., 2011; Vörösmarty et al., 1996).

An alternative to ground measurements is represented by Earth Observation (EO) data. Synthetic Aperture Radar (SAR) satellites show interesting merits w.r.t. observing floods, as they are characterized by a good sensitivity to water and can provide data day and night, regardless of cloud cover. A present limitation is the fact that much of our current data is derived from either low resolution records that lack detail (e.g. ~25 km (Pringent et al., 2007)) or higher resolution data (≤75 m) that are patchy in space and time and yet to be processed globally (Pringent et al., 2007; Brakenridge et al., 2002; Alsdorf, 2007; Bates et al., 2013). However, as discussed by Wagner et al. (2014), EO is now entering a new era where the increasing availability of free, open and reliable global satellite data and high quality measurement from airborne platforms is

expected to trigger a step change in the quality and usefulness of such data. The enhanced observational capabilities, in terms of spatial (ranging between 1m and 20m) and temporal (few days) resolution, of new SAR satellite constellations as TerraSar-X, Sentinel-1 and COSMO-SkyMed render EO a potentially invaluable source of information. The combination of multiple and complementary sensors mounted on airborne and spaceborne platforms will enable monitoring terrestrial water bodies and related impacts in a way that is not achievable using conventional networks of (even densely equipped) measurement stations. These powerful new measurement techniques have the potential to overcome data scarcity by providing water-related information at global scale with unprecedented accuracy and spatiotemporal resolution. However, significant challenges still need to be overcome, particularly in terms of data storage and innovative processing chains for the automated processing of satellite data.

In terms of models, high resolution modelling of hydrological processes across different spatial and temporal scales can be envisaged for the first time. Models provide indications not only in terms of flood extent but also in terms of other related hydraulic variables, such as water elevation, river discharge, flood duration and flow velocity. If used as inputs to different types of impact models, these variables can be used to better assess the economic, social and environmental consequences of floods. Simulating river discharge in a hydraulic model requires runoff data to force the model. Many methods exist to simulate global and/or local runoff, with some approaches performing better than others in locations which cannot always be determined a-priori. Runoff fields are usually represented using an ensemble, examples of which can be obtained from large forecast centres. The spread of this ensemble can be reduced significantly by assimilating observations where they exist. In forecasting mode, such data assimilation applications allow keeping the predictions on track. Ideally, this is achieved via the assimilation of streamflow measurements from distributed hydrometric stations. However, gauging stations are relatively sparse and irregular in space and their number is in decline. An inviting alternative that has obtained increased attention over the last years is to improve the predictions of runoff by assimilating hydrology-related data derived from EO data. The most comprehensive way to estimate inundation dynamics would then be to simulate inundation using an appropriate computer model and assimilate the available EO records to obtain a continuous and spatially complete estimate of global discharge and inundation. Such a model is also essential to understanding how natural variability or longer term changes in the hydrological cycle affect inundation (Pappenberger et al., 2005).

The overall objective of this work is therefore to integrate advanced remote sensing technologies and hydraulic modelling for an improved understanding and prediction of rainfall-runoff transformation processes. Specifically, the aim is to improve water elevation and discharge simulations by correcting hydraulic models using microwave remote sensing-derived flood information.

1.2. Integrating remote sensing and modelling

Recently, a number of international Earth Observation (EO) initiatives have set up a research and development agenda to propose new products that serve user communities, such as emergency response services and insurance companies. The Working group on Disasters of the Committee

on Earth Observation Satellites (CEOS) highlighted the need to exploit the potential of new EO data sets to support flood management in its various phases (CEOS, 2013). In particular, CEOS deems insufficient the revisit rates of current satellite systems for flood extent and water level monitoring. The recent setup of new constellations of SAR satellites, such as COSMO-SkyMed, TerraSAR-X and Sentinel-1, allows for enhanced observational capabilities, in terms of spatial and temporal resolution. In Europe, it is expected to have a revisit time of 2 days, enabling the systematic high-frequency assimilation of remote sensing-derived flood extent maps into numerical prediction models. CEOS identifies as a priority a better integration of satellite observations with numerical prediction models to improve forecasts of water levels and flood extents on a daily basis, with a spatial resolution in the order of 15/20m or better.

Data assimilation is defined as the adaption of model results using externally obtained data sets. In other words, it is the process by which observations are incorporated into a model, in order to put the model in better agreement with observed data, whenever new observations become available. The assumption behind data assimilation is that the combination of uncertain model predictions and uncertain observations will lead to an improved and more reliable forecast.

Fig. 1 shows a scheme of a data assimilation application in the framework of hydraulic forecasting. In this example, the model is a hydraulic one, which predicts state variables such as water stages, discharge, velocities, flood extent. The observations to be assimilated are derived from remote sensing, specifically from SAR imagery. Hydraulically relevant observations that can be derived from SAR image analysis and later assimilated are, for example, flood extent and water stages.

Uncertainty in model forecast mainly derives from input forcings and model's parameters (e.g. Manning's roughness coefficient) and structure (1D flow approximation, geometry errors, …). It is generally taken into account by computing an ensemble of model predictions. This ensemble reflects the uncertainty in the state of the modelled variable(s) of interest. Any time an external observation of a state variable is available, a weighted average can be computed between model results and the external observation. This weighted average can then be used as initial condition for the next forecasting time step.

Several different approaches are available to assimilate measurements into hydraulic models. With the exception of direct insertion (Heathman et al., 2003), all data assimilation methods consist in adjusting model results by weighing model results and observations. The weights assigned to both model results and observations depend on the degree of uncertainty in model results and observations themselves. In order to perform data assimilation, various types of filters have been proposed in literature, such as Kalman filters (Aubert et al., 2003; Pellenq and Boulet, 2004), the Ensemble Kalman filter (EnKF) (Evensen, 1994) and the Particle Filter (PF). In comparison to the widely used EnKF, the PF does not require a Gaussian distribution of observations and model errors, since it can adapt to any probability density functions (Moradkhani, 2008). In other words, the PF allows the propagation of non-Gaussian distributions through nonlinear models.

The following paragraph covers a summary on the state-of-the-art of satellite derived hydraulic information and the subsequent assimilation of these data into hydraulic models.

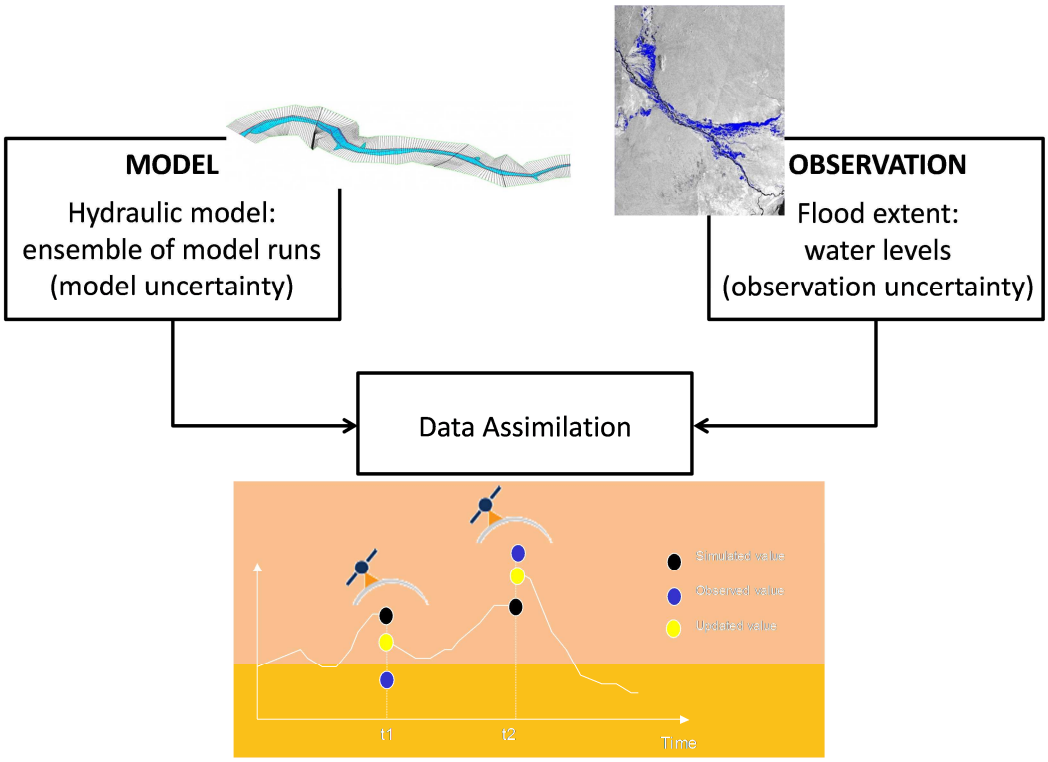

Figure 1: Scheme of a data assimilation approach in hydraulic modelling.

1.3. State-of-the-art

1.3.1. Flood mapping

Nowadays, imaging of flooding is carried out routinely using both satellite and airborne sensors. For inundation detection, SAR sensors are preferred to visible band sensors because of their ability to penetrate clouds that are often present at times of flood and to image at night-time as well as during the day. The ability to obtain a synoptic view of the inundation extent, regardless the light and weather conditions, represents an extremely important feature for operational flood relief management.

A number of active SARs with spatial resolutions as high as 3 m or better have recently been launched that are capable of detecting flooding. They include TerraSAR-X, Sentinel-1 and the four satellites of the COSMO-SkyMed constellation. The latter is particularly useful because it allows image sequences of flooding to be built up with 12- or 24-hour revisit intervals.

In the absence of significant wind, rain or turbulent surface currents, water represents a smooth surface that reflects the radar signal in the specular direction, away from the antenna, producing a very low recorded backscattering. As a result, water has a well-defined backscattering signature (Ulaby and Bare, 1979; Henderson and Lewis, 1998) and it generally appears dark in a SAR image, due to specular reflection from the water surface. Roads and tarmac areas also exhibit low backscatter, though not as low as undisturbed water. For this reason, detection of open water in SAR images is then rather straightforward and a single radar observation of a flood (hereafter indicated as flood image) can be sufficient to detect floodwater on bare soils and scarcely

vegetated terrains. As of today, the exploitation of EO satellite images represents the most powerful means for mapping flood extents in near real time and over large areas.

Many studies in literature have demonstrated that SAR systems are suitable tools for flood mapping. Over the past decades, several analyses have used SAR data to map flood bodies with different techniques. Among the many flood extent mapping techniques currently available, commonly used methods are simple visual interpretation (e.g. Oberstadler et al., 1997), supervised classification (e.g. De Roo et al., 1999; Townsend, 2002), histogram thresholding (e.g. Hostache et al., 2006; Schumann et al., 2007; Pierdicca et al., 2008), and several different multi-temporal change detection methods (e.g. Bazi et al., 2005). Active contour models based on image statistics have also been used by Bates et al. (1997) and Horritt (1999). Mason et al. (2007) proposed a flood extraction algorithm that considers both the SAR image and a DEM of the region, so that waterlines (instantaneous land-water boundaries) in the outcome flood map are conditioned to be smoothly varying in ground height along the river reach. Pulvirenti et al. (2011a) introduced a method that couples segmentation techniques and a SAR backscatter model. On a different note, in a recent study Schlaffer et al. (2015) proposed harmonic analysis of multitemporal ENVISAT ASAR time series to delineate flood events.

One of the main limitations of many of the currently available flood mapping algorithms is their limited level of automation. Generally, their parameters are often determined through visual inspection of the image histograms and are subsequently fine-tuned by the operator based on the subjective analysis of the result. Fully automated image processing algorithms are still surprisingly scarce. In a first attempt towards automation, Martinis et al. (2009) described an automatic split-based thresholding and classification refinement process, as a computationally efficient approach that provides reliable results in a rapid mapping context. Successively, Matgen et al. (2011) introduced a flood mapping hybrid methodology, which combines radiometric thresholding and region growing. Change detection is introduced as an optional final step, in case a reference image is available. The authors showed that the use of a reference image leads to the same results as those obtained with optimized manual approaches. This study is particularly significant because it proposes a robust methodology that reduces the delay between image acquisition and flood map extraction. Moreover, all parameters are automatically optimized by the algorithm itself, with the exception of the tolerance criterion for region growing. The authors acknowledge this limitation of their approach. In all their case studies, an a-priori fixed threshold provided satisfactory results, even though it cannot be excluded that in other situations, better results could be achieved with other threshold values. Matgen et al. (2011) conclude advocating in the future the development of an "all-at-once" calibration that optimizes all algorithms' parameters, including region growing threshold, at the same time. Their study focused on the mapping of rural floods on coarse and intermediate resolution SAR images.

Flood hazard is a major danger in both rural and urban areas worldwide. Nonetheless, it is in urban areas that the risks to people and the economic impacts are most critical. For understandable reasons, stakeholders in flood management are particularly interested in urban areas that are prone to flooding. However, in spite of the progress in the development of flood mapping procedures, the detection of inundation in urban areas still represents a critical issue. A difficulty of urban flood detection using SAR is that, as a consequence of its side-looking nature,

substantial areas of urban ground surface may not be visible to the SAR, due to radar shadowing and layover caused by buildings or taller vegetation. For example, Soergel et al. (2003) found that, in airborne SAR data of Karlsruhe, only one-third of the total road surface was visible to the SAR. Zwenzner and Voigt (2009), while developing a new procedure to improve the matching of flood masks with very high resolution digital elevation models, recognise the difficulty of applying it in urban areas, due to shadow/layover effects and strong backscattering (double bounce).

This makes SAR less effective at detecting urban flooding than it might otherwise be. It is widely recognized that, in order to map floods within urban settlements and also vegetated areas, at least one pre-flood and one flood image have to be combined in a change detection approach. The idea is to search for areas in which the double bounce effect caused by the interaction between the ground surface and the surrounding vertical structures is enhanced by the presence of smooth and reflective floodwater (Pulvirenti et al., 2011b).

Some investigations on mapping flooded urban settlements were carried out by Mason et al. (2010; 2012a). The paper of Mason et al. (2010) is a first attempt at mapping urban water, using a semiautomatic algorithm applied on a single high resolution TerraSAR-X flood image. The authors used the German Aerospace Center (DLR) SAR end-to-end simulator (SETES) and airborne scanning laser altimetry (LiDAR) data to estimate shadow and layover in the image. These are regions unseen by the satellite and, as inundation in this part of the image is considered undetectable, they are masked out in the flood mapping process. Of the remaining urban water pixels that are visible to TerraSAR-X, 76% were correctly detected, demonstrating the capability of detecting water from space in urban area. The algorithm assumes that high-resolution LiDAR data are available for the urban regions in the scene, so that the SAR simulator may be run in conjunction, to generate maps of radar shadow and layover. It is therefore limited to urban regions of the globe that have been mapped using LiDAR. Moreover, the algorithm requires user interaction at a number of stages. The same algorithm was further developed in Mason et al. (2012a) to extract waterline points spatially uncorrelated, to be later used in assimilation studies.

Because of the aforementioned difficulties in detecting water in urban areas, institutional end users (e.g. civil protection agencies) as well as private industry (e.g. insurance companies) still make a relatively limited use of EO data for flood mapping. To increase the usefulness of EO data and to unlock its full potential for operational hydrology, it is presently possible to make use of the enhanced observational capabilities of new SAR satellite constellations.

In addition to enabling flood extent map dissemination, EO-derived flood extent information have a wide potential of applications in hydraulic modelling, especially for model calibration and evaluation (e.g. Pappenberger et al., 2006; Di Baldassarre et al., 2009).

Added value information can be derived from flood extent mapping in the form of water elevations. A well-known technique to derive water elevations from a map of inundation is to extract the heights from a high resolution DEM at the flood shorelines (Oberstadler et al., 1997; Schumann et al., 2008a). Some interesting developments in extracting water levels from remote sensing imagery are those that integrate topographic data (Raclot, 2006) with the aim to retrieve both flooded area and water elevations at the flood edge. Fusing flood edge information with

LiDAR or photogrammetric DEMs might lead to vertical accuracies of 20 to 30 cm (Matgen et al., 2007; Schumann et al., 2007; Hostache et al., 2009). A first attempt at estimating spatially distributed water elevations and their associated uncertainties was carried out by Schumann et al. (2008): they proposed a procedure based on Monte Carlo simulations. Hostache et al. (2009) introduced a slightly different approach, based on a more integrated uncertainty assessment and they built on the analysis of the confidence that can be given to the SAR derived shorelines. Both approaches take into account different sources of uncertainty (i.e. parameters of image segmentation algorithm, co-registration of geo-information layers, accuracy of digital elevation model) that affect the retrieval of water elevation data from remote sensing imagery.

In the last decade, successful studies used SAR-derived water elevations for calibrating uncertain model parameters (e.g. Schumann et al., 2007; Hostache et al., 2009). Moreover, assimilation of remote sensing-derived water levels into flood forecasting systems has gained momentum in recent years with several proof-of-concept studies, demonstrating the ability of these data to improve model predictions (Neal et al., 2007; Neal et al., 2009; Matgen et al. 2010; Hostache et al. 2010). As anticipated, concerning the information content of SAR-derived water elevations, Mason et al. (2012) proposed a method to select a subset of spatially uncorrelated waterline points, in an automated and near real time approach.

Nowadays, SAR-derived water elevations are currently estimated together with their uncertainty, whereas observed flood extent binary maps are still commonly treated as deterministic. It goes without saying that flood extent maps themselves are subject to considerable uncertainty, however, quantifying it remains a rather challenging task. Although accounting for uncertainties and errors has been an implicit exercise in most studies using space-borne images of floods (see e.g. Schumann et al., 2008a; 2008b), a real appreciation and complete account of the uncertainties involved in extracting information has not really been fully explored yet. As a first successful attempt to address this problem, Di Baldassarre et al. (2009) produced an uncertain flood inundation map from near-simultaneous acquisition of two SAR images. They applied five different flood extraction techniques to both images and subsequently fused the derived ten flood extent maps according to a particular measure of consistency into a single fuzzy flood map.

It is argued that such a type of uncertain inundation map may be a useful tool for flood risk mapping, as it expresses our belief in whether a particular image pixel is flooded by an event of a given magnitude (Schumann et al., 2010). However, an issue common to the studies carried out so far is the definition of the type of uncertainty they analyse. In other words, these works do not characterise uncertainty from a statistical point of view, particularly important not only in terms of risk management but also for assimilation purposes.

1.3.2. Data Assimilation

SAR-derived data may be used as calibration, validation and assimilation data for flood inundation models. Such models play a central role in real-time flood forecasting. The cost of damage caused by flooding is highly dependent on the warning time given before an event,

therefore the issue of timely flood alerts is critical and predicting floods remains a key concern of our society.

Flood inundation models are hydraulic models that solve the shallow water equations at each node of a regular or irregular grid covering the river channel and floodplain, subject to boundary conditions that include the input flow rate to the domain (e.g. Bates et al., 2006). They are used to accurately predict the timing and magnitude of a flood. Hydraulic models not only represent valuable tools for independently generating flood extent maps at the time of the satellite acquisition, but also provide additional information, such as water levels, streamflow and inundation duration. Additionally, unlike purely satellite-based observations, these numerical model-based simulations generate flood extent maps that are always consistent with the underlying topography. Another added value is that they can be used to predict the evolution of the flood over several time steps, whereas EO images often provide only one or some snapshots of the flood evolution.

Assimilation may be used to correct the model state and improve estimates of the model parameters and external forcing. There is thus no doubt about the potential of jointly using SAR remote sensing of floods and inundation modelling. A number of recent studies highlight the benefits of this type of integration for model calibration, evaluation and updating procedures. Over the last years, there has been a significant progress with respect to the integration of distributed hydrometric data with hydrodynamic models (e.g. Neal et al., 2007; Andreadis et al., 2007; Matgen et al., 2010; Hostache et al., 2010; Biancamaria et al., 2011).

In such data assimilation studies, modeled state variables and/or model parameters are sequentially verified and updated via measurements. The idea behind this is to merge the high temporal and generally rather poor spatial resolution of model predictions with more accurate but intermittent remote sensing observations, to yield the best possible model simulations. Furthermore, if integrated with parameter estimation techniques, there is the potential to estimate uncertain model parameters, which may be used to increase the accuracy of the model itself (Montanari et al., 2009). Data assimilation techniques based on different versions of the Kalman filter have been used to assimilate ground gauge-based river level data at different points along river reaches (Madsen and Skotner, 2005; Neal et al., 2007), from which discharge can be estimated through state augmentation. Despite this potential, applications of assimilation techniques with distributed elevation data continue to be rare. In one of the few studies of this type, Andreadis et al. (2007) successfully used a square-root ensemble Kalman filter to assimilate synthetic water surface elevation measurements from the proposed SWOT satellite mission, using simulations from a hydrodynamic model for estimating river discharge. Their study showed that the assimilation of 8 successive SWOT overpasses allowed a reduction of the relative error of discharge estimations from 23.2% to 10%. Lai and Monnier (2009) and Hostache et al. (2010) applied a variational data assimilation method using distributed water surface elevations in order to combine in an optimal way measurement data and a 2D shallow water model. This assimilation process allowed the identification of optimal Manning friction coefficients and the identification of areas in the floodplain and the channel where frictions are homogeneous. Smith et al. (2009) assimilated distributed data from wireless sensor networks in a parsimonious time series model to produce forecasts with reduced uncertainty.

Matgen et al. (2010) were among the first to propose an assimilation scheme based on the PF for assimilating EO-based water elevation data into hydraulic models. The experiment of Matgen et al. (2010) with synthetically generated observation data showed that it is possible to correct water depths, forecasted by a 1D hydrodynamic model, by assimilating remote-sensing derived water levels. They showed that the assimilation of synthetic EO water elevations has the potential to lead to increased model accuracy at the time of the satellite data acquisition. It was observed that the mere update of water elevations only improves model forecast for a very short time horizon. A more effective strategy was then tested, updating at the same time model water elevations and input discharge. This correction of the biased forcing led to more persistent improvement in model forecast.

Garcia-Pintado et al. (2013) performed a synthetic analysis to evaluate the sensitivity of sequential assimilation w.r.t. scheduling of satellite acquisitions. They found out that imagery obtained early in the flood is shown to have a large influence on forecast statistics and that the revisit interval is most influential for early observations. In a subsequent study, Garcia-Pintado et al. (2015) assimilated water elevations derived from a sequence of real COSMO-SkyMed overpasses, showing improvements in the forecast. Nevertheless, according to the authors, their study cannot be considered conclusive regarding whether, in an operational situation, the simultaneous estimation of friction and bathymetry helps the current forecast.

There is thus a clear need for a better understanding and parameterization of remote-sensing derived information uncertainty as well as for the development of new retrieval methods that help to improve the quality and reliability of the derived products. Furthermore, it is crucial to continue developing advanced assimilation filters that allow a direct and efficient insertion of flood extent data, particularly over urban areas. So far, the relatively low and irregular sampling rates of existing SAR sensors have clearly hampered the systematic and efficient integration of SAR data with hydrodynamic models.

1.4. Objectives and Method

The main research goal of this thesis is a contribution to the implementation of an end-to-end processing chain that integrates remote sensing information into hydraulic models. The underlining idea is that, from the moment a SAR image is available to the user, it should be rapidly and automatically processed to extract from it hydraulic relevant information, with a characterization of their uncertainty. Subsequently, the data so derived should be assimilated into a hydraulic model, to improve its forecast performances. The main appeal of this approach is the fact that the sequential assimilation of satellite derived data offers a unique opportunity to successively correct and improve the model, any time a remote observation is available. It is legitimate to hope that more frequent observations, and corresponding assimilation of such data, will lead to improvements in the model forecast performances.

Specifically, the objectives of this work are the following:

1) Rapid, accurate and fully automated mapping of rural and/or urban floods from SAR data.

2) Assessment of the uncertainty of SAR-derived hydraulic variables and subsequent assimilation of these observations into hydraulic models.

In terms of flood mapping, several algorithms, already available in literature, have been presented in the previous paragraph. However, a common issue concerns their level of automation. In fact, the ideal algorithm would be, at the same time, fully automated, time-efficient and capable of providing accurate and reliable results. Moreover, it is important to give more attention to flood mapping in urban areas, as it is in built-up environments that risk and cost associated with flooding are highest. The first research goal of this thesis is the development of an algorithm capable of detecting flood extents, in both rural and urban areas, with sufficient accuracy and in a fully automated way. The map product obtained in step 1) is a binary flooded/non-flooded map that represents an invaluable near real-time overview of flood extent and its impact on population and infrastructure.

Given that there is no perfect procedure, the map obtained with the developed algorithm would still be subject to uncertainties, introduced by the flood mapping algorithm itself. However, an additional component of uncertainty is inherent in the SAR image, due to its acquisition process. Therefore, the second scope of this work is the investigation of image uncertainty, focusing on one specific aspect of it which is represented by image uncertainty deriving from speckle. Speckle occurs where distributed targets are imaged and the pixel is representative of the contributions coming from several different scatterers. The main idea is to analyse how speckle uncertainty affects the retrieved flood extent. It is expected that speckle influence would not severely affect parameters of the flood mapping algorithm and, therefore, the corresponding detected flood extent.

As anticipated, a binary flood map already represent, if considered as a stand-alone product, a valuable product for several users. However, deriving additional hydraulic information, such as water elevations, from this binary map is a way of adding value to the product itself. The additional data so derived can be assimilated, as proposed in step 2), into hydraulic models that will fill the gaps where EO, for technical reasons, cannot provide information. Moreover, these updated models will enable a more accurate and reliable short- to medium-range prediction of flooded areas.

In this framework, this work aims to highlight the complementarity of remote sensing-derived inundation maps and hydraulic modelling, with a specific focus on flood mapping in urban areas that are, as anticipated, the most challenging and the most important to be correctly mapped. The objectives listed above were addressed by journal papers, presented in the following paragraphs.

1.4.1. Flood mapping from SAR imagery

The first element of the proposed end-to-end processing chain consists in the processing of SAR images to obtain a flood maps, in both rural and urban areas.

Considering the numerous algorithms developed in literature for flood mapping, one may argue that it is still necessary to further develop their level of automation and objectivity. Generally,

state-of-the-art methods require manual user inputs and/or definition of same parameters. As anticipated, Matgen et al. (2010) already advocated the development of a fully automated algorithm, which optimises in an unsupervised way all its parameters. The ideal algorithm should not only be automated but also capable of accurately detecting water in both rural and urban areas, with minimum data requirements. Additionally, in an operational flood management perspective, such an algorithm should be also computationally efficient.

To contribute to the developments in flood detection algorithms, with a special focus on urban areas, the application of a change detection approach on very high resolution SAR imagery was tested. The idea here proposed is to use two SAR backscattering images as inputs, one imaging the flood event (flood image) and another one observing the area when no flood was present (reference image). The conjunct use of a flood and a reference image is hypothesized to be capable of identifying regions unseen to the satellite. In other words, the benefit of performing change detection w.r.t. a reference image lies in the detection and exclusion from the flood map of areas that are not "visible" to the sensor (i.e., regions affected by "shadow") and that systematically behave as specular reflectors (e.g., smooth tarmac, permanent water bodies), thereby reducing overdetection. This is an alternative approach to the one of Mason et al. (2010), which proposed the use of a LiDAR DEM and a SAR simulator.

Building on the work of Matgen et al. (2010), the development of an "all-at-once" calibration that optimizes all algorithms' parameters was here attempted, to design a flood mapping algorithm, capable of providing satisfactory results in mapping, in a completely unsupervised way, flood extents in both rural and urban areas.

This objective was addressed analysing the case study of the July 2007 Severn River flood (UK). The inundation, one of the highest events in recent history of the UK, was observed by the high resolution SAR sensor on board TerraSAR-X. This study focuses on the city of Tewkesbury, in order to test the potential of SAR sensors to delineate flood in built-up environments, where flood risk is generally highest. For this event, overflights were performed by the Piper Chieftain aircraft operated by the Cambridge University Unit for Landscape Modelling to take aerial photographs of the inundation extent. Validation data was therefore available in the form of very high-resolution photos (0.2 m), from which the actual flood extent was derived through manual delineation. From the archive of TerraSAR-X images, a reference image was selected and used to obtain, in combination with the flood image, a mask of permanent surface-like radar response areas (tarmac, paved roads, parking lots) and of shadow-affected regions.

1.4.2. Flood mapping uncertainty

Flood maps derived from SAR observations are obtained as the result of image processing techniques, such as the one proposed in the previous paragraph. Given that there is no perfect procedure, the chosen mapping algorithm introduces errors and/or uncertainties in the retrieved flood map. Furthermore, SAR observations are susceptible to sources of uncertainty due to imaging characteristics (e.g. imaging modes, speckle, resolution) and/or ground perturbations (e.g. wind, trees, buildings masking water, terrain geometry). Therefore, it is important to assess

the nature and the impact of these uncertainties on the final flood map. Without this information, model calibration/validation or data assimilation activities could yield suboptimal results.

Not only it is necessary to assess flood mapping uncertainty, but an effort should be also made to disentangle its different components. The analysis proposed here was focused on the analysis of one specific component of SAR image uncertainty, i.e. speckle uncertainty. As image speckle directly affect the image which is the input to the flood mapping algorithm, the propagation of this component of uncertainty trough the flood mapping algorithm to the final flood map was investigated.

Analysis of flood mapping uncertainty due to speckle was carried out for the same flood analysed in the previous paragraph, the July 2007 Severn River flood (UK). In this study, other than a couple (flood/reference) of TerraSAR-X images, also a couple of ENVISAT ASAR Wide Swath mode images was considered. In fact, the 2007 flood was observed by two different SAR sensors, providing two flood images with different imaging characteristics.

A non-parametric bootstrap method was introduced to take into account speckle uncertainty. In fact, a flood image can be regarded as a set of pixels that represents the best guess about the population from which the image was taken. Bootstrapping the pixels of the flood image, several synthetic images were constructed and used as input to the flood mapping algorithm to obtain the corresponding flood maps. The accuracy of these flood maps was evaluated w.r.t. an independent validation data set, obtained by manual delineation from very high-resolution photos (see previous paragraph) of actual flood shorelines.

1.4.3. Assimilation of SAR-derived water elevations

Remote sensors provide instantaneous snapshots of an area of the Earth's surface, in this case of a time-specific extent of a flood. To obtain time continuous prediction of the flood evolution, there is a need to combine remote sensing data sets with hydrologic-hydraulic prediction models to generate time-lapses of flooded surfaces. Sequential data assimilation methods can be used to integrate time-continuous model state forecasts (e.g. surface water elevations) with remote sensing observations as they become available.

Most of the studies performed so far in literature, concerns data assimilation of synthetic water elevations. In these experiments, synthetic observations are generally assumed to follow a Gaussian distribution, which is one of the requirements for the use of an EnKF. Matgen et al. (2010) proposed an assimilation scheme based on the Particle Filter (PF), as a possibility to relax the Gaussian assumption in the EnKF while preserving its advantages. In their study, a synthetic experiment was carried out, with artificial observations still assumed to have a Gaussian distribution. Nevertheless, the approach was designed in such a flexible way that the PF can be easily adapted to deal with different (non-Gaussian) distributions of real observed water elevations. The authors stated in their conclusions that one research question of future research would have been testing the proposed PF assimilation scheme with real event data.

In the study here presented, the objective was thus to examine the usefulness assimilating currently available satellite data, characterized by non-Gaussian distributions, to update a hydraulic model in near real time. The PF of Matgen et al. (2010) was adapted to deal with real event data, i.e. non-Gaussian distributions of water level observations. Having at disposal two subsequent satellite observations, problems related to the temporally (and spatially) variable distribution of water level observations were investigated.

A characteristic of synthetic experiments is that it can be assumed that the model is correct in it structure, parameter set and initial or analysis conditions. In fact, the same model is used to create the synthetic observations and, later, to assimilate them. Therefore, the differences between observations and models only derived from inaccuracies in the input data. On the other hand, in a real case study, model structure errors (e.g. 1D flow approximation, errors in geometry) and parameter uncertainties (e.g. Manning's roughness values), cause local bias that need to be taken into consideration. Therefore, an objective of the work here reported was the analysis of potentially biased distribution of water level observations. Two variants of the PF were proposed with a global and local particle weighting procedure. The first option finds the best water elevation line across all cross sections, while the second option finds the best solution at individual cross sections. The final objective was to assess the usefulness of SAR data with respect to in situ hydrometric station data.

The test case of this proof-of-concept study is the Alzette River (Grand Duchy of Luxembourg). The flood event of January 2003 was imaged close to its peak by two different sensors: ERS-2 SAR and ENVISAT SAR. From the two flood images, flood extents were delineated, corresponding to two different snapshots of the flood evolution. Water elevation data, corresponding to two subsequent time steps, were derived intersecting the two detected flood extents with a LiDAR DEM. The quantification of uncertainty for this type of observations was also performed, as this is a pre-requisite to any data assimilation study. It has to be noted that the methodology for flood mapping, water elevation extraction and uncertainty characterization refer to the state-of-the-art literature in 2009, shortly before the analysis here reported was carried out.

Satellite data were assimilated into the hydraulic model set up for the Alzette River for a length of 19 km. Flow direction in this area is mainly parallel to the channel and, as a consequence, the 2D flow field that is typically related to riverbank overtopping can be accurately approximated by a 1D representation. Therefore, the Hydrologic Engineering Center River Analysis System – HEC-RAS (HEC-RAS 4.0, 2008) was chosen as hydraulic model. The upstream boundary condition of the hydraulic model (flow hydrographs) was represented by an ensemble of semi-distributed hydrologic model forecasts. These were generated perturbing model parameters, forcings and initial conditions. On the other hand, for the hydraulic model, an assumption was made that model uncertainties derive only from the upstream boundary condition (output of the hydrologic model), while uncertainties in hydraulic model structure, parameterization, geometry and lateral inflow were not taken into account.

A Change Detection Approach to Flood Mapping in Urban Areas Using TerraSAR-X

Laura Giustarini, Renaud Hostache, Patrick Matgen, Guy J.-P. Schumann, *Member, IEEE*, Paul D. Bates, and David C. Mason

***Abstract*—Very high resolution synthetic aperture radar (SAR) sensors represent an alternative to aerial photography for delineating floods in built-up environments where flood risk is highest. However, even with currently available SAR image resolutions of 3 m and higher, signal returns from man-made structures hamper the accurate mapping of flooded areas. Enhanced image processing algorithms and a better exploitation of image archives are required to facilitate the use of microwave remote-sensing data for monitoring flood dynamics in urban areas. In this paper, a hybrid methodology combining backscatter thresholding, region growing, and change detection (CD) is introduced as an approach enabling the automated, objective, and reliable flood extent extraction from very high resolution urban SAR images. The method is based on the calibration of a statistical distribution of "open water" backscatter values from images of floods. Images acquired during dry conditions enable the identification of areas that are not "visible" to the sensor (i.e., regions affected by "shadow") and that systematically behave as specular reflectors (e.g., smooth tarmac, permanent water bodies). CD with respect to a reference image thereby reduces overdetection of inundated areas. A case study of the July 2007 Severn River flood (UK) observed by airborne photography and the very high resolution SAR sensor on board TerraSAR-X highlights advantages and limitations of the method. Even though the proposed fully automated SAR-based flood-mapping technique overcomes some limitations of previous methods, further technological and methodological improvements are necessary for SAR-based flood detection in urban areas to match the mapping capability of high-quality aerial photography.**

***Index Terms*—Algorithms, flood mapping, image processing, satellites, synthetic aperture radar (SAR).**

I. Introduction

THE support of remote sensing for mapping changes in water surface extents and elevations has been demonstrated widely (for detailed reviews, see [1]–[5]). Recently, the 2009–2010 Data Fusion Contest, organized by the Data Fusion Technical Committee of the IEEE Geoscience and Remote Sensing Society, focused on the evaluation of existing algorithms for flood mapping through change detection (CD) [6]. The success of these research studies together with recent public and political awareness for quantifying global environmental change has led to a significant increase in the number of satellites dedicated to flood monitoring and hydrology in the wider sense. Importantly, flood monitoring from space has the advantage of large area coverage and relatively fast response services (see for example the International Charter "Space and Major Disasters" initiated by major space agencies: http://www.disasterscharter.org/).

The vast majority of a flooded area is rural rather than urban, and accordingly most literature on remote-sensing-based flood detection to date has focused on the rural case. However, it is perhaps more important to detect the urban flooding because of the increased risks and costs associated with it. Flood extent can be detected in rural floods using synthetic aperture radars (SARs) such as ERS and ASAR, but these have too low a resolution (25 m) to detect flooded streets in urban areas. However, a number of SARs with spatial resolutions as fine as 3 m or better have recently been launched and are potentially capable of detecting urban flooding. They include TerraSAR-X, RADARSAT-2, and the four COSMO-SkyMed satellites.

In an operational context, [7] proposed a hybrid methodology which combines radiometric thresholding and region growing as an approach enabling the automated, objective, and reliable flood extent extraction from SAR images. First results on moderate- and low-resolution image data indicate that the proposed method may outperform manual approaches if no training data are available, even if the parameters associated with these methods are determined in a non-optimal way. The results demonstrate the algorithm's potential for accurately processing data from different SAR sensors.

Notable examples of research into automatic near real-time flood detection algorithms using single-polarization high-resolution (greater than a few meters) SAR imagery have been shown by [8] and [9] on TerraSAR-X data and [10] on COSMO-SkyMed data. The algorithms by [8] and [9] search for water as regions of low SAR backscatter using a region-growing iterated segmentation/classification approach, whereas the technique by [10] is based on a fuzzy logic approach which integrates theoretical knowledge about the radar return from inundated areas based on backscattering models, with simple hydraulic considerations and contextual information. Both algorithms are very effective at detecting rural floods, but

Manuscript received October 21, 2011; revised March 2, 2012 and June 7, 2012; accepted July 23, 2012. Date of publication September 7, 2012; date of current version March 21, 2013. This work was part of the HYDRASENS project, supported by the National Research Fund of the Grand Duchy of Luxembourg and the Belgian Federal Science Policy Office in the framework of the STEREO II research program (Contract nr. SR/00/100).

L. Giustarini, R. Hostache, and P. Matgen are with the Département Environnement et Agro-biotechnologies, Centre de Recherche Public - Gabriel Lippmann, 4422 Belvaux, Luxembourg (e-mail: giustari@lippmann.lu; hostache@lippmann.lu; matgen@lippmann.lu).

G. J.-P. Schumann and P. D. Bates are with the School of Geographical Sciences, University of Bristol, Bristol BS8 1SS, U.K. (e-mail: guy.schumann@bristol.ac.uk; paul.bates@bristol.ac.uk).

D. C. Mason is with the Environmental System Science Center, University of Reading, Reading RG6 6AL, U.K. (e-mail: dcm@mail.nerc-essc.ac.uk).

Color versions of one or more of the figures in this paper are available online at http://ieeexplore.ieee.org.

Digital Object Identifier 10.1109/TGRS.2012.2210901

would require substantial modification to work in urban areas containing radar shadow and layover.

A semiautomatic algorithm for the detection of floodwater in urban areas using TerraSAR-X has been developed by [11]. It uses a SAR simulator [12] in conjunction with LiDAR terrain data to estimate regions of the image in which water would not be visible due to shadow or layover caused by buildings and taller vegetation. Ground will be in radar shadow if it is hidden from the radar by an adjacent intervening building. The shadowed area will appear dark and may be misclassified as water even if it is dry. In contrast, an area of flooded ground in front of the wall of a building viewed in the range direction may be allocated to the same range bin as the wall, causing layover which generally results in a strong return and a possible misclassification of flooded ground as unflooded. The algorithm proposed by [11] is aimed at detecting flood extents for validating an urban flood inundation model in an offline situation and requires user interaction at a number of stages.

Follow-up work from this was carried out by [13]. Here, the objective was to build on a number of aspects of the existing algorithms to develop an automatic near real-time method for flood detection in urban and rural areas. In the urban area, 75% of the urban water pixels visible to TerraSAR-X were correctly detected, though this percentage reduced somewhat if the urban flood extent visible in the aerial photos and detected by TerraSAR-X was considered, because flooded pixels in the shadow/layover areas not visible to TerraSAR-X then had to be taken into account. Better flood detection accuracy was achieved in rural areas, with almost 90% of water pixels being correctly detected by TerraSAR-X. The algorithm assumes that high-resolution LiDAR data are available for at least the urban regions in the scene, so that a SAR simulator may be run in conjunction with the LiDAR data to generate maps of radar shadow and layover in urban areas. It is therefore limited to urban regions of the globe that have been mapped using LiDAR.

In an operational flood management perspective, an ideal flood-mapping system operating in near real time should be fully automatic, computationally efficient, independent of the content of local geo-information databases, and, most importantly, capable of providing accurate and reliable results.

To contribute to the recent developments in high-performance flood detection algorithms to obtain timely and more accurate flood warnings, we propose an effective technique based on image differencing as proposed by [7], which may compete with existing algorithms in terms of accuracy and level of automation. For this, we also focus on high-resolution SAR data for flood detection inside urban areas and use the TerraSAR-X image of the England summer 2007 floods as demonstration. Although this is only a single test, and different results may be obtained for other urban areas where the built environment is different to the UK case studied here, it does provide a first demonstration of the potential of the method.

II. Methodology

Martinis *et al.* [8] recently highlighted an apparent lack of traceability and standardization in many SAR-based flood-mapping methodologies. This concern has led to the introduction of two variants of an automated and physically based SAR-based flood-mapping algorithm [7]. Both variants, which are termed M1 and M2a, respectively, exploit the statistics of backscattering coefficients retrieved from SAR to segment an image into its flooded and non-flooded parts. While M1 only considers a single SAR flood image to extract pixels corresponding to "open water" via thresholding and region growing, M2a adds CD with respect to a non-flood reference image to improve the algorithm's performance. In this paper, we introduce an enhanced version of M2a, which we term M2b. This method addresses some of the shortcomings of M2a that [7] identified in two representative case studies.

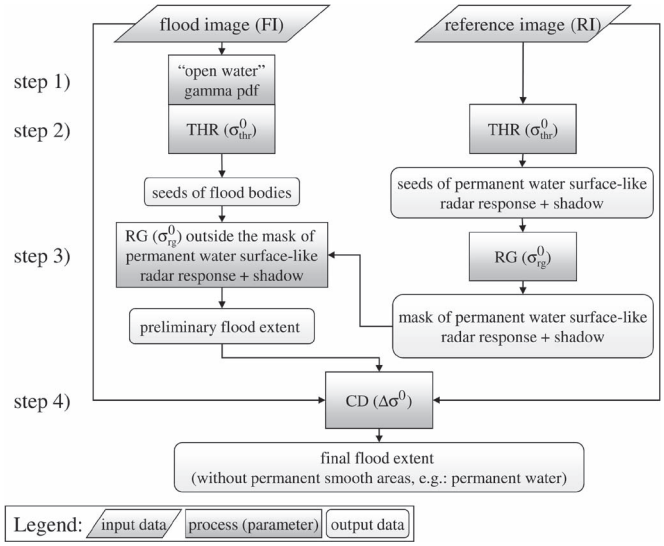

Fig. 1. General scheme of the three processing steps of the flood detection algorithm M2b.

This section provides a detailed overview for all processing steps of the flood extraction algorithm M2b, together with the associated parameters defining each process and a list of differences with respect to the M1 and M2a algorithms previously introduced. In addition to standard pre-processing steps commonly involved with Level 1 SAR data, the M2b algorithm consists of four processing steps (Fig. 1).

A. Statistical Distribution of the "Open Water" Backscatter

The flood extraction algorithm uses as input Level 1 SAR data that are geocoded, coregistered, and calibrated. The first step is the estimation of the probability density function (PDF) of backscattering values associated with "open water." The aim of this processing step is the calibration of a theoretical PDF that optimally fits the empirical distribution of backscatter values from "open water" inferred from the SAR image. According to [14], the backscatter variability on a homogeneous surface is mainly due to speckle and the theoretical PDF that best describes the distribution of backscatter originating from a homogeneous surface is a Gamma PDF. Here, we hypothesize "open water" to be a homogeneous surface, which means that a potential limitation of the approach, and SAR mapping of inundated surfaces in general, relates to the possible roughening

of "open water" caused by emerging vegetation, wind, or rainfall. Alternative PDFs have been parameterized and tested: the K-distribution and the RiIG distribution functions (see, e.g., [15]). However, the goodness of fit provided by the three PDFs was found to be almost equivalent, with the Gamma PDF slightly outperforming the other two functions in this particular case study. Moreover, the Gamma PDF has only two parameters (compared to three parameters for the other PDFs) and the additional advantage of a physically based interpretation for homogeneous areas with fully developed speckle [14]. The latter can be considered a reasonable assumption for "open water." Consequently, the Gamma PDF was preferred over other competing PDFs for approximating the distribution of backscatter values corresponding to "open water"

$$f_{\sigma_m^0}(\sigma^0/k) = \frac{(\sigma^0 - \sigma_1^0)^{(k-1)}}{\left(\frac{\sigma_m^0 - \sigma_1^0}{k-1}\right)^k \cdot \Gamma(k)} e^{-\frac{(\sigma^0 - \sigma_1^0)(k-1)}{(\sigma_m^0 - \sigma_1^0)}} \quad (1)$$

where k is the shape parameter of the gamma distribution and σ_m^0 is the gamma distribution mode. The parameter σ_1^0 is the minimum backscatter value in the SAR image, which needs to be applied so that the gamma distribution is, therefore, only computed for positive values.

Two parameters thus need to be optimized to identify the theoretical gamma function f that best fits the empirical distribution of backscatter values from "open water" h (i.e., image histogram). The optimization of the two parameters k and σ_m^0 consists in minimizing the root mean squared error (RMSE) between the image histogram and the gamma distribution, for backscatter values lower than σ_{thr}^0, with the parameter $\sigma_{thr}^0 \geq \sigma_m^0$ representing the point where the distributions f and h start deviating. The optimization is performed with sequentially increasing values of σ_m^0 and σ_{thr}^0. For both parameters, the proposed sampling step is 0.1 dB. The optimization process is initiated with a first-guess value for σ_m^0 of -25 dB. For each tested mode value, sequentially increasing σ_{thr}^0 values, higher than the corresponding tested σ_m^0 value, are selected. For each set of σ_m^0 and σ_{thr}^0 values, the parameter k is optimized using the nonlinear fitting process of [16], i.e., the nonlinear regression based on the Levenberg–Marquardt algorithm for nonlinear least squares. The RMSE between the theoretical density function f and the empirical density distribution h is calculated for each parameter set and over all backscatter values lower than σ_{thr}^0. Finally, the parameter set $(\sigma_m^0, k, \sigma_{thr}^0)$ providing the lowest RMSE is set as optimal. In case the image histogram is not bimodal, an appropriate option is available for the user to manually set a range of plausible values, inside which the algorithm tests different modes searching for the optimal one.

B. Backscatter Thresholding

The aim of the this step is to extract seeds of "open water" areas from the flood image, being either individual pixels or regions. The parameter σ_{thr}^0 represents the maximum backscatter value for which the fit between the theoretical and empirical PDF is satisfactory. For backscattering values higher than σ_{thr}^0, the distribution functions f and h start deviating. As a matter of fact, σ_{thr}^0 is considered the maximum backscatter value for which there is no significant overlap between radiometric distributions corresponding to water bodies and other land use types. Since the backscatter values from water surfaces are comparatively low, this value is used to extract the seeds of water bodies by selecting the pixels having backscatter values lower than σ_{thr}^0. This thresholding yields a preliminary flood inundation map that represents the seed region for a subsequent region growing process.

Moreover, to be able to map permanent water bodies, the threshold computed on the flood image, σ_{thr}^0, is also applied on the reference SAR image to classify seeds of permanent water bodies. It is worth noting that these seeds include, in addition to permanent water bodies, other smooth surfaces with a water surface-like radar response as well as all shadow-affected areas. The issue related to smooth surfaces will be discussed in more detail in the following sections.

C. Region Growing

Next, the extracted water bodies, representing the seeds, are dilated using the region growing approach of [17]. The procedure iteratively grows the seeds until a given tolerance level is reached. The sequence of thresholding and region growing only adds pixels to the seeds that are located in the vicinity of the preliminary flood extent, thereby limiting the risk of overdetection in areas distant from the flooded area (i.e., misclassification of "dry" pixels as "wet"). The tolerance parameter characterizes the regional homogeneity of the backscattering behavior. The tolerance criterion adopted here is based on the percentiles of the theoretical gamma distribution of "open water" pixels.

The iterative procedure incorporates pixels with backscatter values lower than σ_{rg}^0, corresponding to a given percentile, RG%, of the theoretical gamma distribution of "water" pixels in the image. In this paper, we propose a simultaneous calibration, recently advocated by [7]. The approach optimizes the tolerance criterion together with the CD parameter introduced in the next section.

Region growing, with the same threshold value σ_{rg}^0, is also applied to dilate the seeds of permanent smooth surfaces obtained from the reference image. The approach provides a mask of water surface-like radar response areas that is used to limit the region growing applied on the flood image, thereby preventing the spreading of flooded areas into permanent smooth areas.

D. CD

Matgen *et al.* [7] argued that flood maps resulting from region growing should include all "open water" pixels connected to the seeds. The region growing should thus extend into the high percentiles of the gamma distribution. However, the resulting overdetection needs to be removed by the subsequently applied CD step. CD thus aims at removing pixels from the flood extent map that do not correspond to flood water. To do so, only pixels that significantly change their backscatter values with respect to their baseline backscatter values are kept in the flood extent map, while pixels that did not decrease their backscatter values by a minimum amount are removed. This

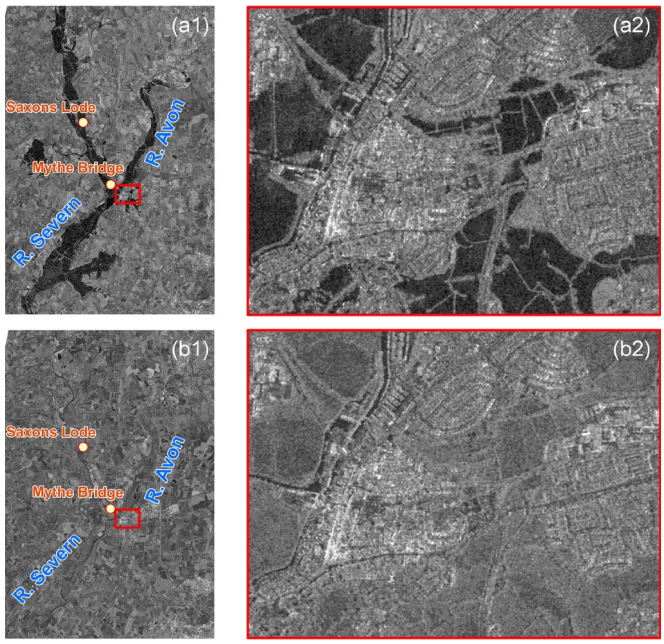

Fig. 2. (a1) Flood image (July 25, 2007) and (b1) postflood reference image (July 22, 2008). Zoom in to the area of interest (city of Tewkesbury) for (a2) the flood image and (b2) the reference one.

means that the main river channel, which is a permanent water body, is not any longer an integral part of the flooded area.

The specific parameter of the CD is $\Delta\sigma^0$, defined as the required minimum change in backscatter between the reference and the flood image for a pixel being considered as flooded. To determine the optimal criterion for the required minimum change in backscatter, an iterative procedure is adopted. As mentioned earlier, the two parameters σ^0_{rg} and $\Delta\sigma^0$ are optimized through a simultaneous calibration, minimizing the RMSE computed over the whole range of backscatter values in the flood image between the theoretical gamma distribution and the empirical distribution of "open water" pixels. This means that different threshold values, σ^0_{rg}, which correspond to different percentiles of the theoretical gamma distribution, are sequentially selected from an interval of plausible values, and a corresponding minimum CD parameter $\Delta\sigma^0$ is optimized for each tested threshold value. We consider as plausible values all values that are greater than σ^0_{thr} and which increase with a sampling step of 1% up to the value of 99% of the Gamma PDF and then with an increment of 0.1% up to the value of 99.9% of the Gamma PDF. For every parameter set (σ^0_{rg}, $\Delta\sigma^0$), the sequence of region growing and CD processes is applied on the area conditioned by the permanent smooth area mask. At the end of each iteration, the histogram of "flood water" pixels is computed. The corresponding empirical PDF is compared against the initially calibrated theoretical gamma distribution (1). The parameter set (σ^0_{rg}, $\Delta\sigma^0$) providing the lowest RMSE value is set as optimal.

To summarize, M2b essentially represents an improved version of the M2a method introduced by [7]. The two algorithms both take into account a reference SAR image and include four inter-related processing steps (i.e., calibration of gamma distribution function, radiometric thresholding, region growing, and CD). However, while M2a predefines the region growing parameter as the 99% percentile of the "water" backscatter gamma distribution, M2b adds flexibility to the optimization process by calibrating the tolerance criterion that, together with the associated CD parameter $\Delta\sigma^0$, minimizes the RMSE between empirical and theoretical distribution functions.

This modification implemented in M2b constitutes an important change as it renders the algorithm fully automated, without any requirement of manual user inputs. Therefore, the mapping process is believed to be entirely objective. Another important improvement is that M2b, unlike M2a, makes use of the reference image to build a mask of permanent water surface-like radar response areas. Indeed, to render the algorithm suitable for urban flood mapping, it is necessary to mask out not only smooth surfaces like tarmac, paved roads, and parking lots, but also all regions in shadow-affected areas unseen by the satellite. In urban areas, the latter are particularly important as they potentially lead to a significant part of overdetected flooded areas. This issue will be thoroughly discussed in Section IV-B2.

It should also be noted that method M2a and its enhanced version M2b both rely on the availability of reference images acquired from the same orbital track, with the same incidence angle, polarization, and resolution, and prior to the onset of flooding. Moreover, the adequate choice of a season-dependent reference image might help reducing the effects of changes in vegetation, as argued recently by [18]. With the advent of relatively new sensors such as TerraSAR-X, it can be difficult to find an image that satisfies these selection criteria. However, as image archives are gradually being built up, this should be less of a problem in the near future. If no reference image is available, method M1 can be applied.

III. Study Area and Available Data Set

This section describes the study area, the flooding event and the available remote-sensing images for testing and evaluating the proposed automated flood delineation algorithm.

The image data used for this study were acquired for the approximately 1-in-150-year flood that took place around Tewkesbury, U.K., in July 2007 [11]. Extreme rainfall intensities resulted in substantial flooding of urban and rural areas; about 1000 properties in the town of Tewkesbury were affected [19]. Tewkesbury lies at the confluence of the River Severn, flowing in from the northwest, and the River Avon, flowing in from the northeast. Bankfull discharge is approximately 350 m.s^{-1} (or 4.5 m in gauged level) at the Saxons Lode gauging station $\sim$7 km upstream of Tewkesbury. The summer 2007 event was unusual for the study site in that the majority of the flow derived from local rainfall. On the 20th July, two days prior to flood peak, more than 12 cm of rain fell on the surrounding area. The flood peak of 5.43 m Ordnance Data Newlyn was measured at Tewkesbury on July 22 with both rivers exhibiting a more rapid increase in flow than a typical autumn or winter event that may build over many weeks, with flows increasing from 100 m.s^{-1} to $>$ 500 m.s^{-1} in 57 h, between the 20th and the 22nd July. The river did not return to below bankfull until July 31. In the region of interest (red

TABLE I
CHARACTERISTICS OF THE AVAILABLE IMAGES (STRIPMAP MODE) FOR THE ANALYZED FLOOD EVENT

IMAGE	Date	track	orbit	pixel spacing (m)	ground resolution (m)	band	wave length (GHz)	polarization	Average mean indicence angle on study area (°)
flood	July 25 2007 6:34	descending	109	1.5	3	X	9.6	H/H	24
reference	July 22 2008 6:34	descending	109	1.5	3	X	9.6	H/H	24

box in Fig. 2), an area of 1.5 km^2 was possibly flooded at the time of the TerraSAR-X overpass, according to a 2 m resolution hydraulic model [20].

The majority of the buildings are two storey houses. In the area of interest, there are some industrial warehouses but no large-size factories. Overall, the study area is rather representative of a typical urban landscape in the UK. To demonstrate the applicability of our proposed SAR image segmentation algorithm, we define urban area as the zone inside and in the vicinity of the built-up region of the town of Tewkesbury.

A. TerraSAR-X Images

A unique data set consisting of numerous types of remotely sensed images over one single event hydrograph were acquired over the selected study area [20]. From this data set, a stripmap TerraSAR-X image acquired on July 25, 2007 (at 06:34 GMT, Wednesday) was selected (see Fig. 2). The image is a multi-look ground range spatially enhanced scene with 1.5 m pixel spacing and has a mean incidence angle of 24°. Its H/H polarization mode arguably allows for the best discrimination between a SAR image's flooded and non-flooded parts [8]. At the time of the satellite overpass and image acquisition, there was relatively low wind speed and no rain [11]. Moreover, no rainfall was recorded in the 30 h preceding the TerraSAR-X acquisition, as well as during the satellite overpass itself.

In their flood delineation study, [11] used the single TerraSAR-X flood image together with airborne scanning laser altimetry (LiDAR) data. Here, we also consider a dry reference image which is a postflood image acquired from the same orbit track and with the same polarization as the flood image. This way, geometric problems related to coregistration can be limited, and baseline backscatter values can be inferred. A single scene having these imaging characteristics and covering all of the azimuth extent of the target is available in the current TerraSAR-X image archive. It was acquired on July 22, 2008 (at 06:34 GMT, Tuesday), almost exactly a year after the flood event had occurred. The flood and non-flood images have both been acquired in the same month of the year. Hence, it can be assumed that the state of vegetation is similar in both images. This is important as decreases in backscatter values between any two images are caused not only by flooding, but also by changes in vegetation.

The two images, whose characteristics are listed in Table I, have been georeferenced and calibrated. These two processes are important to preserve a backscatter consistency and an accurate coregistration between the images. Hence, it can be avoided to erroneously consider as flooding related those changes in backscattering values that are due to differences in image acquisition characteristics.

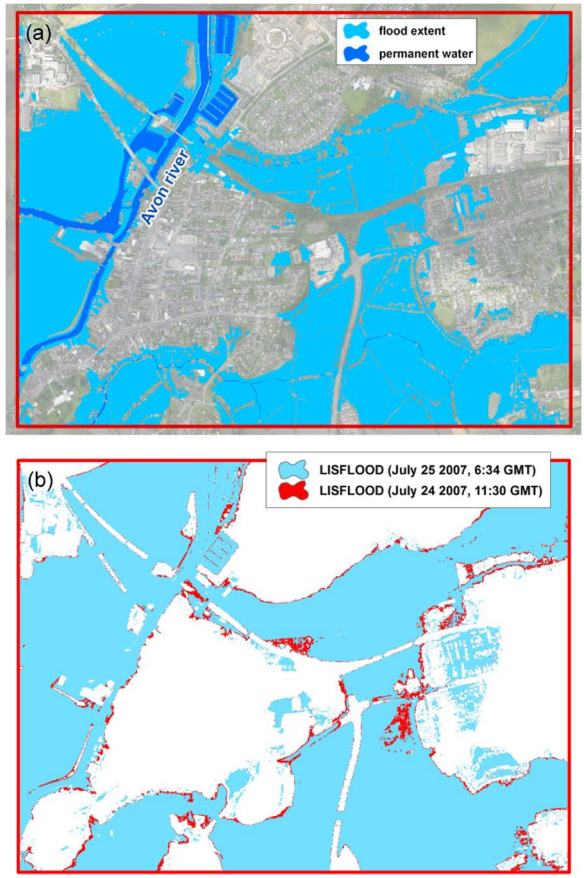

Fig. 3. (a) Flood validation map obtained from high-resolution aerial photography on July 24, 2007 at 11:30 GMT: The permanent water bodies are also displayed; (b) comparison between the LISFLOOD computed flood extent at the time of aerial photographs acquisition (July 24, 2007 at 11:30 GMT) and TerraSAR-X overpass (July 25, 2007 at 6:34 GMT).

The TerraSAR-X images used in this study have a 1.5 m pixel spacing and a ground resolution of the order of magnitude of 3 m. This means that each pixel represents a 1.5×1.5 m^2 area on the ground and that only individual objects of dimensions bigger than 3 m can be discriminated in the image. In an operational context, the reference image would ideally consist of a preflood satellite acquisition. However, in this particular case, given the relative novelty of a sensor such as TerraSAR-X, it was not possible to find a reference image, prior to the onset of flooding, acquired from the same orbital track and with same polarization. Therefore, a postflood image was selected.

Particular attention has been given to an adequate coregistration of the images, as an accurate overlapping is a prerequisite for detecting flooding-related changes in the backscattering behavior. The accuracy of the georeferencing is of subpixel precision. Next, the images have been filtered with a 5×5 Gamma-MAP filter to decrease the speckle contribution. This

filter smoothes out the speckle granularity while preserving details, such as the contours of buildings and flooded areas [21]. It also impacts the parameterization of the gamma PDF (1) by reducing the spread of backscattering values associated with "open water." The red box area in Fig. 2 presents the area of interest for the city of Tewkesbury: it refers to a rectangular area of 1135 $\times$ 998 pixels (1.5 m pixel spacing) for a total surface of $\sim$3 km^2.

B. Validation Data Set

The validation data set, consisting of very high resolution 0.2 m aerial photographs acquired during the flooding event in July 2007, enables a comprehensive evaluation of the algorithm's performance in terms of SAR-based flood delineation. An aircraft operated by the Environment Agency of England and Wales carried out the overflights.

The flood extent was obtained through manual photo-interpretation [Fig. 3(a)]. Taking advantage of existing landuse maps of the area, permanent water bodies associated with rivers and canals have been removed from the validation map. While in general the delineation of flood boundaries from such high-resolution optical products is relatively straightforward, it is important to note that the flooding of densely vegetated and built-up environments can lead to some ambiguities. For instance, in the case of bare soil fields, the accurate positioning of the separation line between muddy flood waters and non-flooded areas is nontrivial. However, for this case study, difficulties in shoreline delineation were encountered only in a limited number of locations.

In addition, it is important to bear in mind that the aerial photographs were acquired on July 24 (at 11:30 GMT) while the TerraSAR-X image was obtained 19 h later on July 25 (at 06:34 GMT). Although there was no significant decrease in gauged water levels between the acquisition time of aerial photographs and the TerraSAR-X overpass [22], this time gap might be responsible for some discrepancies between the aerial photography-derived and SAR-derived flooded areas. To estimate the potential variation of flood extent between the two acquisition times, simulations with a previously calibrated hydraulic 2 m LISFLOOD-FP flood model [23] have been carried out both at the acquisition time of the aerial photographs and at the TerraSAR-X overpass. It is here assumed that the model provides a satisfactory representation of the time variation of the flood extent, since an evaluation of the model results showed that the model predicts water levels with a mean error of less than 30 cm [20]. The simulations show a reduction of the flooded area of approximately 5% between the two time steps. In particular, Fig. 3(b) shows the differences between the two simulated flood inundation maps. The most notable differences can be observed on a triangular-shaped field (see middle-right part in the domain of interest) from which, according to the model simulations, flood water was drained between the two overpasses. This location was also problematic in terms of identifying its flooding status through photo-interpretation, as explained in more details in the discussion section. These factors, all unrelated to the processing of the SAR images, need to be taken into account during the analysis, as all the observed differences may not be necessarily due to the inability of the proposed algorithms for accurately extracting the flood extent from SAR imagery.

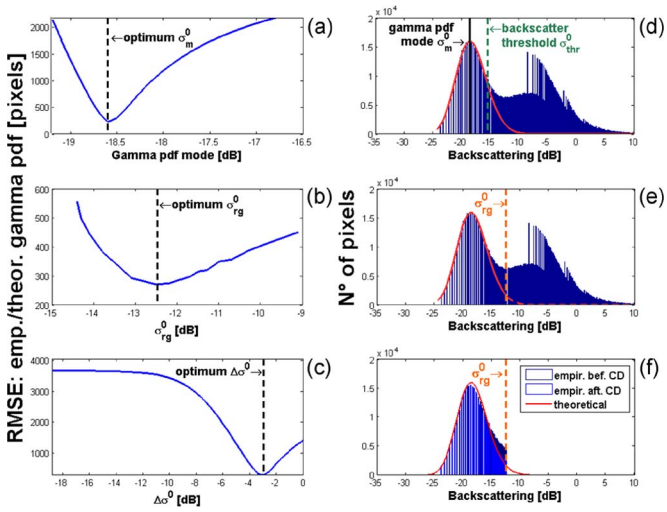

Fig. 4. Optimization of the parameters of the automated algorithm for M2b method. (a) RMSE calculated by comparing the empirical image histogram with several competing Gamma PDFs, obtained with different values for the mode, σ^0_m. (b) RMSE calculated by comparing the optimized Gamma PDF and the empirical image histogram after region growing and change detection, for different tested values of the region growing parameter, σ^0_{rg}. (c) Example of RMSE calculated by comparing the optimized Gamma PDF and the empirical image histogram obtained, for a given fixed region growing parameter, σ^0_{rg}, testing several change detection values, $\Delta\sigma^0$. (d) Empirical image histogram and optimized Gamma PDF. (e) Empirical image histogram with the optimized region growing parameter, σ^0_{rg}, displayed. (f) Example of the effect deriving from the application of the optimized change detection value, $\Delta\sigma^0$, for a given region growing parameter, σ^0_{rg}.

IV. Results and Discussion

This section assesses the classification accuracy obtained with the fully automated flood detection algorithm M2b and contrasts its performance with those of the previously introduced M1 and M2a algorithms. It also provides insights into the added value of reference images for flood delineation in urban areas.

A. Extraction of Flooded Areas

The flood extent has been extracted from the TerraSAR-X image using the three methods M1, M2a, and M2b.

In particular, for method M2b, Fig. 4 illustrates the optimization of the four parameters: the mode of the "open water" backscatter gamma PDF, σ^0_m, the backscatter threshold, σ^0_{thr}, the tolerance criterion for the region growing step, σ^0_{rg}, and the minimum CD value, $\Delta\sigma^0$.

Panel (a) reports the optimization of the mode parameter, while panel (d) provides the corresponding optimized gamma PDF in red, together with the histogram of the backscatter values in the flood image. Panel (d) displays the value of the second parameter, σ^0_{thr} (i.e., in this case study equal to -15.5 dB) as the maximum backscatter value for which there was no overlap between the empirical histogram and the theoretical gamma PDF. The optimized value is also provided in

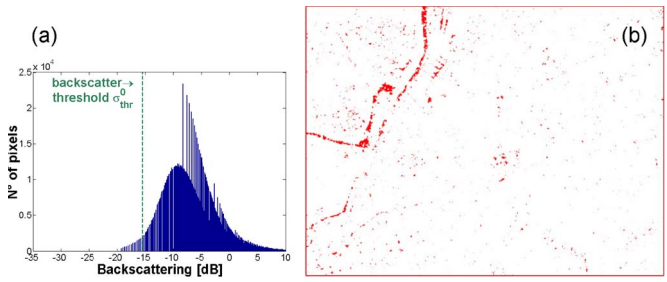

Fig. 5. (a) Backscatter histogram of the reference image with superimposed threshold value σ^0_{thr}, computed on the flood image; (b) reference mask.

Fig. 5(a), together with the backscatter histogram of pixels in the reference image. This value is used to derive the reference mask of permanent water surface-like radar response areas through thresholding of the reference image [Fig. 5(b)]. From Fig. 4(d) and Fig. 5(a), it can be observed that for high backscatter values, there is a systematic noise in the return signal of both TerraSAR-X images. This is arguably due to the high complexity of urban topography and its considerable impact on the high-resolution backscattering signal. However, at this stage, this is only a hypothesis that could not be verified: other inherent technological reasons related to very high resolution SAR data could be at the origin of the noisy data. Considering the region growing step of method M2b, it is important to mention that the parameters σ^0_{rg} and $\Delta\sigma^0$ are optimized together. Therefore, the subplot in panel (b) of Fig. 4 illustrates the impact that different σ^0_{rg} parameters (each associated with a corresponding optimal $\Delta\sigma^0$ value) have on the RMSE. Similarly, panel (c) provides an example of the performance of $\Delta\sigma^0$ values for a given σ^0_{rg} value: Fig. 4(c) refers to the optimal σ^0_{rg} value for the case study. The backscatter value corresponding to the optimized σ^0_{rg} value is also displayed in panels (e) and (f). Finally, panel (f) shows the empirical histogram of flood pixel values before and after CD: these histograms are computed only with the pixels inside the SAR-derived flooded area. The reduction of the distribution tail and the related reduction of overdetection are indicated by the empirical histogram approaching the theoretical gamma PDF.

B. Evaluation at City Level (Quantitative Analysis)

1) Overview of Flood Maps: Three flood extent maps were obtained through the application of the three image processing algorithms. The corresponding contingency matrices were computed using the evidence provided by aerial photography. The binary pattern of flooded and non-flooded pixels was compared against the reference flood map (in this case, see Fig. 3). The result is a matrix (or contingency table) of four possible outcomes. With respect to the reference flooded area, there are two ways for a remote-sensing-derived flooded area to be correct (either by correctly representing flooded or non-flooded pixels) and two ways to be incorrect (either by erroneously under- or overpredicting the observed inundation extent). The values of the contingency matrix for all methods are reported in Table II (and also displayed as contingency maps in Fig. 6) for a quantitative evaluation of the performances. Moreover,

TABLE II
QUANTITATIVE EVALUATION OF TERRASAR-X DERIVED FLOOD EXTENT

	σ^0_{rg}	$RG_{\%}$	$\Delta\sigma^0$	over detection	under detection	total good	total error
	(dB)	(%)	(dB)	(%) area of interest, red box in Figures			
M1	-13.4	96	-	2.8	15.6	81.6	18.4
M2a	-11.7	99	-3.1	2.6	15.6	81.8	18.2
M2b	-12.5	98	-3.0	2.1	16.2	81.7	18.3

the optimized (and/or fixed) parameter values for the region growing and the CD are indicated.

From Table II, it can be concluded that in the present case study, the three algorithms provide very similar performance levels. When the evaluation is carried out at a regional scale (i.e., at city level), the differences seem to be marginal. Methods M2a and M2b slightly outperform method M1 with respect to the main performance measures provided in Table II. For example, the total error is lower when CD is applied. While the underdetection obtained with M2b is slightly higher than with M1 and M2a, this is compensated with a lower overdetection. Overall, M2b and M2a perform better than M1, as it was expected, suggesting that CD with respect to a non-flood reference image does provide some advantages.

The results do not reflect the added value that we expected from the methodological improvements of method M2b. This result is due to the fact that, in this particular case study, the optimized region growing threshold σ^0_{rg} equals 98%, which is very close to the pre-defined 99% value that [7] proposed for M2a. A similar result was obtained in a pretest of the fully automated algorithm with an ENVISAT ASAR WSM image available for the same flood. These two case studies on the one hand suggest that the threshold chosen by [7] is rather plausible and, on the other hand, validate the applicability of the procedure to images with different resolution. Here, the tradeoff involves a controlled growing of the seed region to be able to limit the overdetection of flooded areas. While the latter can be partly removed by the subsequent CD, the results indicate that the reduced overdetection comes at the cost of an increased underdetection of flooded areas. The results also indicate that method M2b, which provides an optimal empirical distribution with respect to the targeted gamma distribution of "open water" backscatter values, does not necessarily generate a more accurate flood inundation map than M2a. On a more positive note, it can be observed that the simultaneous optimization of region growing threshold σ^0_{rg} and CD parameter $\Delta\sigma^0$, computed by minimizing the RMSE between empirical and theoretical distribution functions, nearly led to the maximum value of correctly detected pixels (81.7% as reported in Table II). Moreover, from Fig. 7, it can be observed that in this case study, the optimum parameter set also yields the best performance with respect to the validation data.

A comparison with the flood extent detected for the same test case with the semiautomatic procedure of [11] cannot be carried out in a very meaningful way due to the fact that the input data sets in the two studies are different. Mason *et al.* [11] took advantage of a regional DEM, so that SAR-derived water ground heights smoothly vary along the river reach, but did

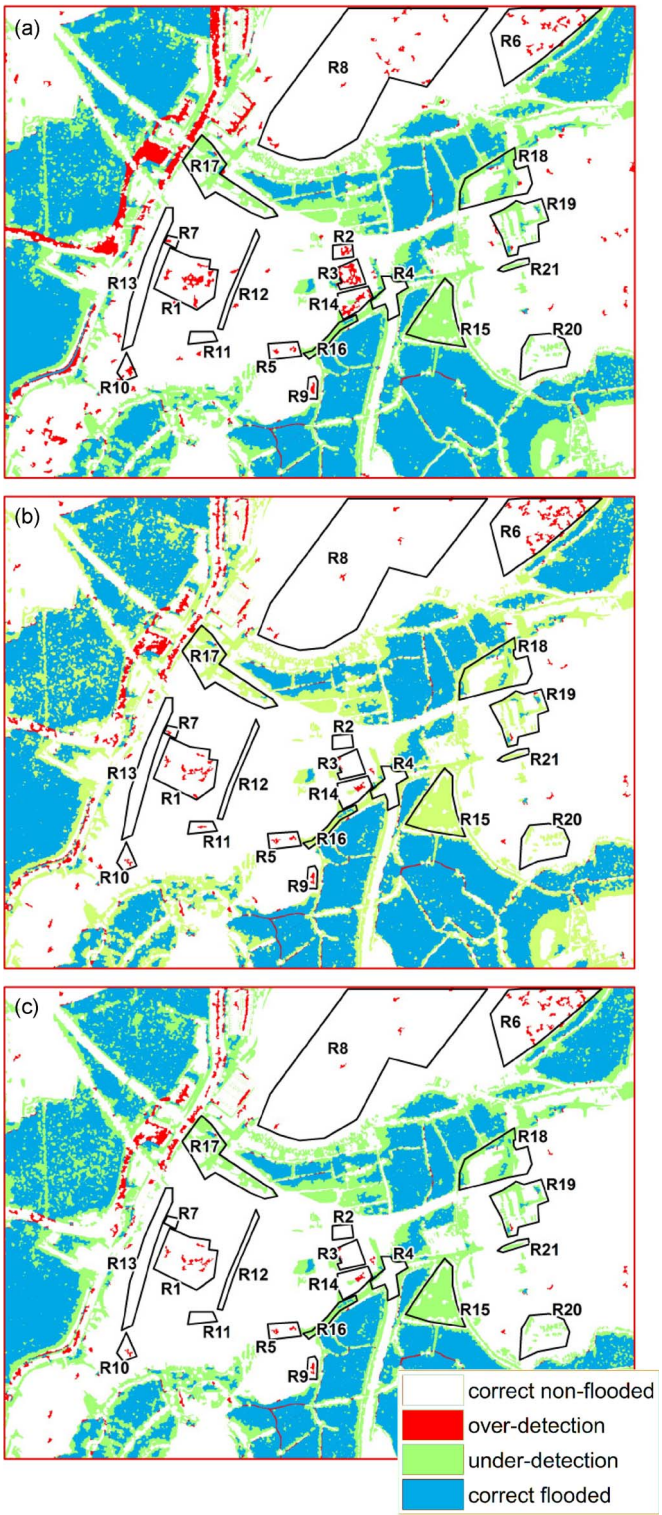

Fig. 6. Contingency map deriving from method: (a) M1, (b) M2a, (c) M2b. For the sake of clearness in the representation, the displayed maps have been cleaned by neighborhood analysis in post-processing step.

not make use of a preflood reference image. However, the comparison of contingency matrices, on a common area of interest and validation data set, reveals that the M2b method performance of 81.7% of correctly detected pixels is rather close to the percentage of 85.4% obtained with the flood inundation map provided by [11]. This result indicates that

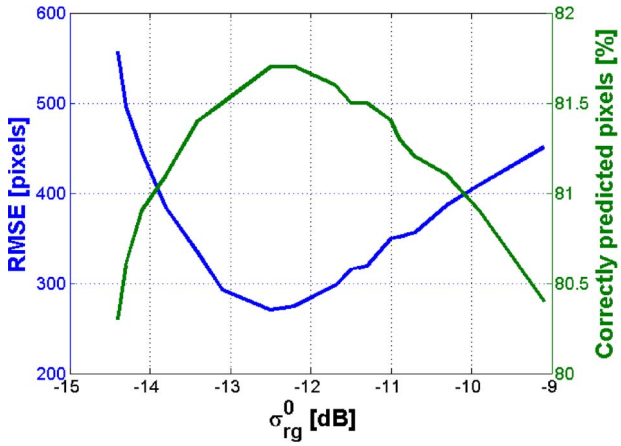

Fig. 7. RMSE values computed for different region growing thresholds (M2b method) during the optimization process and corresponding performances in terms of correctly predicted pixels (as flooded and as nonflooded).

topography data could be used more efficiently than preflood reference images for increasing the accuracy of SAR-derived flooded areas. However, this assessment needs to be confirmed in future studies.

To better appreciate the advantages of these methodological enhancements, it is worth analyzing the PDF of backscattering values associated with pixels located inside the flood extents, the latter corresponding either to the validation map obtained from aerial photographs or the flood extents computed with the different versions of the image-processing algorithm. The different PDFs are displayed in Fig. 8. It becomes evident from the panels that the PDF of "flood water" pixels from high-resolution photos is reasonably close to a gamma distribution, albeit characterized by a heavy tail end. M1 does enable the identification of a majority of water pixels but it misses out the tail of the distribution. M2a yields a better performance, as it adds more pixels to the flood extent, thereby reducing the number of underdetected flood pixels. However, there is still a tendency to slightly overestimate part of the tail of the theoretical gamma PDF. Because of its enhanced CD procedure, M2b method is capable of growing the seeds further into the high percentiles of the gamma distribution, reducing the heavy tail end and keeping the PDF of detected water pixels closer to the theoretical one. It is worth noting here that the PDF of backscattering values inside the area delimited by the high-resolution photos exhibits a particular tail that is missed by all three versions of the flood detection algorithm. Surprisingly, the high number of pixels with associated high backscatter values is not only due to the expected increased backscatter response from urban structures. In fact, the probability distribution from pixels located in rural areas exhibits the same heavy tail end as the one of pixels located in urban areas (Fig. 9).

Further research is needed to get a better understanding of the particular shape of the PDF of backscatter values. One possible explanation can be that some of the pixels changed their status from "flooded" to "nonflooded" between the two data acquisitions, as already shown in Fig. 3(b).

From this first overview of results, it can be concluded that the strength of CD is that it allows the region growing to extend further into the high percentiles of the gamma distribution

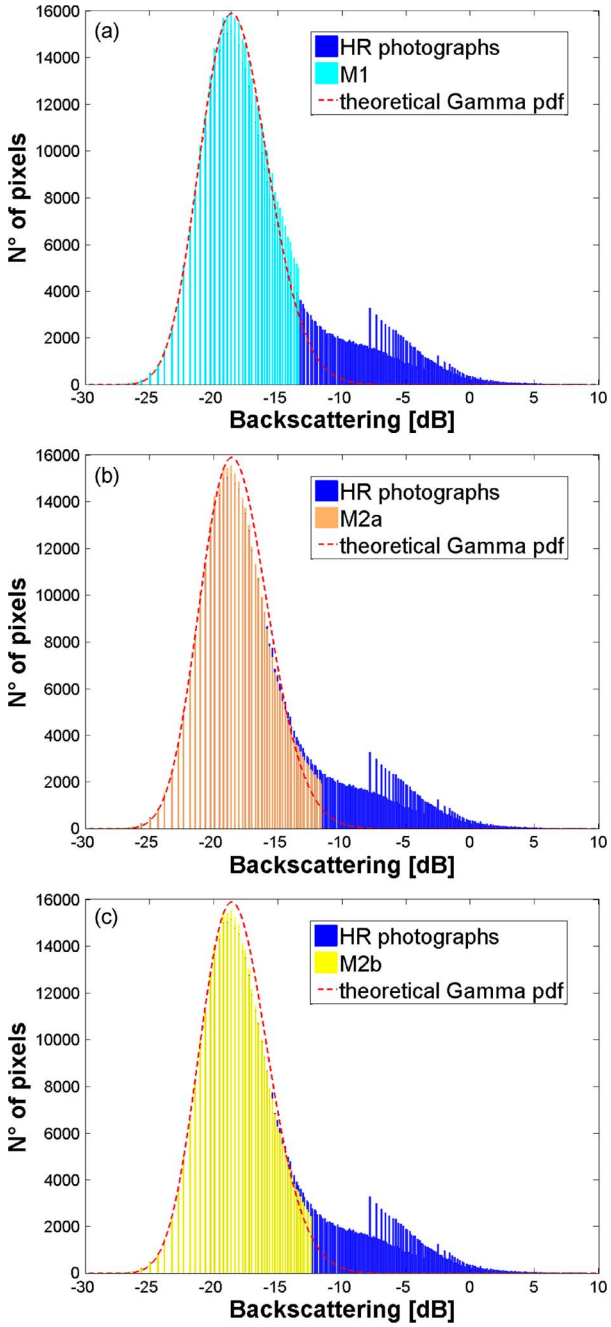

Fig. 8. Backscatter probability density function of water pixels from the high-resolution photographs and water pixels from the method: (a) M1, (b) M2a, (c) M2b. The histograms refer to the algorithm output, with no post-processing cleaning step included.

as it efficiently removes part of the resulting overdetection. More case studies are needed before a generalization of these findings can be done in a meaningful way. Nevertheless, these preliminary results corroborate those reported by [7] in case studies dealing with moderate- and low-resolution SAR imagery.

On the selected domain (i.e., rectangular area of 1135 × 998 pixels), the running time of the complete M2b process on an Intel Core 2Quad CPU, 2.66 GHz and 3.24 GB RAM is less than 30 min, indicating the appropriateness of the method also for near real-time applications.

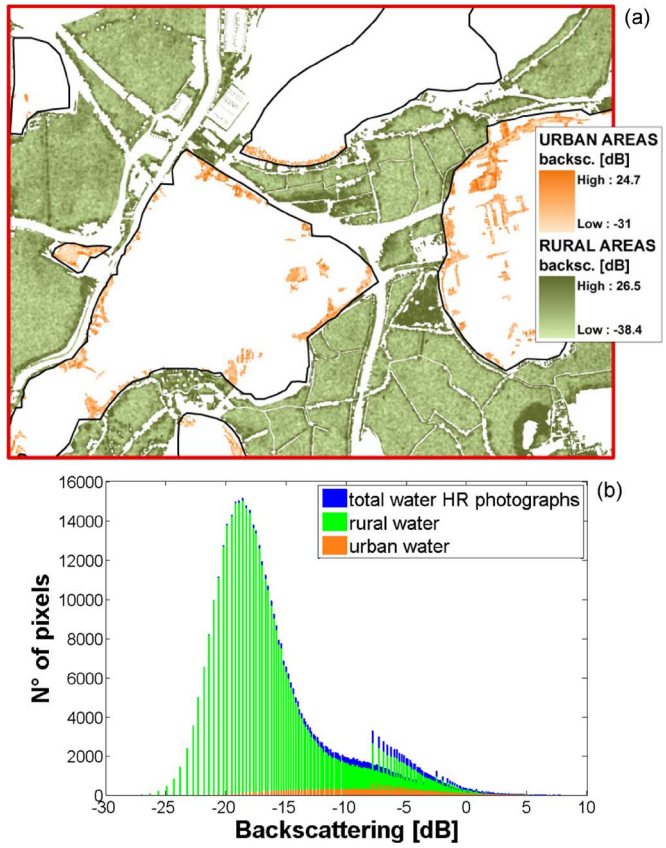

Fig. 9. (a) Main rural and urban areas overlapped on the pixels in the flood image covered by water according to the high-resolution aerial photographs; (b) corresponding backscatter probability density functions.

To summarize, it can be observed that the results obtained with the three versions of the algorithm are rather similar, with the performance of the fully automated M2b being comprised between those obtained with the simplified but fully automated approach M1 and the more subjective one M2a. Moreover, since the correct classification rate of the proposed methods are comparable to those obtained by [11], it could be argued that the main part of the 18% misclassification still remaining can be imputed to limitations of the SAR imaging technique.

2) The Problem of Unseen Regions: One feature that requires special attention relates to regions in a SAR image that cannot be seen by the radar sensor because of its side-looking nature. The affected regions are commonly referred to as "shadow" and "layover." In the context of urban flood mapping, "shadow" and "layover" are due to geometric distortions caused mainly by the presence of buildings. Their impact on SAR-based flood mapping is twofold. First, flooding does not impact the radar response from shadow areas and, consequently, SAR-based detection of flooded shadow areas is not possible (i.e., problem of underdetecting floods). Second, the low radar response from shadow regions might erroneously lead to their classification as "flooded" even in the case they are not (i.e., problem of overdetecting floods). Here, we assume that the resulting overdetection might be addressed through CD since urban shadow areas do not change between two images acquired with the same imaging characteristics. This is confirmed by the reduction in overdetection shown in Table II.

Fig. 10. Mask of regions unseen by TerraSAR-X due to shadow and layover, from [11].

On the other hand, due to double-bounce reflection effects, the urban layover backscatter could be different in the flood and reference images. This phenomenon typically occurs in vegetated areas, where flooding yields an increased backscatter due to the double bouncing between the flooded ground and branches or leaves, resulting in a higher return signal in the flood image. A similar mechanism of multiple reflections between flooded streets and walls could potentially result in a brighter backscatter in the urban areas covered by the flood image. Classification errors are expected to be higher in urban areas than in forested regions [24], and therefore the layover contribution should be taken into account when mapping flooded urban areas. In fact, the inherent underdetection problem can only be addressed through technological advances (e.g., look angles closer to nadir) or the use of ancillary data (e.g., topography data).

For the imaging characteristics of the July 25, 2007 TerraSAR-X image, [11] computed a mask of areas affected by "shadow" and "layover" in the city of Tewkesbury (Fig. 10). They used the German Aerospace Center (DLR) SAR end-to-end simulator in conjunction with airborne scanning laser altimetry (LiDAR) data to estimate regions of the image in which water would not be "visible" to the instrument. In this paper, we made use of the shadow/layover mask from [11] to evaluate the risk of misclassifying pixels in areas not "visible" to the SAR sensor. In the area of interest (red box in relevant figures), the shadow/layover mask of [11] covers a total area of $\sim$1 km^2, which represents a significant percentage ($\sim$39%) of the total area. However, according to the validation map, the flooded area not visible to the satellite reduces to 0.25 km^2, over a total flood extent of 1.22 km^2 (see Table III). Moreover, due to the 24° look angle, in this particular case study, the effect of layover is greater than shadow, as it covers a much larger flooded area. This is mostly due to the diffuse presence of hedges along the borders of the different fields in the rural areas.

As flooding in shadow/layover areas is undetectable for SAR, the corresponding regions would need to be delineated *a priori* and considered as areas with an "unidentifiable status of flooding." In fact, even if a flood is correctly classified in a shadow region, this result should be viewed as an error as the right answer is obtained for the wrong reason. As the objective of the developed method was to generate a mask of surfaces that produce a radar signal response similar to that of inundated areas to constrain the flood extent outside the shadow areas, in the following, we focus only on the overlap between the obtained flood extent and the shadow areas derived by [11]. Note that the shadow mask itself, obtained with the SAR simulator and the LiDAR data, might contain some degree of uncertainty. In general, the overlap between the SAR-derived flood extent and the shadow mask is restricted to the border regions of large clusters of pixels, which were correctly classified as "flooded." The number of such pixels is not significant in comparison to the total number of extracted flood pixels (see Table III): furthermore, it can be observed that M2b helps in significantly reducing the number of pixels classified as "flood water" in the shadow regions. This is due to the fact that parts of the shadow-affected areas are included in the mask of permanent water surface-like radar response areas described earlier. By considering a reference image acquired from the same orbital track as the target image, M2b method reduces the risk of classifying "shadow" areas as "flooded."

TABLE III
QUANTITATIVE ANALYSIS OF WATER PIXELS (PIXEL SIZE 1.5 m) IN THE SHADOW REGIONS [11]

	n° of water pixels in shadow	n° of total water pixels	water pixels in shadow (%)
M1	8648	374060	2.3
M2a	8738	371734	2.3
M2b	7304	357616	2.0

C. Evaluation at Street Level (Qualitative/Thematic Analysis)

The benefits of using a reference image, including the masking of permanent smooth areas representing in this case study $\sim$20% of the area of interest, become obvious when looking at the spatial distribution of errors (Fig. 6). The application of algorithms M2a and M2b leads to the expected reduction of misclassified pixels in urban areas. Numerous scattered clusters of pixels that were initially erroneously classified as "flooded" could be removed, thereby significantly reducing overdetection. In Table IV, a thematic analysis with a special focus on urban features complements the quantitative analysis presented earlier (Table II).

The objective is to understand the advantages and limitations of the three variants of the SAR-based flood delineation algorithms for correctly identifying flooding in urban areas. From the results shown in Table IV, it can be observed that in spite of the high-resolution SAR imagery used in this study, the detection of flooding in built-up environments remains a very challenging task. All algorithms struggle to recognize the flooding status of many small-scale features that might be crucial, as their state of flooding could mean significant interruptions of everyday life. However, overall, the enhanced algorithm M2b performs best, with a slightly reduced number of misclassified areas. In particular, M2b enables the *a priori*

TABLE IV
IMPROVEMENT DERIVING FROM THE USE OF A REFERENCE IMAGE: COMPARISON OF THE DIFFERENT METHODS FOR SOME REGIONS, WITH A SPECIAL EMPHASIS ON URBAN FEATURES. SEE FIG. 6 FOR THE LOCATION OF STREETS, CROSSINGS, AND URBAN/RURAL AREAS (THE CORRECTLY CLASSIFIED REGIONS OF EACH METHOD ARE IN BOLD FONT)

ID	region	HR photographs	method M1	method M2a	method M2b
R1	parking lots	non-flooded	flooded	partially flooded	partially flooded
R2	tarmac area	non-flooded	flooded	**non-flooded**	**non-flooded**
R3	supermarket roof (Morrisons Store)	non-flooded	flooded	**non-flooded**	**non-flooded**
R4	road crossing	non-flooded	**non-flooded**	**non-flooded**	**non-flooded**
R5	Road (Barton Road)	non-flooded	flooded	flooded	flooded
R6	field on hillslope	non-flooded	flooded	flooded	flooded
R7	roof	non-flooded	flooded	flooded	**non-flooded**
R8	urban area	non-flooded	partially flooded	less flooded	less flooded
R9	roof	non-flooded	flooded	flooded	flooded
R10	road crossing	non-flooded	flooded	partially flooded	partially flooded
R11	Road (East Street)	non-flooded	**non-flooded**	flooded	**non-flooded**
R12	Road (Chance Street)	non-flooded	**non-flooded**	**non-flooded**	**non-flooded**
R13	Road (High Street)	non-flooded	**non-flooded**	**non-flooded**	**non-flooded**
R14	parking lot	partially flooded	flooded	**partially flooded**	**partially flooded**
R15	field	flooded (dubious)	non-flooded	non-flooded	non-flooded
R16	Road (Ashchurch Road)	flooded	partially flooded	partially flooded	partially flooded
R17	road crossing	flooded	non-flooded	non-flooded	non-flooded
R18	parking lot	flooded	partially flooded	partially flooded	partially flooded
R19	urban area	flooded	partially flooded	partially flooded	partially flooded
R20	urban area	flooded	non-flooded	non-flooded	non-flooded
R21	Road (Knights Way)	flooded	non-flooded	non-flooded	non-flooded

delineation of areas characterized by specular-like reflections (i.e., areas with permanent water surface-like radar responses). This is helpful given that smooth areas (e.g., R2 & R3) tend to be systematically classified as flooded by M1 and, to a lesser extent, by M2a. On the other hand, more open areas, such as the main roads R12 and R13, are correctly classified by all three methods. It is worth mentioning that, despite these somewhat encouraging results, M2b fails to correctly delineate flooding in many densely vegetated and built-up environments.

These errors will be analyzed in more detail in the following sections. In this analysis, we will consider ancillary data (e.g., land use map, oral communications from local experts) to better understand the reasons that are at the origin of the remaining misclassifications. Moreover, the mask of regions unseen by the satellite, i.e., shadow and layover, has also been taken into account for error detection at street level.

1) The Problem of Overdetection: As it can be seen from the urban flood maps presented in Fig. 6, both over- and under-detection are reduced as a result of applying the M2b algorithm rather than its predecessors. This is particularly evident in the case of the large shopping mall labeled R3. Due to the flatness of its roof and resulting specular reflection, it was erroneously classified as flooded by M1, while M2a and M2b correctly excluded it from the flooded area. This emblematic example best illustrates the potential added value of reference images, as they enable the *a priori* identification of the majority of smooth areas.

Similarly, other wide flat regions, such as parking lots and airfields, are recognizable in the reference image. For instance, the region labeled R1 corresponds to a large parking lot composed of three parts. M2b completely removes one of them from the flood extent map, while the two other parts are significantly reduced in size. The sub-optimal performance of M2b is arguably due to a difference in the number and placement of vehicles at the time of the two satellite overpasses. In very high resolution SAR imagery the presence or not of an object like a car inevitably impacts the radar response. This necessarily influences the capability of the M2b algorithm to reliably identify areas of smooth tarmac and unfortunately may not be resolvable at all, for obvious reasons.

The region labeled R2, an area both flat and made of tarmac but not used as a parking space, shows the capability of M2b to avoid the typical misclassifications of smooth areas as flooded.

Finally, the thematic analysis confirms the algorithm's ability for identifying permanent water bodies. The permanently flooded bed of the River Avon and some adjacent boat marinas are removed from the flood extent map when taking into account the reference image: this becomes evident when looking at the areas of overdetection in the panels (b) and (c) of Fig. 6. Clearly, this result is not achievable with a single flood image, as M1 would invariably classify permanent water bodies as flooded (see panel (a) of Fig. 6).

Despite the previously mentioned ability of M2b to detect areas with permanent low backscatter values, there are still some shadow-affected areas that are erroneously classified as "flooded." A typical example is a large inclined rooftop in region R9. This is classified as "flooded" by all three methods due to the fact that one side is not "visible" to the SAR sensor. Other examples of this behavior can be found on various inclined rooftops in the R7 region.

To summarize, some risk of overdetecting flooded areas in built-up environments inevitably remains. Non-flooded areas that appear smooth and water-surface like at radar wavelengths as well as areas unseen by the satellite because of the side-looking nature of SAR systematically produce very low signal returns and are not easily distinguishable from flooded areas. The results of this study suggest that taking into account the baseline backscatter values from "dry" reference images partly addresses the problem. Wide, open areas of tarmac or concrete (roads, parking lots, airfields, etc.) can be identified and removed from the final flood map (or, alternatively, categorized as areas impossible to classify), while the situation is more problematic with shadow areas. To check the plausibility of both types of regions to be flooded, we expect that the use of high-resolution high-precision DEM data may be helpful. More research on the integration of additional data sources into the image-processing algorithm is needed for this to provide significant advantages.

2) The Problem of Underdetection: With respect to the problem of underdetecting the true flood extent using SAR observations, the results shown in Table II indicate that method M2b leads to a decrease in performance. In fact, the percentage of underdetected flood pixels rises from 15.6% obtained with the initial M2a method to its M2b-related value of 16.2%. The increase in underdetection between M2a and M2b is mainly due to the fact that the optimized value of RG% is lower than the *a priori* one. However, it has to be underlined that this type of error is generally to be found on the edge of inundated fields or in the vicinity of the main riverbed with tall vegetation surrounding the areas. While the algorithm accurately retrieves most of the flooded areas in wide, open areas, it can be observed that it systematically fails to retrieve flooding under the vegetation canopy. These errors are not related to the image-processing algorithm; rather they are due to the fact that with X-band radar systems volume scattering originating from the vegetation canopy causes increased signal return. Furthermore, as already mentioned in Section III-B, it cannot be ruled out that the validation flood extent itself is affected by a slight overestimation, as it was acquired closer to peak discharge than the satellite images. This could also at least partly explain the underdetection documented in the contingency matrix. Also, the uncertainties in the delineation of the flood validation extent from aerial photography are expected to have some marginal effect.

For example, an important area of apparent underdetection is the triangular shaped field labeled R15. However, due to the time difference between the acquisitions of aerial photographs satellite imagery, it is likely that most of the floodwater was drained from the field in the 19 h preceding the TerraSAR-X acquisition. This hypothesis is confirmed by hydraulic model simulations [see Fig. 3(b)].

The roughening of water surfaces due to wind is another inherent and potentially significant limitation of the algorithm proposed in this study. When there are regular waves on the surface of the water, Bragg resonance can result in very high signal returns [25]. The misclassification of the area labeled R18 as non-flooded represents a typical example. From the air photos and model simulations, there can be no doubt about the flooding of the area. However, waves are clearly identifiable on the standing water. This renders accurate flood detection extremely difficult (if not impossible), as it violates the algorithm's main underlying assumption of flooded areas behaving as specular reflectors.

V. Conclusion and Perspectives

This study proposes a promising methodology that is shown to be capable of providing satisfactory results in mapping, in a completely unsupervised way, flood extent in a challenging case study, such as an urban flooding.

A. New Findings and Conclusion

The proposed algorithm is based on the calibration of a PDF on the backscatter values associated with "open water." Next, a sequence of optimized backscatter thresholding, region growing, and CD is applied on the flood image and a pre- or postflood reference image acquired with the same imaging characteristics. Since no manual (and subjective) input is required from the end user, the algorithm enables automated, objective, and repeatable flood detection. It operates with minimum data requirements, considering as input data a flood image and a reference image acquired before or after the flooding, also maintaining the option of functioning with only a crisis image. The algorithm is efficient in both the two fully automated versions (M1 and M2b), as the processing time on an Intel(R) Core (TM) 2Quad CPU, 2.66 Ghz, and 3.24 GB RAM for a study area of 1135x998 pixels is less than 30 min. With a classification accuracy of around 82%, the algorithm yielded satisfactory results with respect to aerial photography-derived flooded areas in an urban case study. Since the classification accuracies of the proposed methods are comparable to those obtained by [11], it could be argued that the main part of the 18% of the remaining misclassification can be imputed to limitations of the SAR imaging technique.

The difficulty of detecting flooded areas in a built-up environment has been partially addressed by a CD approach that makes use of pre- or postflood reference images available in the data archives of satellite data providers. In particular, the shadow effect stemming from man-made structures can be taken into account through a mask of permanent water surface-like radar response areas. This approach overcomes the need of a high-resolution DEM and a SAR simulator for determining shadow regions that are not visible to the satellite. On the other hand, it requires a reference image with the same imaging characteristics as the flood image. While the number of suitable candidate images can be very limited in case of relatively new satellites, such as TerraSAR-X, it is important to note that image archives are gradually being built up, which will progressively increase the likelihood of finding adequate reference images in the online archives.

B. Future Research

Some further improvements are still necessary before the deployment of a fully automated SAR-based flood delineation

algorithm operating in a near-real time can be envisaged. Our results indicate that in spite of the high-resolution SAR imagery used in this study, the detection of flooding in built-up environments remains a very challenging task. To further improve the method, we aim at taking advantage of topographic and land use data, which are now becoming more readily available at global scale, albeit with variable accuracy and resolution. We hypothesize that such ancillary data will help reduce the elevation curvature along the flood edges as argued by [11] and identify parts of the underdetection caused by emerging objects such as trees or buildings. In addition, future research should investigate the usefulness of alternative distribution functions for optimally fitting the distribution of backscatter values corresponding to "open water" over different study areas.

We consider this study to be timely because there is a clear need for rapidly acquiring, processing, and distributing hydrology-related information derived from SAR imagery. In a crisis management context, where the situation on the ground can change very fast, data are more valuable if available shortly after the acquisition. The lag time between satellite acquisition and availability of information for efficient data assimilation can be variable from hours, in case of basins with small contributing areas and low response times, to days for much larger catchments. In fact, for near real-time applications in hydrology, where flood extent data is systematically assimilated into hydrologic-hydraulic models, the value of remote-sensing data is much higher if rapidly accessible [26], [27].

APPENDIX
OBTAINING THE CODE

The flood-mapping code here described is a science tool developed by a team of researchers, and we are happy to provide a copy of it for non-commercial studies. The code is reasonably well documented and has been tested in different case studies; however, it has not been through the same quality control procedure you would expect for a commercial software package. Using the code also requires some basic computing expertise. If you would like to obtain a copy of the code or are interested in collaborative research, then please contact us at one of the following addresses: giustari@lippmann.lu, hostache@lipmman.lu, matgen@lippmann.lu

ACKNOWLEDGMENT

The authors wish to thank the Environment Agency of England and Wales for the aerial photography of the Tewkesbury flood and the UK Meteorological Office for granting access to the NERC BADC for the rainfall records used in the analysis. The TerraSAR-X flood image was received under DLR SSS project HYD0363.

REFERENCES

[1] D. E. Alsdorf, E. Rodriguez, and D. P. L. Lettenmaier, "Measuring surface water from space," *Rev. Geophys.*, vol. 45, p. RG2 002, May 2007.

[2] W. A. Marcus and M. A. Fonstad, "Optical remote mapping of rivers at sub-meter resolutions and watershed extents," *Earth Surf. Process. Landforms*, vol. 33, no. 1, pp. 4–24, Jan. 2008.

[3] G. Schumann, P. D. Bates, M. S. Horritt, P. Matgen, and F. Pappenberger, "Progress in integration of remote sensing-derived flood extent and stage data and hydraulic models," *Rev. Geophys.*, vol. 47, p. RG4 001, Nov. 2009.

[4] G. Nico, M. Pappalepore, G. Pasquariello, S. Refice, and S. Samarelli, "Comparison of SAR amplitude vs. coherence flood detection methods—A GIS application," *Int. J. Remote Sens.*, vol. 21, no. 8, pp. 1619–1631, 2000.

[5] M. Chini, L. Pulvirenti, and N. Pierdicca, "Analysis and interpretation of the COSMO-SkyMed observations of the 2011 Japan tsunami," *IEEE Geosci. Remote Sens. Lett.*, vol. 9, no. 3, pp. 467–471, May 2012.

[6] N. Longbotham, F. Pacifici, T. Glenn, A. Zare, M. Volpi, D. Tuia, E. Christophe, J. Michel, J. Inglada, J. Chanussot, and Q. Du, "Multi-modal change detection, application to the detection of flooded areas: Outcome of the 2009-2010 data fusion contest," *IEEE J. Sel. Topics Appl. Earth Observ. Remote Sens.*, vol. 5, no. 1, pp. 331–342, Feb. 2012.

[7] P. Matgen, R. Hostache, G. Schumann, L. Pfister, L. Hoffmann, and H. H. G. Savenije, "Towards an automatic SAR-based flood monitoring system. lessons learned from two case studies," *Phys. Chem. Earth*, vol. 36, no. 7/8, pp. 241–252, 2011.

[8] S. Martinis, A. Twele, and S. Voigt, "Towards operational near real-time flood detection using a split-based automatic thresholding procedure on high resolution TerraSAR-X data," *Nat. Hazards Earth Syst. Sci.*, vol. 9, no. 2, pp. 303–314, Mar. 2009.

[9] S. Martinis, A. Twele, and S. Voigt, "Unsupervised extraction of flood-induced backscatter changes in SAR data using Markov image modeling on irregular graphs," *IEEE Trans. Geosci. Remote Sens.*, vol. 49, no. 1, pp. 251–263, Jan. 2011.

[10] L. Pulvirenti, N. Pierdicca, M. Chini, and L. Guerriero, "An algorithm for operational flood mapping from synthetic aperture radar (SAR) data using fuzzy logic," *Nat. Hazards Earth Syst. Sci.*, vol. 11, no. 2, pp. 529–540, Feb. 2011.

[11] D. C. Mason, R. Speck, B. Devereux, G. Schumann, J. Neal, and P. D. Bates, "Flood detection in urban areas using TerraSAR-X," *IEEE Trans. Geosci. Remote Sens.*, vol. 48, no. 2, pp. 882–894, Feb. 2010.

[12] R. Speck, P. Turchi, and H. Süß, "An end-to-end simulator for high resolution spaceborne SAR systems," in *Proc. SPIE Defense Security*, 2007, vol. 6568, p. 656 80H.

[13] D. C. Mason, I. J. Davenport, J. C. Neal, G. J.-P. Schumann, and P. D. Bates, "Near real-time flood detection in urban and rural areas using high resolution synthetic aperture radar images," *IEEE Trans. Geosci. Remote Sens.*, vol. 50, no. 8, pp. 3041–3052, Aug. 2012.

[14] F. Ulaby, R. Moore, and A. Fung, *Microwave Remote Sensing, Active and Passive: Volume Scattering and Emission Theory, Advances System and Applications*. Norwood, MA: Artech House, 1986.

[15] T. Eltoft, "The Rician inverse Gaussian distribution: A new model for non-Rayleigh signal amplitude statistic," *IEEE Trans. Image Process.*, vol. 14, no. 11, pp. 1722–1735, Nov. 2005.

[16] G. A. F. Seber and C. J. Wild, *Nonlinear Regression*. Berlin, Germany: Wiley, 2003.

[17] R. M. Haralick and L. G. Shapiro, "Image segmentation techniques," *Comput. Vis. Graph. Image Process.*, vol. 29, no. 1, pp. 100–132, Jan. 1985.

[18] R. Hostache, P. Matgen, and W. Wagner, "Change detection approaches to flood extent mapping: How to select the best pre-flood reference image from on-line archives?" *J. Appl. Earth Observation Geoinf.*, vol. 19, pp. 205–213, 2012.

[19] E. Agency, Review of 2007 summer floods, Environment Agency, Bristol, U.K. [Online]. Available: http://publications.environment-agency.gov.uk/PDF/GEHO1107BNMI-E-E.pdf

[20] G. J.-P. Schumann, J. C. Neal, D. C. Mason, and P. D. Bates, "The accuracy of sequential aerial photography and SAR data for observing urban flood dynamics, a case study of the UK summer 2007 floods," *Remote Sens. Environ.*, vol. 115, no. 10, pp. 2536–2546, Oct. 2011.

[21] A. Lopès, E. Nezry, R. Touzi, and H. Laur, "Structure detection and statistical adaptive speckle filtering in SAR images," *Int. J. Remote Sens.*, vol. 14, no. 9, pp. 1735–1758, 1993.

[22] H. Zwenzner and S. Voigt, "Improved estimation of flood parameters by combining space based SAR data with very high resolution digital elevation data," *Hydrol. Earth Syst. Sci.*, vol. 13, no. 5, pp. 567–576, May 2009.

[23] J. C. Neal, G. Schumann, T. Fewtrell, M. Budimir, P. D. Bates, and D. C. Mason, "Evaluating a new LISFLOOD-FP formulation with data from the summer 2007 flood in Tewkesbury, UK," *J. Flood Risk Manage.*, vol. 4, no. 2, pp. 88–95, Jun. 2011.

[24] E. Malnes, S. Solbo, I. Lauknes, G. J. Evertsen, T. A. Tllefsen, I. Solheim, and M. Indregard, "Floodman-global near real-time flood monitoring for hydrological users," in *Proc. Int. Conf. Innov., Adv. Implement. Flood Forecast. Technol.*, 2005, vol. 4, pp. 1–9.
[25] D. O'Grady, M. Leblanc, and D. Gillieson, "Use of ENVISAT ASAR global monitoring mode to complement optical data in the mapping of rapid broad-scale flooding in Pakistan," *Hydrol. Earth Syst. Sci.*, vol. 15, no. 11, pp. 3475–3494, Nov. 2011.
[26] P. Matgen, M. Montanari, R. Hostache, L. Pfister, L. Hoffmann, D. Plaza, V. R. N. Pauwels, G. J. M. D. Lannoy, R. D. Keyser, and H. H. G. Savenije, "Towards the sequential assimilation of SAR-derived water stages into hydraulic models using the particle filter: Proof of concept," *Hydrol. Earth Syst. Sci.*, vol. 14, no. 9, pp. 1773–1785, Sep. 2010.
[27] L. Giustarini, P. Matgen, R. Hostache, D. Plaza, V. R. N. Pauwels, G. J. M. D. Lannoy, R. D. Keyser, L. Pfister, L. Hoffmann, and H. H. G. Savenije, "Assimilating SAR-derived water level data into a flood model: A case study," *Hydrol. Earth Syst. Sci.*, vol. 15, no. 7, pp. 2349–2365, Jul. 2011.

Laura Giustarini received the B.Sc. and M.Sc. degrees in environmental engineering from the University of Perugia, Perugia, Italy, in 2003 and 2006, respectively.

She has worked for the National Research Council, Research Institute for Geo-Hydrologicl Protection, Perugia, Italy. Since 2010, she has been with the Department of Environment and Agro-Biotechnologies, Public Research Center - Gabriel Lippman, Belvaux, Luxembourg. Her current research interests are the integration, through data assimilation techniques, of radar remote sensing into coupled hydrologic and hydraulic models for surface water management.

Renaud Hostache received the Engineering degree in hydraulics and environmental sciences from Grenoble Institute of Technology-National School of Hydraulics and Mechanism of Grenoble, the M.Sc. degree in mechanics of geophysical media and environment from the Joseph Fourier University, Grenoble, France, in 2003, and the Ph.D. degree in water sciences from the National School of Agriculture, Water, and Forest Engineering, Montepellier, in 2006. During the Ph.D. work at the Cemagref, Montepellier, France, he investigated the fine 3-D characterization of flood hazard, through satellite imagery and its integration in flood inundation models.

Since 2007, he has been with the Department of Environment and Agro-Biotechnologies, Public Research Center - Gabriel Lippman, Belvaux, Luxembourg. His research interests are focused on the integration of remote-sensing observations in hydraulic models and on the hydrologic and hydraulic model uncertainty characterization and reduction.

Patrick Matgen received the M.Sc. degree in environmental engineering from the Ecole Polytechnique Fédérale de Lausanne, Lausanne, Switzerland. In 2011, he was awarded the Ph.D degree from the water resources section of the Technical University in Delft, The Netherlands, for his dissertation on the retrieval of surface and subsurface water from microwave remote-sensing observations and the integration of the data with flood prediction systems.

Currently, he holds the position of Project Leader responsible for microwave remote-sensing and hydrologic-hydraulic modeling projects at the Centre de Recherche Public - Gabriel Lippmann (Grand Duchy of Luxembourg).

Guy J.-P. Schumann (S'06–A'08–M'09) received the M.A. degree in geography and environmental science and the M.Sc. degree in remote-sensing image processing and applications from the University of Dundee, Dundee, U.K., in 2003 and 2005, respectively, and the Ph.D. degree in collaboration with the Public Research Centre - Gabriel Lippmann, Belvaux, Luxembourg, in 2008.

From August 2008 to March 2011, he was a Full-time Lecturer and Research Fellow in hydrology at the School of Geographical Sciences, University of Bristol, Bristol, UK: he currently is an Honorary Research Fellow at the same university. His research interests include flood hydrology and hydraulics and remote sensing in hydrology, in particular, radar remote sensing for flood hydrology and management.

Paul D. Bates received the Ph.D. degree from the University of Bristol, Bristol, U.K., in 1993, with support from a Natural Environmental Research Council studentship.

Subsequently, he has worked with the University of Bristol as a Postdoctoral Researcher and Lecturer and has been a Full Professor since 2003. Currently, he is the Director of the Hydrology Research Group with the School of Geographical Sciences, Bristol. He has been a Visiting Scientist with the Laboratoire National D'Hydraulique, Princeton University, Paris, and the European Union Joint Research Centre, Ispra, Italy. His research concerns the development and analysis of numerical models for predicting river flood flows, principally using data derived from remote-sensing sources. He has specific interests in spatial prediction, risk, and uncertainty.

Prof. Bates is the Editor-in-Chief of the International Journal of River Basin Management.

David C. Mason received the B.Sc. and Ph.D. degrees in physics from the University of London, London, U.K., in 1963 and 1968, respectively.

He has worked for the U.K. Medical Research Council and Plessey Electronic Systems Research. Since 1984, he has been with the Natural Environment Research Council Environmental Systems Science Center, University of Reading, Reading, U.K., carrying out research on the automated extraction of information from remotely sensed data and linking these data to environmental models. His current interests include using remotely sensed data for validation and parameterization of river flood models and assimilation into coastal orphodynamic models.

International Journal of Applied Earth Observation and Geoinformation 34 (2015) 70–77

Contents lists available at ScienceDirect

International Journal of Applied Earth Observation and Geoinformation

journal homepage: www.elsevier.com/locate/jag

Accounting for image uncertainty in SAR-based flood mapping

L. Giustarini[a,*], H. Vernieuwe[b], J. Verwaeren[b], M. Chini[a], R. Hostache[a], P. Matgen[a], N.E.C. Verhoest[c], B. De Baets[b]

[a] Centre de Recherche Public – Gabriel Lippmann, Belvaux, Luxembourg
[b] KERMIT, Department of Mathematical Modelling, Statistics and Bioinformatics, Ghent University, Coupure links 653, 9000 Gent, Belgium
[c] Laboratory of Hydrology and Water Management, Ghent University, Coupure links 653, 9000 Gent, Belgium

ARTICLE INFO

Article history:
Received 22 January 2014
Accepted 23 June 2014

Keywords:
Flood mapping
Speckle
Bootstrap
Synthetic aperture radar
Uncertainty

ABSTRACT

Operational flood mitigation and flood modeling activities benefit from a rapid and automated flood mapping procedure. A valuable information source for such a flood mapping procedure can be remote sensing synthetic aperture radar (SAR) data. In order to be reliable, an objective characterization of the uncertainty associated with the flood maps is required.

This work focuses on speckle uncertainty associated with the SAR data and introduces the use of a non-parametric bootstrap method to take into account this uncertainty on the resulting flood maps. From several synthetic images, constructed through bootstrapping the original image, flood maps are delineated. The accuracy of these flood maps is also evaluated w.r.t. an independent validation data set, obtaining, in the two test cases analyzed in this paper, *F*-values (*i.e.* values of the Jaccard coefficient) comprised between 0.50 and 0.65. This method is further compared to an image segmentation method for speckle analysis, with which similar results are obtained. The uncertainty analysis of the ensemble of bootstrapped synthetic images was found to be representative of image speckle, with the advantage that no segmentation and speckle estimations are required.

Furthermore, this work assesses to what extent the bootstrap ensemble size can be reduced while remaining representative of the original ensemble, as operational applications would clearly benefit from such reduced ensemble sizes.

Introduction and objective

Rapid flood mapping, together with uncertainty assessment and delivery of flood maps, are of considerable importance for response activity planning during emergencies and as a support for long-term risk management. Given its cloud penetrating and night/day operational capabilities and its skill in capturing the different scattering behavior between flooded and non-flooded areas (Pierdicca et al., 2013), synthetic aperture radar (SAR) constitutes a valuable source of information to provide flood maps. Such maps can then be used for the calibration or validation of hydraulic models (Di Baldassarre et al., 2009; Hostache et al., 2009; Montanari et al., 2009; Stephens et al., 2012; Mason et al., 2012; Schumann et al., 2014). Hydraulic information derived from flood maps, such as flood extents or water stages, can also be employed in a data assimilation (DA) framework in order to improve model predictions (Matgen et al., 2010; Hostache et al., 2010; Giustarini et al., 2011).

Flood maps derived from SAR observations are the result of image processing procedures. Given that there is no perfect procedure and no best practice on selecting one over another, the chosen mapping procedure may introduce errors or uncertainties in the retrieved flood map. Furthermore, SAR observations are susceptible to sources of uncertainty due to imaging characteristics (*e.g.* imaging modes, speckle, resolution) and ground perturbations (*e.g.* wind, trees, buildings masking water, terrain geometry). Therefore, it is important to assess the impact of these uncertainties on the final flood map. Without this information, model calibration/validation or DA activities could yield suboptimal results (Quaife et al., 2008).

In order to assess uncertainty in flood delineation methods, the few approaches proposed in literature employ an ensemble of flood maps (Schumann et al., 2008; Di Baldassarre et al., 2009). However, the number of ensemble members and the procedure to obtain the different ensemble members tend to be subjective. For example, Schumann et al. (2008) investigated uncertainty in SAR-derived water stages, for a single SAR image and a single flood mapping

* Corresponding author at: 41, rue du Brill, L-4422 Belvaux, Luxembourg. Tel.: +352 470261 479.
E-mail address: giustari@lippmann.lu (L. Giustarini).

http://dx.doi.org/10.1016/j.jag.2014.06.017
0303-2434/

procedure, identifying two main sources of uncertainty. The first one corresponds to the parameter value applied to classify a pixel as flooded (*i.e.* wet/dry classification threshold), whereas the second one stems from the geocoding of the image itself. They decided to test four different threshold values and fifty image geocodings, to obtain an ensemble of flood maps and corresponding SAR-derived water levels. In a second study, Di Baldassarre et al. (2009) considered uncertainty due to both the available SAR image and the applied procedure. They computed ten flood maps, combining two available SAR images, acquired at nearly the same time but having a different resolution, with five different flood mapping procedures. These case studies show that it is important, yet not trivial, to correctly and objectively quantify uncertainty in flood mapping. In flood mapping, uncertainty principally stems from the image input to the algorithm and from the algorithm itself.

The flood mapping procedure (Giustarini et al., 2013) employed in this paper, deterministically fits its parameter values to a given SAR image. The uncertainty we focus on stems from image uncertainty, which is propagated through the flood mapping procedure.

SAR image uncertainty is mainly due to speckle, leading to random changes in the pixel's brightness and usually hampering decision making on a pixel basis (Oliver and Quegan, 1998). This phenomenon occurs where distributed targets are imaged and the pixel is therefore representative of the contributions coming from many scatterers with random phase. These contributions cause interference and result in speckle. In an amplitude or intensity image, speckle appears as a noise-like multiplicative modulation of backscatter. As a consequence, the individual value of a pixel represents a rather inaccurate measurement of its true backscatter. In order to account for speckle in uncertainty analysis, each pixel can be characterized by its speckle distribution, which is different for each particular land cover class. This speckle characterization can be accomplished with speckle reconstruction techniques (Frost et al., 1982; Durand et al., 1987; Lee et al., 2009), which try to approximate the backscatter over the entire image, or with segmentation methods, which hypothesize the presence of structures in the image and are potentially powerful techniques for extracting information from SAR images (Lee and Jurkevich, 1989; Horritt, 1999; Zhang et al., 2008; Sui et al., 2012). These latter methods assume that the image is composed of relatively homogeneous regions, whereas adjacent regions are separated by edges corresponding to changes in some local statistic, such as mean brightness or texture (Caves et al., 1998). The assumption of a uniform backscatter within each segment is useful to extract speckle from the given image by first segmenting the image into uniform regions and by then extracting the speckle distribution of each region.

In this work, differently from already published methods, a non-parametric bootstrap method is proposed to account for the influence of speckle. Bootstrap methods (Efron, 1979; Efron and Tibshirani, 1993) belong to the class of resampling methods in which multiple new samples are drawn from the data sample at hand in order to estimate a statistical unknown population parameter. Resampling methods are generally used when it is not straightforward to use the classical statistical methods in the estimation of the parameter, for instance, when one disposes of a small data set. In this work, only one SAR image is available, which can be regarded as a set of pixels that represents the best guess about the population from which the image was formed. A first advantage of the proposed bootstrap method is that it is fully automatic, in the sense that it does not require specific knowledge on image processing, in contrast to, *e.g.* segmentation methods. Moreover, while image segmentation could result in a rather time-consuming process, particularly for large images, the proposed method should be rather independent of the image size in terms of process time. Eventually, since the bootstrap method can result in a large set of bootstrap data sets, we also assess the smallest appropriate number of data sets needed to still adequately describe the uncertainty in the flood maps due to speckle.

Methodology

Flood mapping procedure

In this work, the flood mapping procedure described in Giustarini et al. (2013) and based on Matgen et al. (2011) is applied for flood delineation. It is a hybrid procedure combining backscatter thresholding, region growing and change detection w.r.t. an available reference image. The procedure assumes that the histogram of backscatter values in a SAR flood image can be modeled as two partially overlapping histograms: one histogram derived from the backscatter values representing "open water" in the image and the other one from the backscatter values representing the non-flooded areas (Ulaby et al., 1986). The flood mapping method is based on fitting a scaled gamma curve to the backscatter values that represent "open water" in the flood image:

$$f(\sigma^0; k, \sigma_m^0) \frac{(\sigma^0 - \sigma_1^0)^{k-1}}{((\sigma_m^0 - \sigma_1^0)/(k-1))^k \Gamma(k)} \exp\left(-\frac{(\sigma^0 - \sigma_1^0)(k-1)}{\sigma_m^0 - \sigma_1^0}\right) \quad (1)$$

where k is the shape parameter of the scaled gamma curve, σ^0 is the backscatter value of a pixel in the SAR image, σ_m^0 is the mode of the scaled gamma curve and σ_1^0 is the minimum backscatter value in the SAR image, applied so that the curve only takes positive values. Next, a sequence of three steps, optimized backscatter thresholding, region growing, and change detection, is applied on the flood image and on a pre- or post-flood reference image with the same imaging characteristics (track, orbit, polarization, acquisition mode). In the first step, based on the fitted curve, a backscatter threshold parameter σ_{thr}^0 is determined, and the flooded area is extracted by selecting the pixels with a backscatter value lower than σ_{thr}^0. Concerning the second step, the region growing parameter σ_{rg}^0 is the one on whose basis pixels in the vicinity of the water bodies are included in the flood area. The change detection parameter $\Delta\sigma^0$ is defined as the required minimum change in backscatter between the reference and the flood image for a pixel being retained as flooded. The second and the third step, *i.e.* region growing and change detection, are simultaneously and iteratively performed. This means that several different σ_{rg}^0 values are sequentially tested and a corresponding $\Delta\sigma^0$ is optimized for each tested σ_{rg}^0 value. At the end of each iteration, the histogram of "open water" pixels is computed and it is compared with the initially calibrated theoretical gamma curve. The parameter set $(\sigma_{rg}^0, \Delta\sigma^0)$ providing the lowest RMSE value, computed between the histogram of "open water" pixels and the theoretical gamma curve, is set as optimal.

Since no manual and subjective input is required from the end user, the procedure enables automated, objective and repeatable flood detection. The parameters, σ_m^0 and σ_{thr}^0 only depend on the histogram shape and the gamma curve optimized on it, whereas σ_{rg}^0 and $\Delta\sigma^0$ also depend on the geographical patterns in the SAR image.

The flood mapping procedure automatically optimizes its parameters in a deterministic way for a couple of given input SAR images. However, the uncertainty stemming from the image acquisition process, affecting the actual images used as input to the flood mapping procedure, influences the parameter values. In order to take into account this uncertainty and its effect on the pixel histogram and flood mapping classification accuracy, several synthetic flood images are generated and provided as input for the procedure itself. It has to be noted that only for the flood image, synthetic images are generated, whereas the reference image is

kept unchanged. Synthetic flood images are obtained with two different approaches: image segmentation and the non-parametric bootstrap method.

Image segmentation method

The objective of image segmentation is to produce a set of non-overlapping homogeneous regions, requiring that the union of two adjacent regions should be heterogeneous (Pal and Pal, 1993; Fu and Mui, 1981). This method has also been fruitfully used to cope with SAR speckle (Lee and Jurkevich, 1989; Zhang et al., 2008; Pulvirenti et al., 2011), which is a multiplicative noise-like phenomenon, preventing the direct retrieval of the backscatter per pixel. The segmentation of a SAR image helps to identify regions corresponding to different land cover classes such as fields, urban area, water bodies and so on. Thus, the hypothesis of the segmentation method is that the entire image is composed of relatively uniform backscatter regions, showing local changes at their borders. In contrast to filtering approaches, segmentation does not try to reconstruct the backscatter value of each pixel, but focuses on the explicit description of image structures (Caves et al., 1998). Therefore, in the segmentation method there is no need to determine in advance the speckle models, a task that could even be unfeasible in the case of non-completely developed speckle. As can be the case with high resolution SAR data, the number of scatterers per pixel is then limited, leading to the fact that the speckle appears with wide spatially correlated patterns depending on the scene geometry (Quartulli and Datcu, 2004). Setting a speckle model for filtering such imagery is then a rather difficult task.

Using the segmentation method, each region can be decomposed into its mean backscatter value and its speckle distribution, computed as the empirical distribution of the residuals between the mean backscatter value of the region and the backscatter value of each pixel inside the specific region (Oliver and Quegan, 1998). Based on the aforementioned considerations, the segmentation method can be profitably used to generate a set of synthetic speckle-dependent flood images, where each pixel is the sum of two terms, the mean backscatter value of the segment and a random speckle value, sampled from its segment speckle distribution. Thus, each synthetic flood image can be used as input to the flood mapping procedure, together with the unchanged reference image, to compute the associated flood map, with its corresponding classification accuracy. In this work, 1000 synthetic flood images and hence 1000 flood maps were generated.

In order to produce a map of homogeneous regions, we adopted the segmentation method of Pulvirenti et al. (2011), which is basically composed of two main steps. In the first step, the input space (see further) is clustered by the *K*-means algorithm (Duda and Hart, 1973; Haralick and Dinstein, 1975), while in the second step, the map showing the clusters is transformed into a segmented map, through segmenting each cluster into many connected regions, considering eight neighbors in the connectivity rule (Pulvirenti et al., 2011, 2013). In order to efficiently perform the clustering, the input features should describe several characteristics of SAR images. Different land cover classes have their own unique geometric structures, roughness, soil moisture levels and so on, resulting in different brightness and textures. However, one single feature, as in our case the backscatter values of a single SAR image, cannot describe in sufficient detail different regions and objects in a SAR image. Therefore, it is useful to add other pieces of information, *i.e.* contextual features, to improve the performance of SAR image segmentation (Dekker, 2003; Yu et al., 2013). In our work, the second order spatial statistical parameters (Haralick et al., 1973; Haralick, 1979) have been added in this respect as input to the clustering algorithm. The resulting input space is thus composed of 4 features: the SAR backscatter values and the three most effective second order statistical parameters, *i.e.* homogeneity, contrast and dissimilarity (Baraldi and Parmiggiani, 1995; Pacifici et al., 2009).

These statistical parameters have been computed using a 5×5 moving window, and a horizontal and vertical shift of one pixel. The size of the moving window and the shift parameter have been selected based on results recently published in Pierdicca et al. (in press). Additional tests have been performed with different values of these parameters. The evaluation of the corresponding performance is carried out in the first step of the segmentation procedure (*i.e.* clustering), based on the Jeffries–Matusita (J-M) distance, such that values that maximize the spectral cluster separability are selected. Indeed, the J-M distance has been calculated for each spectral cluster w.r.t. all the others: it provides information on separability between two classes and takes values in the interval [0,2), according to Richards and Jia (1999). Values close to 2 indicate a higher degree of separability, while those close to 0 a lower one.

Non-parametric bootstrap method

The non-parametric bootstrap method (Efron, 1979; Efron and Tibshirani, 1993) belongs to the class of resampling methods. It is based on the idea that the sample itself, *i.e.* the entire set of pixel values in the image, offers the best guess about the population from which the sample was taken. The bootstrap method, in which bootstrap replicas of an original data set are generated, has already been applied in a similar optimization problem in remote sensing, *i.e.* the estimation of aboveground biomass (Carreiras et al., 2012). The application of the bootstrap method as a possible way to account for speckle stems from the idea that speckle is present in the entire image. Therefore, resampling the image could globally take into account speckle, with the advantage of not having to segment the image into uniformly textured regions. In the non-parametric bootstrap method, the entire initial data set of n observations (where n is the total number of pixel values within the image) is first randomly sampled with replacement. The result is a bootstrap data set of n resampled observations. A pixel histogram can be computed for each bootstrap data set, in order to assess the effect of image uncertainty on the histogram itself. The bootstrap data set is a vector of resampled pixels values, where geographical patterns are lost. Therefore, to create a synthetic flood image preserving geographic pattern, the pixels of the original image and the bootstrap data set are first ordered according to their backscatter value. Second, a synthetic flood image is created by replacing the pixels of the original image with the pixels having the same rank in the ordered bootstrap data set. In other words, the smallest backscatter value in the bootstrap data set is positioned in the same location as the smallest backscatter value in the original image, and so on. The flood mapping procedure is applied on this synthetic flood image, together with the unchanged reference image, to compute the associated flood map with its corresponding classification accuracy. These steps are repeated m times (according to Efron and Tibshirani (1993) m should be between 1000 and 2000. We chose $m = 1000$) in order to obtain an estimate of the bootstrap distribution of the respective values of interest, *e.g.* the classification accuracy.

This bootstrap distribution consists of 1000 values, corresponding to 1000 bootstrap data sets or 1000 synthetic flood images, leading to a high computational cost when flood maps should be delineated for each of these images. This would be rather inefficient, particularly in near real time applications. Therefore, it is essential to identify the smallest size m for the ensemble of bootstrap data sets that is still capable of maintaining the representation of the uncertainty as given by the entire estimate of the bootstrap distribution. In this way, the full distribution of 1000 values would no longer be necessary. To this end, different ensembles with sizes $k = 10, 20, \ldots, 100, 200, \ldots, 1000$ are repeatedly (1000 times for each tested ensemble size k) drawn with replacement from the

Table 1
Characteristics of the images for the summer flood event in 2007.

Image	Date and time of acquisition	Image type	Pixel size (m)	Ground resolution (m)	Band	Polarization
Flood	Jul 23 2007 10:27 am	ENVISAT ASAR WSM	75	150	C	VV
Reference	Oct 01 2007 10:25 am	ENVISAT ASAR WSM	75	150	C	VV
Flood	Jul 25 2007 6:34 am	TerraSAR-X Stripmap	1.5	3	X	HH
Reference	Jul 22 2008 6:34am	TerraSAR-X Stripmap	1.5	3	X	HH

entire bootstrap distribution. For each ensemble size, the standard deviations, both on the mean and on the standard deviation of the accuracies of the ensemble members, are computed. On the basis of these results, it is possible to identify the smallest ensemble size that is still meaningful and representative for the entire bootstrap distribution, and applicable for further use.

Case studies and available data

The proposed procedure has been tested on the July 2007 flood event in the Tewkesbury region (UK), which was observed by two different SAR sensors, providing images with different characteristics. The study data set is composed of the following couples of satellite images: two ENVISAT ASAR Wide Swath images and two StripMap TerraSAR-X images, whose characteristics are listed in Table 1.

As displayed in Fig. 1, the chosen area of interest (AOI) for the ENVISAT image corresponds to a large area (~730 km^2), with 303 × 649 pixels (n = 196,647) having a pixel size of 75 m × 75 m. For the high-resolution TerraSAR-X image, the selected AOI corresponds to the city of Tewkesbury (~3 km^2), with 1335 × 998 pixels (n = 1,332,330) having a pixels size of 1.5 m × 1.5 m. In order to evaluate the classification accuracy of the flood maps derived on the basis of each couple of SAR images, a validation data set is available, composed of very high-resolution 0.2 m aerial photographs, acquired during the flood event on July 24 at 11:30 am. The observed flood extent was delineated in the form of a binary flooded/non-flooded map through manual photo-interpretation (see in Fig. 1), such that a validation flood map is obtained. This validation map is compared to those obtained as output of the flood mapping procedure, using the Jaccard coefficient (Jaccard, 1908; see also De Baets et al., 2001) as a measure of the classification accuracy (denoted F by Horritt et al. (2007)):

$$F = \frac{A}{A + B + C} \tag{2}$$

where A is the number of pixels of the flooded area correctly predicted by the model, B is the number of pixels predicted as flooded that are observed to be non-flooded (over-prediction) and C is the

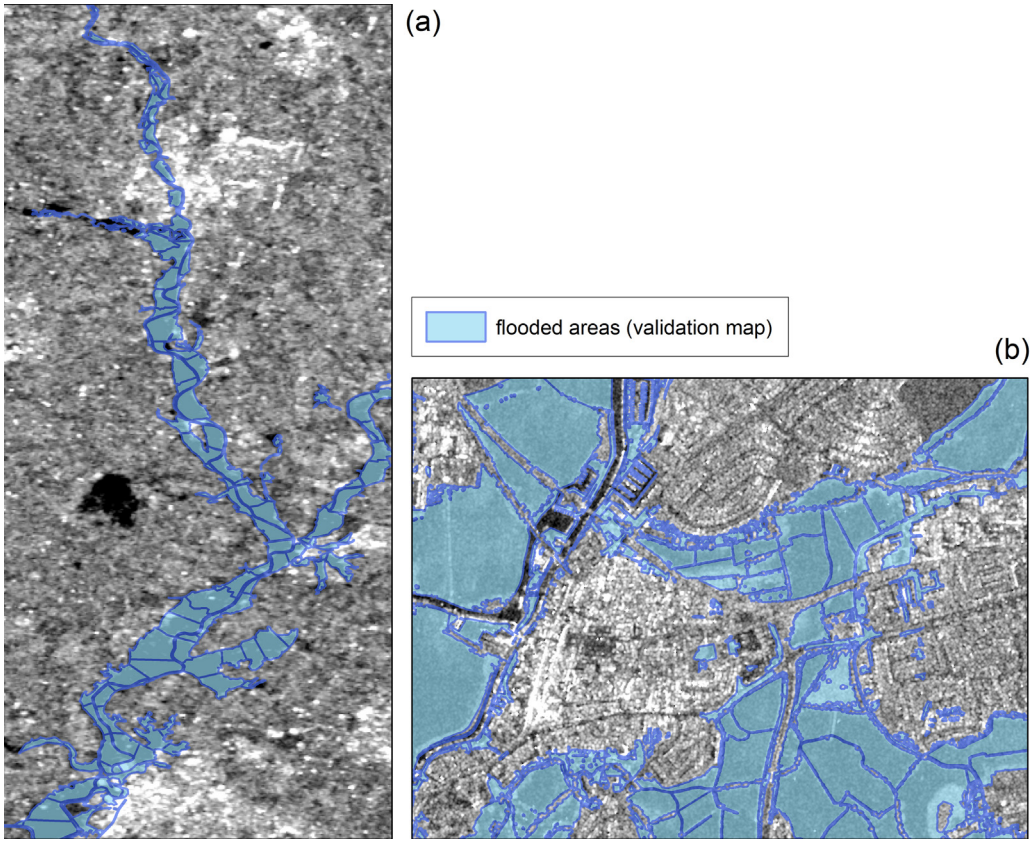

Fig. 1. Study site, showing the larger area of interest (AOI) of the couple of ENVISAT images (a) and the smaller AOI, centered on the city of Tewkesbury, of the TerraSAR-X images (b). The validation map is obtained from high-resolution aerial photos through manual delineation.

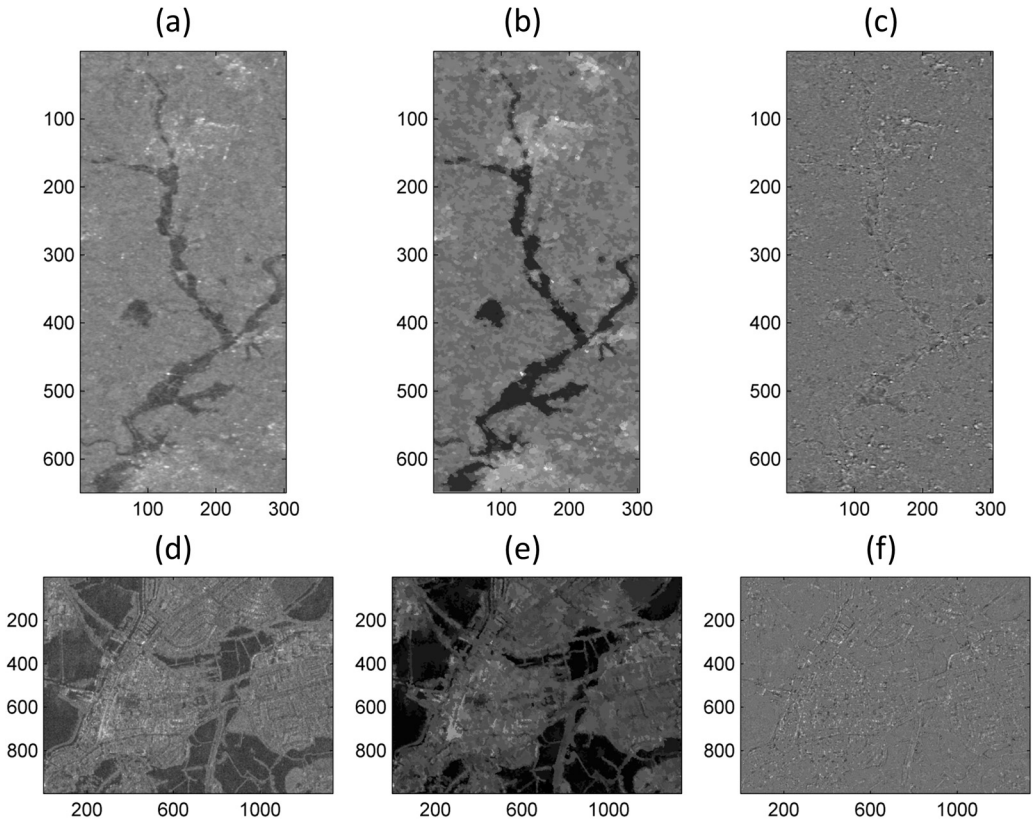

Fig. 2. Original SAR images (a and d), mean backscatter values in the segmented images (b and e) and speckle residuals (c and f), for the ENVISAT flood image and the TerraSAR-X flood image.

number of pixels that are predicted as non-flooded and yet are observed to be flooded. *F* ranges from 0 to 1, where 1 represents perfect classification. It has to be pointed out that the flood mapping procedure classifies the entire AOI, however, in the evaluation we only focus on the flooded area and its surroundings through excluding the pixels that are correctly classified as non-flooded (Horritt et al., 2007).

Results and discussion

Analysis of the segmentation method

The final maps resulting from the entire segmentation method are shown in Fig. 2. This figure shows the original SAR images ((a) and (d)), the segmented images or the map/image with the mean backscatter value of each segment ((b) and (e)), and the speckle maps/images ((c) and (f)), obtained by subtracting the second from the first one. A visual inspection of the results shows that the segmented images, (b) and (e), still contain all the well-defined structures that are also present in the original images, (a) and (d). To evaluate the performance of the segmentation method, it is verified whether the defined segments correspond to homogeneous regions in space, *i.e.* whether the statistics of backscatter values within a segment are similar to that of a fully developed speckle. To this aim, it is essential to check the speckle maps, which in case of a successful segmentation should not contain any structure or spatial pattern associated to the scene (Oliver and Quegan, 1998). As shown in Fig. 2(c) and (f), a very limited number of objects is still partly detectable in the images of speckle residuals.

Comparison of both methods

Each of the above described methods, *i.e.* both the image segmentation method and the non-parametric bootstrap method, results in 1000 synthetic flood images. In order to investigate whether both methods yield similar results, one could employ a statistical test that compares the obtained image histograms. However, to our knowledge, no statistical test exists that allows comparing two groups of 1000 image histograms. Nevertheless, a visual inspection of the panels in Fig. 3 indicates the similarity for the mean, maximum and minimum values in each histogram bin, for the ENVISAT and the TerraSAR-X images.

The similarity in the image histograms, as derived by bootstrap or by segmentation, is reflected in similar values of the procedure's parameters, σ_m^0 and σ_{thr}^0, those that only depend on the histogram shape and the gamma curve optimized on it. The results are not shown here, as the main issue of the paper does not concern the analysis of the specific parameters of the flood mapping procedure. On the other hand, a conclusion can be drawn on the fact that speckle, as modeled by the bootstrap or by the segmentation method, has an extremely similar effect on the method's parameters.

Subsequently, the flood mapping procedure was applied on the synthetic flood images, given as input to the flood mapping algorithm, together with the unchanged reference image. Since validation data are available in this case study, the *F*-values (cfr. Eq. (2)) that reflect the classification accuracy, can be computed. Table 2 lists the obtained ranges of *F*-values for the synthetic flood images obtained by both methods. This table shows that both methods yield comparable *F*-values, although the ranges of *F*-values obtained with the two methods on the TerraSAR-X flood image

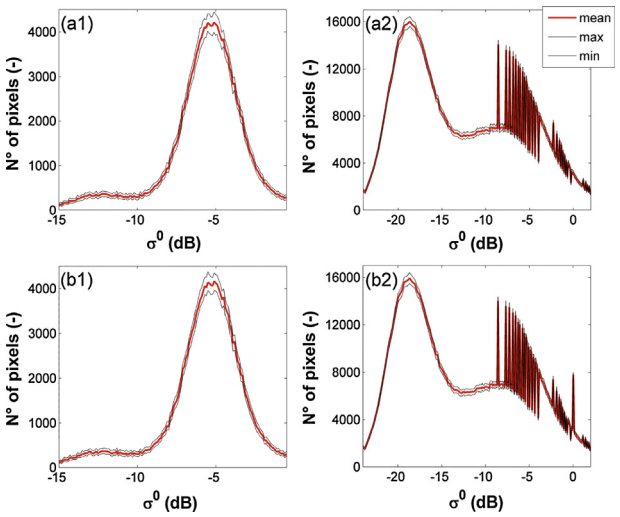

Fig. 3. Mean, maximum and minimum values for each bin of the 1000 histograms after application of the bootstrap method (top panels) and segmentation method (bottom panels) on the original ENVISAT (a1 and b1) and TerraSAR-X (a2 and b2) flood images.

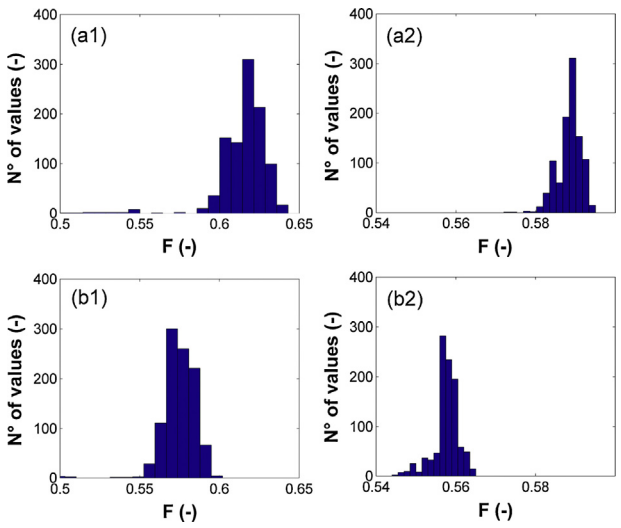

Fig. 4. Histograms of the *F*-values of the flood maps obtained after application of the flood mapping procedure on the synthetic images generated by applying the bootstrap (top panels) or the segmentation method (bottom panels) on the original ENVISAT (a1 and b1) and TerraSAR-X (a2 and b2) flood images.

do not overlap. The matching in terms of flood mapping accuracy shows that the ranking step in the bootstrap method compensates for the loss of geographical patterns due to bootstrapping the image pixel values. The obtained *F*-values denote that misclassifications are still present, which can be addressed to limitations of the flood mapping method and the SAR imaging technique itself (shadowed areas and a possible double-bounce effect).

Table 2
Range of *F*-values obtained for the synthetic flood images after application of the segmentation and the bootstrap method on the ENVISAT and TerraSAR-X original flood images.

	Segmentation method	Bootstrap method
ENVISAT	[0.50 0.60]	[0.50 0.64]
TerraSAR-X	[0.54 0.57]	[0.57 0.60]

A statistical comparison was performed on the resulting *F*-values to test for significant differences. First, a Shapiro–Wilk test (Shapiro and Wilk, 1965) was performed to check whether the *F*-values, displayed in Fig. 4, are normally distributed. As this is not the case (p-value <0.05), a non-parametric Wilcoxon rank sum test (Mann and Whitney, 1947) was further performed to test for significant differences. p-values smaller than 0.05 were obtained for comparison of both methods on the ENVISAT and TerraSAR-X original flood images. The test hence reveals that there exists a significant difference between the two methods. However, it has to be noted that the obtained *F*-values only differ slightly. As the Wilcoxon rank sum test is based on a ranking of the *F*-values, the obtained results indicate that the ranking of the *F*-values consequently places the *F*-values of one method before the *F*-values of the other method. Yet, as the *F*-values themselves do not differ much

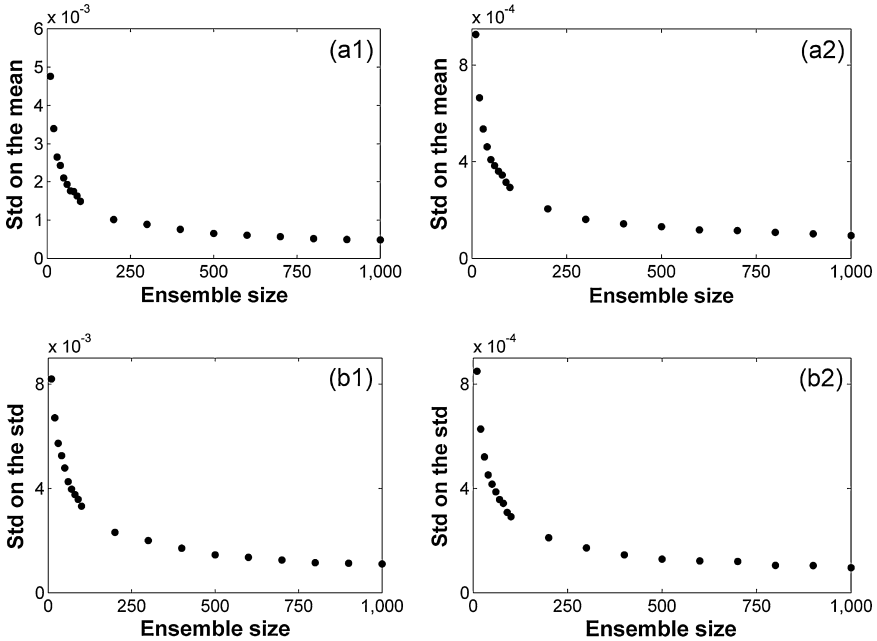

Fig. 5. Standard deviations on the mean (a1 and a2) and on the standard deviation (b1 and b2) of the *F*-values of 1000 ensembles randomly drawn from the bootstrap distribution of *F*, for each tested ensemble size, for the ENVISAT (a1 and b1) and the TerraSAR-X flood image (a2 and b2).

(see Table 2), we still conclude that both methods yield comparable results.

Both methods involve resampling the pixel values of the original image. The bootstrap method resamples at the image scale, whereas the segmentation method locally resamples according to different speckle patterns. Furthermore, the bootstrap method uses a ranking step that is essential for preserving geographical patterns, whereas the segmentation method inherently takes into account the structure present in the image. The bootstrap method has the advantage of being extremely straightforward and efficient, as it does not require any specific image-processing knowledge and extra computation time for segmentation. Therefore, it represents an effective method for assessing speckle influence on flood extent.

Reducing the ensemble size

In order to increase the computational efficiency when the bootstrap method is to be used in an operational mode, it was tested whether the size of the ensemble of bootstrap data sets, *i.e.* the ensemble of synthetic flood images, could be reduced while still obtaining a representative distribution of *F*-values. To this end, sets of different sample sizes were repeatedly sampled with replacement from the bootstrap distribution of *F*-values. For each of these sets, the mean *F*-value and the standard deviation were calculated. In order to estimate the reliability of these means and standard deviations, the standard deviations on these means and on the standard deviations were calculated for each of the sample sizes. Fig. 5 shows the standard deviation on the mean (top panels) and on the standard deviation (bottom panels) of the *F*-values of 1000 repeatedly sampled sets for different sample sizes, for the ENVISAT (left panels) and the TerraSAR-X (right panels) test cases. The results show that the values of standard deviation do not differ much for ensemble sizes ranging from *ca.* 200 to 1000. However, for ensemble sizes smaller than *ca.* 200, the value of the standard deviation increases exponentially, indicating that these samples do not adequately reflect the bootstrap distribution. Therefore, a bootstrap distribution of *ca.* 200 values, which corresponds to an ensemble of *ca.* 200 synthetic flood images, is considered to be an ensemble with a reasonable size, still representative of the entire bootstrap distribution. However, the eventual choice of the number of images is user-defined and should be regarded as a trade-off between computational cost and representativeness.

Conclusions

In this paper, two methods have been compared to take into account speckle uncertainty in a flood mapping procedure. In this paper we assessed only speckle-induced uncertainty, which represents one of several components of the total uncertainty. An image segmentation method has been applied to determine different speckle patterns on the basis of which speckle can be resampled and added to the mean backscatter value of the segment such that synthetic flood images can be generated. Alternatively, a procedure based on the non-parametric bootstrap method was proposed. The method takes into account speckle uncertainty by resampling with replacement the pixel values of the original image. In order to preserve the geographic location in the creation of a synthetic flood image, a ranking procedure was used to position the bootstrapped values within the synthetic flood image.

The image histograms of the synthetic flood images obtained after application of both methods have been visually compared. It was observed that the local resampling according to the speckle distribution, as performed in the segmentation method, yields similar histograms as those obtained by globally resampling the original image, as performed with the bootstrap method.

Furthermore, the flood mapping procedure has been applied on both sets of 1000 synthetic flood images. On the basis of an independent validation set, the *F*-value that reflects the classification accuracy of the flood maps was calculated. It was observed that although slightly higher *F*-values were obtained with the bootstrap method, one can still conclude that both methods yield similar values. This indicates that the ranking step in the bootstrap method compensates for the loss of geographical patterns due to bootstrapping the image pixel values.

In addition, it was checked whether the size of the ensemble of bootstrap data sets, *i.e.* the ensemble of synthetic flood images, could be reduced such that the computational efficiency of the bootstrap method is increased. This would facilitate its use in further applications. It was found that an ensemble of *ca.* 200 synthetic flood images is still representative for the entire bootstrap distribution.

Acknowledgements

This work was supported by the National Research Fund of Luxembourg and the Belgian Science Policy through the FLOODMOIST project (INTER/STEREOII/11/02). Marco Chini's contribution was supported by the National Research Fund of Luxembourg through the PAPARAZZI project (C11/SR/1277979). Additional funding was obtained through other projects financed by the Belgian Science Policy (SR/00/100) and the Research Foundation Flanders (G.0837.10).

References

Baraldi, A., Parmiggiani, F., 1995. An investigation of the textural characteristics associated with gray level co-occurrence matrix statistical parameters. IEEE Trans. Geosci. Remote Sens. 33, 293–304.
Carreiras, J.M.B., Vasconcelos, M.J., Lucas, R.M., 2012. Understanding the relationship between aboveground biomass and ALOS PALSAR data in the forests of Guinea-Bissau (West Africa). Remote Sens. Environ. 121, 426–444.
Caves, R., Quegan, S., White, R., 1998. Quantitative comparison of the performance of SAR segmentation algorithms. IEEE Trans. Image Process. 7, 1534–1546.
Di Baldassarre, G., Schumann, G., Bates, P.D., 2009. A technique for the calibration of hydraulic models using uncertain satellite observations of flood extent. J. Hydrol. 367, 276–282.
De Baets, B., De Meyer, H., Naessens, H., 2001. A class of rational cardinality-based similarity measures. J. Comput. Appl. Math. 132, 51–69.
Dekker, R.J., 2003. Texture analysis and classification of ERS SAR images for map updating of urban areas in The Netherlands. IEEE Trans. Geosci. Remote Sens. 41 (9), 1950–1958.
Duda, F., Hart, P., 1973. Pattern Classification and Scene Analysis. Wiley and Sons, New York.
Durand, S.J.M., Gimonet, B.J., Perbos, J.R., 1987. SAR data filtering for classification. IEEE Trans. Geosci. Remote Sens. 25 (5), 629–637.
Efron, B., 1979. Bootstrap method: another look at the Jackknife. Ann. Stat. 7, 1–26.
Efron, B., Tibshirani, R.J., 1993. An Introduction to the Bootstrap. Chapman & Hall, New York.
Frost, V.S., Stiles, J.A., Shanmugan, K.S., Holtzman, J.C., 1982. A model for radar images and its application to adaptive filtering of multiplicative noise. IEEE Trans. Pattern Anal. Mach. Intell. 4, 157–166.
Fu, K.S., Mui, J.K., 1981. A survey on image segmentation. Pattern Recognit. 13, 3–16.
Giustarini, L., Matgen, P., Hostache, R., Montanari, M., Plaza, D., Pauwels, V.R.N., De Lannoy, G.J.M., De Keyser, R., Pfister, L., Hoffmann, L., Savenije, H.H.G., 2011. Assimilating SAR-derived water level data into a hydraulic model: a case study. Hydrol. Earth Syst. Sci. 15, 2349–2365.
Giustarini, L., Hostache, R., Matgen, P., Schumann, G., Bates, P.D., Mason, D.C., 2013. A change detection approach to flood mapping in urban areas using TerraSAR-X. IEEE Trans. Geosci. Remote Sens. 51 (4), 2417–2430.
Haralick, R.M., Shanmuga, K., Dinstein, I.H., 1973. Textural features for image classification. IEEE Trans. Syst. Man Cybern. SMC-3, 610–621.
Haralick, R.M., Dinstein, I., 1975. A spatial clustering procedure for multi-image data. IEEE Trans. Circuits Syst. CAS-22, 440–450.
Haralick, R.M., 1979. Statistical and structural approaches to texture. Proc. IEEE 67, 786–804.
Horritt, M.S., 1999. A statistical active contour model for SAR image segmentation. Image Vis. Comput. 17, 213–224.
Horritt, M.S., Di Baldassarre, G., Bates, P.D., Brath, A., 2007. Comparing the performance of a 2-D finite element and a 2-D finite volume model of floodplain inundation using airborne SAR imagery. Hydrol. Process. 21, 2745–2759.
Hostache, R., Matgen, P., Schumann, G., Puech, C., Hoffmann, L., Pfister, L., 2009. Water level estimation and reduction of hydraulic model calibration

uncertainties using Satellite SAR images of floods. IEEE Trans. Geosci. Remote Sens. 47 (2), 431–441.
Hostache, R., Lai, X., Monnier, J., Puech, C., 2010. Assimilation of spatially distributed water levels into a shallow-water flood model. Part II: use of a remote sensing image of Mosel River. J. Hydrol. 390 (3–4), 257–268.
Jaccard, P., 1908. Nouvelles recherches sur la distribution florale. Bull. Soc. Vaud. Sci. Nat. 44, 223–270.
Lee, J.S., Jurkevich, I., 1989. Segmentation of SAR images. IEEE Trans. Geosci. Remote Sens. 27 (6), 674–680.
Lee, J.S., Wen, J.H., Ainsworth, T.L., Chen, K.S., Chen, A.J., 2009. Improved sigma filter for speckle filtering of SAR imagery. IEEE Trans. Geosci. Remote Sens. 47 (1), 202–213.
Mann, H.B., Whitney, D.R., 1947. On a test of whether one of two random variables is stochastically larger than the other. Ann. Math. Stat. 18 (1), 1–164.
Mason, D.C., Schumann, G.J.-P., Neal, J.C., Garcia-Pintado, J., Bates, P.D., 2012. Automatic near real-time selection of flood water levels from high resolution Synthetic Aperture Radar images for assimilation into hydraulic models: a case study. Remote Sens. Environ. 124, 705–716.
Matgen, P., Montanari, M., Hostache, R., Pfister, L., Hoffmann, L., Plaza, D., Pauwels, V.R.N., De Lannoy, G.J., De Keyser, R., Savenije, H.H.G., 2010. Towards the sequential assimilation of SAR-derived water stages into hydraulic models using the Particle Filter: proof of concept. Hydrol. Earth Syst. Sci. 14, 1773–1785.
Matgen, P., Hostache, R., Schumann, G., Pfister, L., Hoffmann, L., Savenije, H.H.G., 2011. Towards an automatic SAR-based flood monitoring system. Lessons learned from two case studies. Phys. Chem. Earth 36 (7-8), 241–252.
Montanari, M., Hostache, R., Matgen, P., Schumann, G., Pfister, L., Hoffmann, L., 2009. Calibration and sequential updating of a coupled hydrologic–hydraulic model using remote-sensing derived water stages. Hydrol. Earth Syst. Sci. 13, 367–380.
Oliver, C., Quegan, S., 1998. Understanding Synthetic Aperture Radar Images. Artech-House.
Pacifici, F., Chini, M., Emery, W.J., 2009. A neural network approach using multi-scale textural metrics from very high resolution panchromatic imagery for urban land-use classification. Remote Sens. Environ. 113 (6), 1276–1292.
Pal, R., Pal, K., 1993. A review on image segmentation techniques. Pattern Recogn. 26, 1277–1294.
Pierdicca, N., Pulvirenti, L., Chini, M., Guerriero, L., Candela, L., 2013. Observing floods from space: experience gained from COSMO-SkyMed observations. Acta Astronaut. 84, 122–133.
Pierdicca, N., Chini, M., Pelliccia, F., 2014. The contribution of SIASGE radar data integrated with optical images to support thematic mapping at regional scale. IEEE J. Sel. Top. Appl. Earth Obs. Remote Sens., http://dx.doi.org/10.1109/JSTARS.2014.2330744 (in press).
Pulvirenti, L., Chini, M., Pierdicca, N., Guerriero, L., Ferrazzoli, P., 2011. Flood monitoring using multi-temporal COSMO-SkyMed data: Image segmentation and signature interpretation. Remote Sens. Environ. 115, 990–1002.
Pulvirenti, L., Pierdicca, N., Chini, M., Guerriero, L., 2013. Monitoring flood evolution in agricultural areas using COSMO-SkyMed data: the Tuscany 2009 case study. IEEE J. Sel. Top. Appl. Earth Obs. 6 (4), 1807–1816.
Quaife, T., Lewis, P., De Kauwe, M., Williams, M., Law, B.E., Disney, M., Bowyer, P., 2008. Assimilating canopy reflectance data into an ecosystem model with an Ensemble Kalman Filter. Remote Sens. Environ. 112, 347–1634.
Quartulli, M., Datcu, M., 2004. Stochastic geometrical modeling for built-up area understanding from a single SAR intensity image with meter resolution. IEEE Trans. Geosci. Remote Sens. 42, 1996–2003.
Richards, J.A., Jia, X., 1999. Remote Sensing Digital Image Analysis: An Introduction. Springer-Verlag, New York.
Schumann, G., Matgen, P., Pappenberger, F., 2008. Conditioning water stages from satellite imagery on uncertain data points. IEEE Geosci. Remote Sens. Lett. 5 (4), 810–813.
Schumann, G., Vernieuwe, H., De Baets, B., Verhoest, N.E.C., 2014. ROC-based calibration of flood inundation models. Hydrol. Process., http://dx.doi.org/10.1002/hyp.10019 (in press).
Shapiro, S.S., Wilk, M.B., 1965. An analysis of variance test for normality (complete samples). Biometrika 52 (3–4), 591–611.
Stephens, E.M., Bates, P.D., Freer, J.E., Mason, D.C., 2012. The impact of uncertainty in satellite data in the assessment of flood inundation models. J. Hydrol. 414–415, 162–173.
Sui, H., Xu, C., Liu, J., Sun, K., Wen, C., 2012. A novel multi-scale level set method for SAR image segmentation based on a statistical model. Int. J. Remote Sens. 33 (17), 5600–5614.
Ulaby, F., Moore, R., Fung, A., 1986. Microwave Remote Sensing, Active and Passive. Volume Scattering and Emission Theory, Advances Systems and Applications, vol. III. Artech House, Norwood (MA), USA.
Yu, H., Zhang, X., Wang, S., Hou, B., 2013. Context-based hierarchical unequal merging for SAR image segmentation. IEEE Trans. Geosci. Remote Sens. 51 (2), 995–1009.
Zhang, X., Jiao, L., Liu, F., Bo, L., Gong, M., 2008. Spectral clustering ensemble applied to SAR image segmentation. IEEE Trans. Geosci. Remote Sens. 46 (7), 2126–2136.

Hydrol. Earth Syst. Sci., 15, 2349–2365, 2011
www.hydrol-earth-syst-sci.net/15/2349/2011/
doi:10.5194/hess-15-2349-2011

Hydrology and Earth System Sciences

Assimilating SAR-derived water level data into a hydraulic model: a case study

L. Giustarini[1], P. Matgen[1,4], R. Hostache[1], M. Montanari[1], D. Plaza[2], V. R. N. Pauwels[2], G. J. M. De Lannoy[2], R. De Keyser[3], L. Pfister[1], L. Hoffmann[1], and H. H. G. Savenije[4]

[1]Centre de Recherche Public – Gabriel Lippmann, Département Environnement et Agro-biotechnologies, Belvaux, Luxembourg
[2]Laboratory of Hydrology and Water Management, Ghent University, Ghent, Belgium
[3]Department of Electrical Energy – Systems and Automation, Ghent University, Ghent, Belgium
[4]Water Resources Section, Faculty of Civil Engineering and Geosciences, Delft University of Technology, GA Delft, The Netherlands

Received: 4 February 2011 – Published in Hydrol. Earth Syst. Sci. Discuss.: 25 February 2011
Revised: 14 June 2011 – Accepted: 18 July 2011 – Published: 21 July 2011

Abstract. Satellite-based active microwave sensors not only provide synoptic overviews of flooded areas, but also offer an effective way to estimate spatially distributed river water levels. If rapidly produced and processed, these data can be used for updating hydraulic models in near real-time. The usefulness of such approaches with real event data sets provided by currently existing sensors has yet to be demonstrated. In this case study, a Particle Filter-based assimilation scheme is used to integrate ERS-2 SAR and ENVISAT ASAR-derived water level data into a one-dimensional (1-D) hydraulic model of the Alzette River. Two variants of the Particle Filter assimilation scheme are proposed with a global and local particle weighting procedure. The first option finds the best water stage line across all cross sections, while the second option finds the best solution at individual cross sections. The variant that is to be preferred depends on the level of confidence that is attributed to the observations or to the model. The results show that the Particle Filter-based assimilation of remote sensing-derived water elevation data provides a significant reduction in the uncertainty at the analysis step. Moreover, it is shown that the periodical updating of hydraulic models through the proposed assimilation scheme leads to an improvement of model predictions over several time steps. However, the performance of the assimilation depends on the skill of the hydraulic model and the quality of the observation data.

Correspondence to: L. Giustarini
(giustari@lippmann.lu)

1 Introduction

Due to its all weather and day and night capability, Synthetic Aperture Radar (SAR) is regarded as the most promising technology to monitor floods from space. Since the launch of the ENVISAT mission in 2002 and more recently the successful launches of the high-resolution COSMO Skymed, TerraSAR-X and Radarsat-2 missions in 2007, considerable progress has been made with respect to SAR-based flood delineation algorithms (e.g. Zwenzner and Voigt, 2009; Martinis et al., 2009; Mason et al., 2010; Matgen et al., 2010, 2011). These methods were specifically developed for rapid, repeatable and reliable flood mapping. Remote sensing data have become more frequent and rapidly available and accuracies of SAR-derived flood detection have improved due to higher spatial resolutions and enhanced image processing algorithms. There is a growing pressure on the scientific community to find new ways to use the increased volume and accuracy of remote sensing data in order to improve near real-time flood monitoring and prediction applications (Di Baldassarre et al., 2009).

The retrieval of water level data by merging remote sensing-derived shorelines with a digital elevation model ("indirect measuring technique") can be viewed as a way to add value to remote sensing data for hydrological applications (e.g. Hostache et al., 2009; Raclot, 2006; Schumann et al., 2007). Direct measuring techniques such as those from the proposed swath altimetry "Surface Water and Ocean Topography" (SWOT) mission (Alsdorf et al., 2007) represent a potential enhancement of the indirect measuring techniques as they enable the systematic acquisition of elevation data

of inland water surfaces with an observation uncertainty of 50 cm for a 50 m spatial resolution (Lee et al., 2010). Both techniques enable the monitoring of changes in water volume in ways that are not possible using hydrometric station data.

However, as space-borne sensors provide instantaneous snap-shots of an area of the Earth's surface, there is a need to combine remote sensing data sets with hydrologic-hydraulic prediction models to generate time-lapses of flooded surfaces. Sequential data assimilation methods can be used to integrate time-continuous model state forecasts (e.g. soil moisture, surface water storage) with remote sensing observations as they become available. The quantification of uncertainty for all observations is a pre-requisite to any meaningful data assimilation study. To date, only a few studies have investigated the uncertainty description of remote sensing derived water stages. According to Schumann et al. (2008), geo-location accuracy of the flood extent and parameter uncertainty in flood delineation algorithms are the most significant sources of uncertainty in a high resolution ENVISAT ASAR-based flood mapping application. In a water level retrieval process, which consists in merging the remote sensing-derived shorelines with a digital elevation model, these errors add up to the errors that are inherent in the topography data. The uncertainty assessment approach of Schumann et al. (2008) results in cross-section specific cumulative distribution functions (cdfs) of water elevation estimates. In the case study of the Alzette 2003 flood, the indirect water stage measuring technique yields cdfs that indicate non-normal distributions and skewness of the SAR-based water level estimates for many cross-sections. Uncertainty of stage over the entire river reach was on the order of 2 m.

In situ measurements are routinely assimilated for hydrologic-hydraulic modelling applications (e.g. Neal et al., 2007; Madsen and Skotner, 2005; Pauwels and De Lannoy, 2009). However, only a few studies have attempted to assimilate remote sensing-derived water stage data into hydraulic models. Matgen et al. (2007) used a direct insertion method that forced water stage data simulated by a hydraulic model to fall within the confidence interval of ENVISAT and European Remote Sensing satellite (ERS-2) SAR-derived water stages. They showed that the insertion of remote sensing derived water levels increased the accuracy of modelled water levels. However, this version of a direct insertion method is not an optimal sequential assimilation method and appears as a useful approach only if uncertainties associated with observation data are much smaller than simulation uncertainties and distribution functions of observations are unknown.

Different variants of the Kalman filter present dynamic methods for merging uncertain simulation data with uncertain observations. Andreadis et al. (2007) and Biancamaria et al. (2010) successfully applied an ensemble Kalman filter (EnKF) to assimilate synthetic water level measurements from the proposed SWOT mission with simulations from the LISFLOOD-FP 2-D hydraulic model (Bates and De Roo, 2000). Durand et al. (2008) assimilated virtual SWOT-derived water level observations into a hydraulic model of the Amazon River to improve the estimates of bathymetric depths by 84 % compared to the model runs without assimilation.

Neal et al. (2009) used the EnKF with a real event SAR image of the flood extent. The ensemble uncertainty was estimated by image histogram thresholding with different backscattering values and repeatedly shifting the resulting flood boundaries in space in order to approximate geo-location errors. The measurement error covariance was defined from the perturbations of this ensemble of water level estimates around the mean. Neal et al. (2009) only considered the measurement members with the smallest inter-quantile range over the ensemble at any river section. This was suggested as a quality control step prior to assimilation that was needed because some locations produced biased data (e.g. shorelines next to steep slopes and tall vegetation). They also argue that, because of the spatial coverage offered by remote sensing, it is not necessary to use all measurements. Following this approach, they showed that it is possible to significantly reduce discharge and water level uncertainty of a hydraulic model by using ENVISAT Advanced SAR-derived water stage estimates.

Since the Gaussian error assumption may not be satisfied for most remote sensing observations of water stage, Matgen et al. (2010) proposed an assimilation scheme based on the Particle Filter (PF) as a possibility to relax the Gaussian assumption in the EnKF while preserving its advantages. Their experiments showed that the PF is able to correct water depths from a corrupted 1-D hydrodynamic model by assimilating synthetic observations that are realistic in terms of accuracy for remote sensing-derived water levels. In this case, the PF leads to a significant increase of the accuracy and a reduction of the model forecast uncertainty. Matgen et al. (2010) further state that problems related to a spatially and temporally variable non-Gaussian distribution of water level observations still need to be solved.

The objective of this paper is thus to examine the usefulness of currently available satellite data to update a hydraulic model in near real time, through a PF-based assimilation scheme. The specific objectives are: (1) to adapt the PF assimilation scheme in order to deal with non-Gaussian distributions of remote sensing derived (RSD) water levels; (2) to deal with model structural errors and parameter uncertainties, proposing two variants of the PF; (3) to assess the usefulness of SAR data with respect to in situ hydrometric station data.

2 Study area and available data

The area of interest is situated in the Grand Duchy of Luxembourg (Fig. 1).

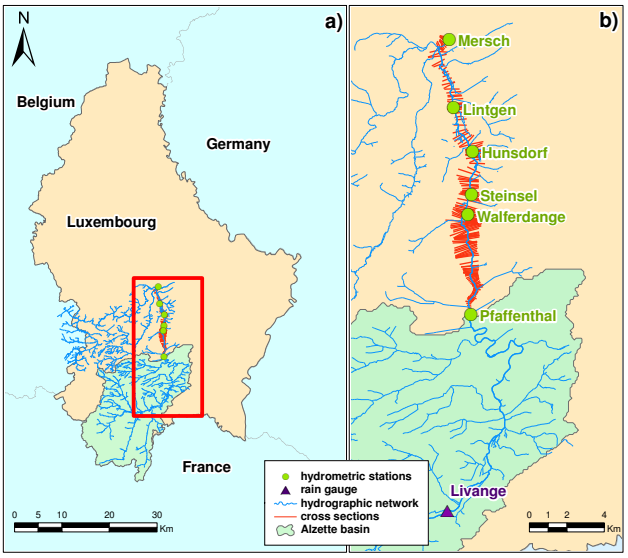

Fig. 1. Study site in the Alzette River basin showing: **(a)** the drainage area down to Pfaffenthal and the 19 km river reach whose geometry is represented by the cross sections, **(b)** the hydrometric stations along the river.

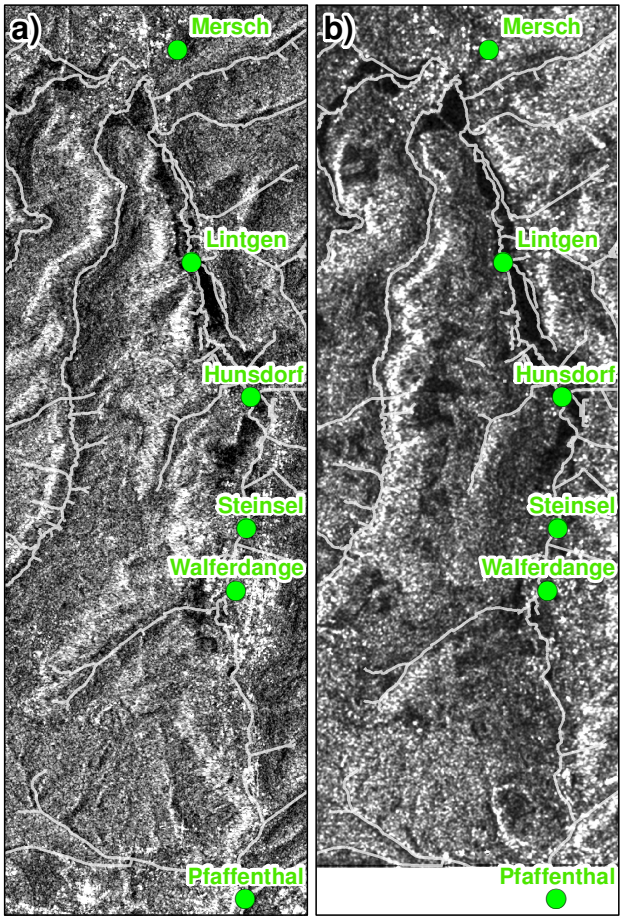

Fig. 2. The 2 available satellite images in backscatter values: **(a)** ERS-2 SAR image, **(b)** ENVISAT ASAR image. The hydrometric stations are also shown. In radar imagery, flooded areas appear in black colour due to the comparatively low signal return on open water bodies.

The hydrologic model is applied to a basin area of 356 km^2 draining to a stream gauge located in Pfaffenthal. This produces the upstream boundary condition for the hydrodynamic model, which simulates the 19 km reach of the Alzette River between hydrometric stations at Pfaffenthal and Mersch (Montanari et al., 2009). The river reach is described by 144 ground-surveyed and evenly spaced (∼130 m) channel cross sections.

The investigated event was a flood recorded in January 2003. Hydrometric data were recorded every 15 min at six stream gauges interspersed throughout the 19 km reach (Pfaffenthal, Walferdange, Steinsel, Hunsdorf, Lintgen and Mersch). Moreover, information about the maximum water level reached along the river during the flood was available, as measured by means of a theodolite (altimetric accuracy around ±2 cm) at distributed points across the floodplain. The availability of in situ data not only allows evaluating the results of the assimilation of remote sensing data, but also helps to contrast the use of space-based and in situ based water level monitoring in a data assimilation exercise. The comparison of results provides insights on the advantages and limitations of each data set.

This paper makes use of the measured precipitation rate to drive the hydrologic model: hourly rainfall data observed in Livange between 1 and 7 January 2003 are available. Contrary to Neal et al. (2009), who used predictions of convective and stratiform precipitation and evaporation, in this case the forcings of the hydrologic model can be considered as the best available representation of the rain field, potentially leading to a more accurate basin response. The set-up of this case study can be viewed as a realistic representation of an operational application of the proposed methodology.

Two subsequent SAR images, acquired at two distinct stages of the 2003 flood event have been used in this study: one was acquired by the ERS-2 satellite during the rising limb of the flood wave; the second image by the ENVISAT satellite just after the flood peak. The two images are shown in Fig. 2 as well as the six stream gauges distributed along the river. A LiDAR DEM of the floodplain at a spatial resolution of 2 m and a vertical accuracy of ±15 cm was fused with remote sensing derived flood boundaries to retrieve the water stages (Schumann et al., 2009). RSD observations of the water stages in the river were retrieved from the two available images, which have a spatial resolution of 12.5 m: in other words, at each cross section more or less independent water stages were observed.

Uncertainty assessment for RSD water stages

Different approaches can be used to estimate spatially distributed water levels and their associated uncertainties from a sequence of wet/dry flood edges extracted from radar imagery and fused with a DEM.

Schumann et al. (2008) proposed a procedure to estimate uncertainty associated with RSD water stage data using a Monte Carlo-based statistical analysis. Hostache et al. (2009) introduced a slightly different approach based on a more integrated uncertainty assessment and based on the analysis of the confidence that can be given to the SAR derived shorelines. Both approaches take into account different sources of uncertainty (i.e. parameters of image segmentation algorithm, co-registration of geo-information layers, accuracy of digital elevation model) that affect the retrieval of water elevation data from remote sensing imagery. First, flood extension limits with their respective geo-location uncertainty are derived from a SAR image using a radiometric thresholding-based procedure. Next, the part of the SAR derived shoreline having a high probability of being erroneous (close to building and trees) due to the incapability of the SAR sensor to detect water in the corresponding areas are removed from the analysis. This provide pertinent shorelines that will be used for the water level estimation. Finally, the ensemble of relevant flood boundaries is superimposed on a DEM in order to estimate water levels. The method takes into account the uncertainty stemming from the underlying DEM and ultimately provides empirical distribution functions of water level data from space at every river cross section (Fig. 3). In assimilation studies, this approach thus potentially allows exploiting the full empirical distribution of observed water levels. However, the resulting uncertainty can be very high (Fig. 3). Moreover the distribution functions often exhibit bias and skewness, especially in the vicinity of steep embankments. All of these factors render the use of the empirical distribution functions in data assimilation studies problematic.

In order to reduce the estimation uncertainty, all water level estimates were hydraulically constrained. The procedure was first introduced by Raclot (2006) and consisted in applying hydraulic rules, governing overland flow in a floodplain, on water level intervals derived from aerial photographs. The hypothesis for applying this procedure is that the uncertainty on the estimated water level is known accurately enough to assume that the real water level is included inside the water level estimate intervals. Considering the effort that was made to take account of all sources of uncertainty and remove errors impacting the extraction of water levels from remote sensing imagery, it is reasonable to assume that the "true" water level is included inside each interval. This hypothesis is supported by the fact that all ground-surveyed measurements of water elevation are included in the above-mentioned intervals (Hostache et al., 2009). Up-/downstream relationships between water level

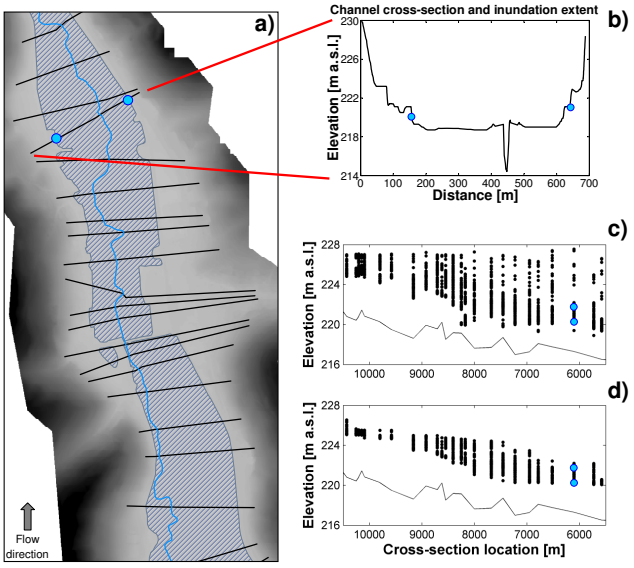

Fig. 3. Diagram showing an example of: **(a)** flood extent derived from a satellite image superimposed on the DEM and the river cross-section location, **(b)** illustration of water level extraction method from inundation extent and cross-section and c) the remote sensing derived water levels along a portion of stream **(c)** before and **(d)** after the hydraulic coherence constrain.

estimates were first defined depending on the location of the water stage estimates within the floodplain. Knowing that the water level decreases from upstream to downstream, an algorithm imposed the following two constraints on the water stage estimate intervals: (1) the upper bounds of the water stage intervals have to decrease from upstream to downstream and (2) the lower bounds of the water stage intervals have to increase from downstream to upstream. This algorithm allowed a significant reduction of the mean water level estimation intervals, as shown in the panels on the bottom right in Fig. 3. As a result, water level information was available as cross-section specific values of the possible local water levels.

3 Simulation design

Figure 4 shows the setup of the data assimilation experiments using event data. The methodology consists of assimilating remote sensing-derived water stage observations into an ensemble of 1-D hydraulic model integrations for a number of cross sections. The upstream boundary conditions (flow hydrographs) are produced using an ensemble of semi-distributed hydrologic model forecasts with perturbed parameter sets, initial conditions and precipitation data.

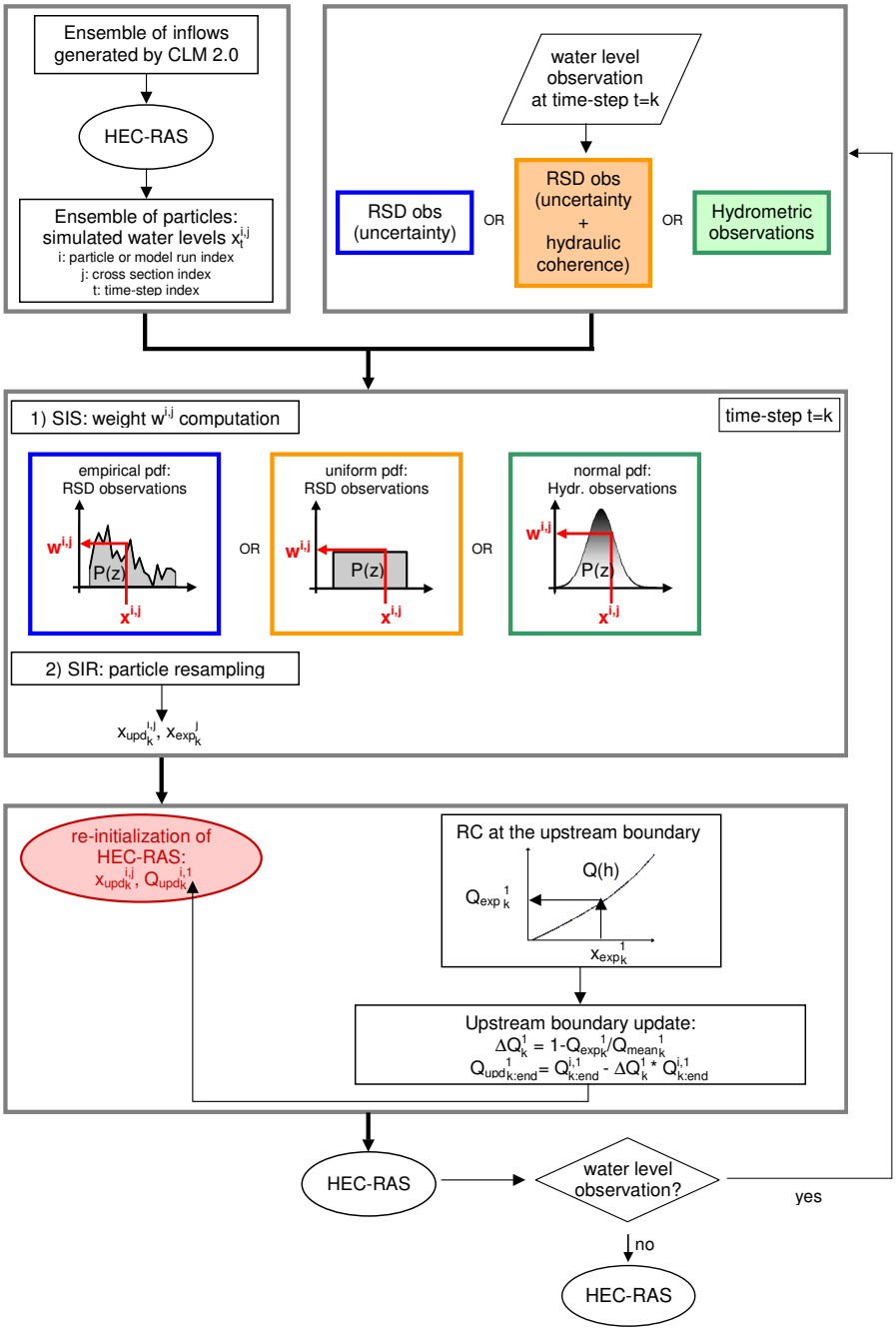

Fig. 4. Flowchart of the data assimilation experiment.

3.1 Coupled hydrologic-hydraulic model

The semi-distributed hydrologic model is loosely coupled to a 1-D hydraulic model: the discharge hydrograph computed by the hydrologic model is used as upstream boundary condition to drive the hydraulic simulation, but the hydraulic model does not feed back into the hydrologic model.

The rainfall-runoff transformation is carried out using the Community Land Model version 2.0 (CLM 2.0) (Dai et al., 2003), a global land surface model built over the 356 km^2 drainage area of the Alzette River extending upstream from the gauging station at Pfaffenthal. To generate meaningful ensembles of model predictions, we followed the procedure of De Lannoy et al. (2007). Model parameters, forcings and initial conditions of the hydrologic model were perturbed in such a way that the ensemble mean differs from the observation by a value that is equal to the time average of the

ensemble spread (De Lannoy et al., 2006). More details on the ensemble generation and the verification measures that were used to monitor the ensemble spread can be found in Matgen et al. (2010). The land surface model was initialized a month before the analyzed flood event to allow spin up and balancing of the state variables in each ensemble member.

The assumption is made that model uncertainties derive only from the upstream boundary condition, which means that uncertainties in hydraulic model structure, parameters, geometry and lateral inflow are not accounted for. Moreover, it is worth mentioning that errors in the inflow peak timing are not taken into account. Therefore, in order to represent the hydrodynamic model uncertainty, an ensemble of 64 upstream boundary conditions (i.e. discharge) was generated with CLM 2.0, adopting the same methodology as discussed in Matgen et al. (2010). The hydrographs are shown in Fig. 5 together with the 2 time steps of satellite overpasses for the 2003 flood event. As opposed to the synthetic experiment by Matgen et al. (2010), no artificial bias was added here to the output of the hydrologic model. However, we noticed that during the receding limb of the hydrograph, the ensemble did not bracket the observed discharge, indicating a tendency of the hydrologic model to underestimate the inflow during that period. The ensemble of the hydraulic model realizations or particles (see box on top-left of Fig. 4) has been produced by integrating the hydrodynamic model with all the members of the discharge ensemble generated by the hydrologic model for the analysis period 1 January 15:00–7 January 23:00, 2003 (GMT+1).

The hydraulic model is implemented over a 19 km reach of the Alzette River between the gauging stations of Pfaffenthal and Mersch. Since flow direction in this area is mainly parallel to the channel, the 2-D flow field that is typically related to riverbank overtopping can be accurately approximated by a 1-D representation and thus, the Hydrologic Engineering Center River Analysis System – HEC-RAS (HEC-RAS 4.0, 2008) – was set-up for 1-D river flow computation.

3.2 Data assimilation algorithm

The data assimilation technique applied in this study is a sequential Particle Filter (PF), an ensemble filtering method that has its origin in Bayesian estimation. Unlike the widely used EnKF (e.g. Burgers et al., 1998; Evensen, 1994), which simplifies the recursive estimation by assuming a Gaussian distribution for both the model and the observation error structure, the PF relaxes the need for restrictive assumptions regarding the shape of the probability density functions and can easily manage the propagation of a non-Gaussian distribution through nonlinear hydrologic and hydrodynamic models (Moradkhani, 2008). In the PF the assumption of Gaussianity is relaxed and the fundamental idea is to represent the required posterior density by a set of properly weighted samples (Smith et al., 2008), named particles, and to compute the estimate based on these samples and weights.

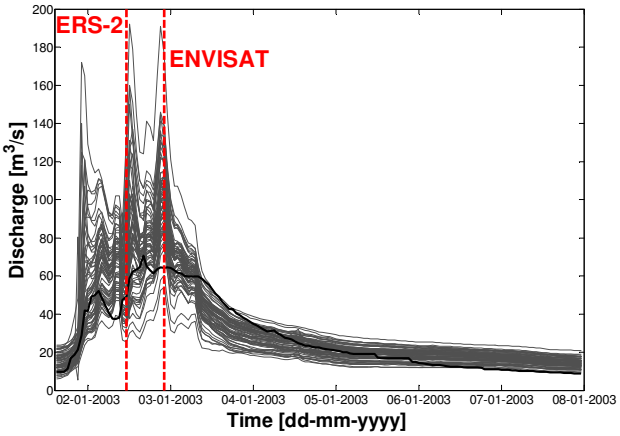

Fig. 5. Ensemble of the 64 upstream boundary conditions generated by the CLM 2.0. The gauged flow is also shown in bold line and the time of the two satellite overpasses are overlaid.

3.2.1 Sequential Importance Sampling (SIS)

The simplest implementation of the PF is based on the Sequential Importance Sampling (SIS) method (see box in the middle of Fig. 4). Each particle consists of a possible value of the state. The filtering density is approximated by a discrete distribution, whose support is the set of particles. The probability mass assigned to each particle is proportional to that particle's weight, which, in turn, is proportional to the likelihood of the observation at the assimilation time step (Fearnhead, 2002).

In this case study, a particle represents the water surface line resulting from one hydrodynamic model run at the assimilation time step $t = k$, and the number of state variables corresponds to the number of cross sections. The particles are sampled directly from the state-space to represent the posterior probability, and a weight is computed for each particle according to the information contained in the RSD water level observations. In this case study, the SIS algorithm was implemented using two different distribution functions that are characteristic for the data sets at hand. A local weight, $w^{i,j}$, is assigned to any state variable j for any particle i (the index k is left out to avoid confusion but the weights are recomputed at any time-step of observation acquisition). Note that the weighting procedure can be adapted to any kind of distribution function.

Section 2.1 describes an approach for retrieving for each cross section an interval of possible water stage values. In this case, as only the maximum and minimum water level values are available for each cross section, we assimilate the observation data assuming a uniform distribution, whose boundaries are the derived maximum and the minimum water stage estimates. Therefore, the likelihood or weight, $w^{i,j}$, of the water level, $x^{i,j}$, simulated by particle i at cross section

j for the time-step of the observation acquisition is simply computed as:

$$w^{i,j} = \begin{cases} \frac{1}{b-a} & \text{for } a^j \le x^{i,j} \le b^j \\ 0 & \text{for } x^{i,j} < a^j \text{ (or) } x^{i,j} > b^j \end{cases} \quad (1)$$

where x is the state vector of the state variables (simulated water stages at any cross section j for any particle i), a and b are the lower and upper observed endpoints or minimum and maximum, respectively, for any cross section j. All assimilation experiments were also carried out using hydrometric station data as it allowed contrasting results obtained with relatively uncertain but densely distributed satellite-derived data with those obtained with accurate but poorly distributed in situ measurements. When assimilating data from these stations, a Gaussian distribution was used, assuming the recorded water level to be the mean of a normal distribution whose shape is also defined by a pre-defined value of standard deviation (Matgen et al., 2010). Note that water stage estimates obtained from space-borne swath altimeters were assumed to be normally distributed as well (Andreadis et al., 2007). One weight, $w^{i,j}$, for any water level, $x^{i,j}$, simulated by particle i at cross section j for the time-step of the observation acquisition is therefore computed as:

$$w^{i,j} = \frac{1}{\sigma\sqrt{2\pi}} e^{\frac{-\left(x^{i,j}-\mu^j\right)^2}{2\sigma^2}} \quad (2)$$

where x is the state vector of the state variables (simulated water stages at any cross secrtion j for any particle i), μ is the observation vector and σ is the standard deviation associated to the observations.

Regardless of the way the weights of the individual particles are computed (e.g. assuming a normal or uniform distribution of residuals), the matrix of weights contains all local weights, $w^{i,j}$, that are obtained for any model run or particle i at all the N_o observed cross sections j. Subsequently, an overall likelihood of the water level globally simulated along the river reach for any particle or model run is computed by applying the joint probability theory for independent variables:

$$w^i = \prod_{j=1}^{N_o} w^{i,j} \quad (3)$$

where N_o is the number of observations.

The resulting global weight is then normalized.

$$W^i = \frac{w^i}{\sum_{i=1}^{N_p} w^i} \quad (4)$$

N_p is the number of particles or water surface lines.

The probability obtained with the global weights at the previous steps allows computing an expectation of the updated water stage as follows for the assimilation time-step k:

$$E(x_k) = x_{exp} = \sum_{i=1}^{N_p} x^i W^i \quad (5)$$

3.2.2 Sequential Importance Resampling (SIR)

Because of the stochastic behaviour of the system, the particles tend toward dispersion and there is a risk that many of them obtain negligible weight during the analysis. This behaviour, called degeneracy, is defined as the tendency to converge to a single point estimate (Moradkhani et al., 2005). To avoid unnecessarily high computational resources, a resampling step is carried out to eliminate samples with low weight and to replicate samples with high weight. In other words, the HEC-RAS model is re-initialized at the time-step of the observation acquisition, k, replicating the water lines with higher weight (see box on the bottom of Fig. 4). The resampled particles have the same weight, until the next assimilation step. The most common resampling scheme is the Sequential Importance Resampling (SIR) developed by Gordon et al. (1993). The authors refer to Moradkhani et al. (2005) and Weerts et al. (2006) for more detailed explanations of the SIR and its use in hydrologic applications.

It should be mentioned that resampling is independent of the proposal distribution (Fearnhead, 2002) but it is also possible to implement a PF without resampling. In any case, the SIR algorithm also suffers from particle degeneracy. Smith et al. (2008) showed that the resampling step only reduces the degeneracy of the particles. Moreover, a different problem may arise, known as sample impoverishment, causing particles with high weight to be selected many times, which leads to a loss of diversity in the sample. In fact, due to the discrete approximation of the filtering density, inaccuracies accumulate over many time steps and the result is often a clustering of particles in small areas of the state-space (Fearnhead, 2002).

The experimental set-up of this case study avoided the problem of sample impoverishment through a loose coupling of the hydrologic and hydraulic model components. Only the water levels were resampled, while the spread in the input data was maintained. Therefore, even in the extreme case where a single particle was retained and replicated, the spread in the discharge hydrographs ensured that shortly after the assimilation a sufficient spread of the state variables was obtained. As in Matgen et al. (2010), at the assimilation time-step k, the estimate of the upstream water level x^1_{exp} (Eq. 5) was used to compute the corresponding estimate of the discharge $E\left(Q^1_k\right)$, using the HEC-RAS internal rating curve. A simple algorithm was then applied for the updating

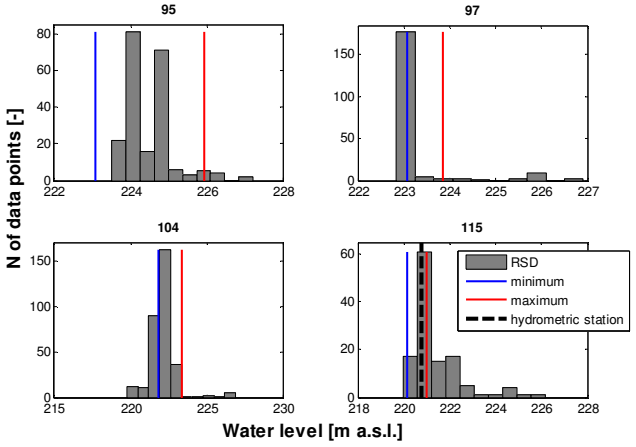

Fig. 6. Cross section specific empirical histograms of RSD water levels for four hydrometric sections, shown with numbers increasing in river flow direction, for the first satellite overpass (ERS-2 on 2 January 2003 at 22.00 GMT+1). RSD, minimum, maximum and station recorded water levels (where available) are also shown.

of the forcings (i.e. discharge Q) until the next assimilation time-step (see box on bottom right of Fig. 4):

$$Q_i^1 = Q_i^1 - \left(\frac{\overline{Q_k^1} - E\left(Q_k^1\right)}{\overline{Q_k^1}} \right) \cdot Q_i^1 \quad (6)$$

where Q_i^1 is the upstream discharge of particle i and $\overline{Q_k^1}$ is the average, computed during the analysis step k, of the hydrograph ensemble. The forcing update was applied until the next assimilation time-step, based on the assumption that relative model errors remain constant and that correcting the inflows by the same relative error term at subsequent time steps will improve the accuracy of the model prediction.

3.3 Synthetic experiment vs. real-event case study

The set-up of the case study was very similar to the one presented for the synthetic experiment in Matgen et al. (2010), but there were some significant differences that need to be highlighted.

3.3.1 First assumption: observations

In the synthetic experiment, one of the basic assumptions was that the observed and assimilated (synthetic) satellite water level data were unbiased and normally distributed. In a real case study, the Gaussian assumption may not be satisfied for at least some of the remote sensing-derived water stage observations. Examples of cross-section specific pdfs of RSD data retrieved with the procedure proposed by Schumann et al. (2008) are shown in Fig. 6. The data obtained from the first satellite overpass (ERS-2 on 2 January 2003 at 11.00 GMT+1) are given for four representative cross sections. As it can be seen, the data at each section exhibit a different pdf shape. Obviously, the normal distribution is not a suitable candidate distribution for representing the pdf. In the same panels, the maximum and minimum water levels deriving from the hydraulic coherence concept (Hostache et al., 2009) are also shown. It can be seen from these results that a significant reduction of the water level estimation intervals was obtained (see also Fig. 3). Here we assume that within each interval the RSD water levels are uniformly distributed.

Furthermore, Fig. 6 highlights bias and skewness in the RSD data retrieved using the first image. The RSD water levels at the first satellite overpass (ERS-2 on 2 January 2003 at 11.00 GMT+1) for the gauged cross section of Lintgen (named 115 in the hydraulic model) were not centered on the in situ water level measurements. For this cross section and the considered time step, the RSD water levels showed a tendency to overestimate the actual water level. After applying the hydraulic coherence concept, the plausible interval was significantly narrowed and, most importantly, included the ground "truth". Therefore, the data assimilation algorithm was run assuming the uniform pdf to represent the statistical distribution of RSD water levels.

3.3.2 Second assumption: model

A further characteristic of the synthetic experiment by Matgen et al. (2010) was that the hydraulic model was correct in it structure, parameter set and initial or analysis conditions. Therefore, the differences between observations and models only derived from inaccuracies in the input data (i.e. hydrographs at the upstream boundary). This means that, for a given forcing (Q), the model generally performs equally well (or poorly) at all cross sections along the river. In other words, due to the fact that the same model is used both to generate the artificial satellite observations and to assimilate them, a model run that is good at a given cross section performs well at all the other cross sections.

In a real case study, model structure errors (e.g. 1-D flow approximation, errors in geometry) and parameter uncertainties (e.g. Manning's roughness values), cause local bias that need to be taken into consideration. We expect such models to have a less uniform behavior along the river reach. This raises difficulties in the selection of a good model run, as it might happen that one model performs globally well over the whole river reach but at the same time has a poor performance at a local level (i.e. at some cross sections).

In the present case study, a first assimilation test was carried out with the same Manning's values as in Montanari et al. (2009): one value for the channel and one for the floodplain. However, by using spatially-distributed stage-discharge measurements it is possible to further reduce potential errors that may originate from a too simplistic parameterization of the model. By introducing additional model parameters, we expect the resulting model to have potentially better behaviour at a local scale.

For the Alzette River and for the considered flood event, previous studies have shown that the floodplain does not play a significant role in the flood hydraulics (Hostache et al., 2009; Montanari et al., 2009). Therefore, for the floodplain a Manning's coefficient equal to $0.184\,s\,m^{-1/3}$ was assumed (Montanari et al., 2009). The Manning friction coefficients for the channel was calibrated by means of discharge measurements carried out in the period 2001–2009 along the river reach on the hydrometric stations of Pfaffenthal, Steinsel, Hunsdorf and Lintgen. The geometry of the river is described by the 144 channel cross sections that were surveyed in 2001. It is important to note that the SAR-observed flooding event occurred in January 2003. All cross sections with available simultaneous measurements of water level and discharge were analyzed by comparing the cross section of the hydraulic model with those observed during each discharge measurement campaign. As there is no evidence that would indicate any significant changes in riverbed geometry, we assume the river geometry to be temporally stable.

Measurements of both water levels and discharge taken at the same time allowed calibrating Manning's roughness values for the four cited cross sections in the main channel. Following the random sampling of 4 values for the channel roughness from a range of plausible values (i.e. 0.030–$0.060\,s\,m^{-1/3}$), parameters of the cross sections that are located between the 4 gauging stations were estimated through linear interpolation. As upstream boundary discharge, we used the January 2003 discharge data that was estimated from recorded water levels and a calibrated rating curve. The model was evaluated by comparing the observed rating curves at the 4 cross sections with the internal rating curves of HEC-RAS. The selected model set is the one that minimizes the difference between simulated and observed water levels for a range of observed and simulated discharge values.

The calibration reproduced the high discharge values reasonably well, with Manning's roughness coefficients set equal to 0.042, 0.044, 0.053 and $0.039\,s\,m^{-1/3}$, for Pfaffenthal, Steinsel, Hunsdorf and Lintgen, respectively. The plots in Fig. 7 display the calibrated rating curves for the cross sections with available measurements. For the cross sections in between, the friction coefficient was linearly interpolated. It has to be noted that the distance between Pfaffenthal and Steinsel is nearly 8 km, which is rather significant with respect to the total river reach length (19 km). Therefore we expect model errors to be higher in the upper part of the river reach. In particular, the cross section of Walferdange did not have measurement data and its friction value was deduced from the one in Steinsel, the nearest calibrated cross section.

The observed January 2003 discharge hydrograph at the upstream boundary condition was used as input for the calibrated model to assess its capability in reproducing observed spatio-temporal fluctuations of water surface elevation. This assessment was made by comparing the observed and the simulated hydrographs at all the gauged cross sections. The

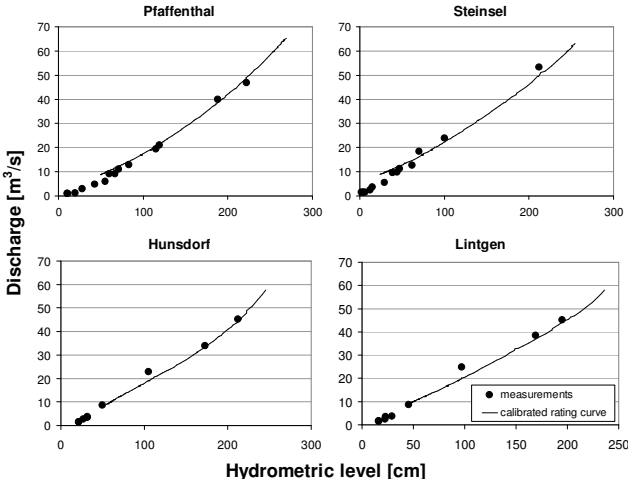

Fig. 7. Calibrated rating curves for the cross sections with available discharge measurements.

Nash-Sutcliffe efficiency was computed obtaining an average value on the gauged cross sections of 0.84, indicating a satisfactory result in terms of model performance.

4 Results and discussion

The hydrodynamic model, built from the 144 surveyed cross sections, was used to simulate water levels along the river reach, considering as inputs the ensemble of 64 hydrographs generated by the CLM 2.0. At each satellite overpass, RSD water level estimates were assimilated into the coupled hydrologic-hydraulic model following the procedure outlined in Sect. 3.2. The results are compared against in situ observed station data. It is important to note that in situ data were assimilated only at the time steps of the satellite overpasses. This analysis can be considered as a benchmark test that enables contrasting the performances obtained when assimilating, respectively, very precise but poorly distributed ground-surveyed information and spatially distributed but highly uncertain satellite data.

4.1 Global weighting procedure (gw)

4.1.1 Analysis step

When a satellite observation becomes available, weights are computed for all the simulations at any cross section. A global weight is computed for every particle according to the procedure outlined in Sect. 3.2.1.

Figure 8 shows the histograms of computed water stages before and after resampling the particles during the assimilation procedure. The histograms shown here correspond to the four intermediate gauging stations in Walferdange, Steinsel, Hunsdorf and Lintgen. The two groups of four panels on top refer to the first satellite overpass (i.e. ERS-2 image), while

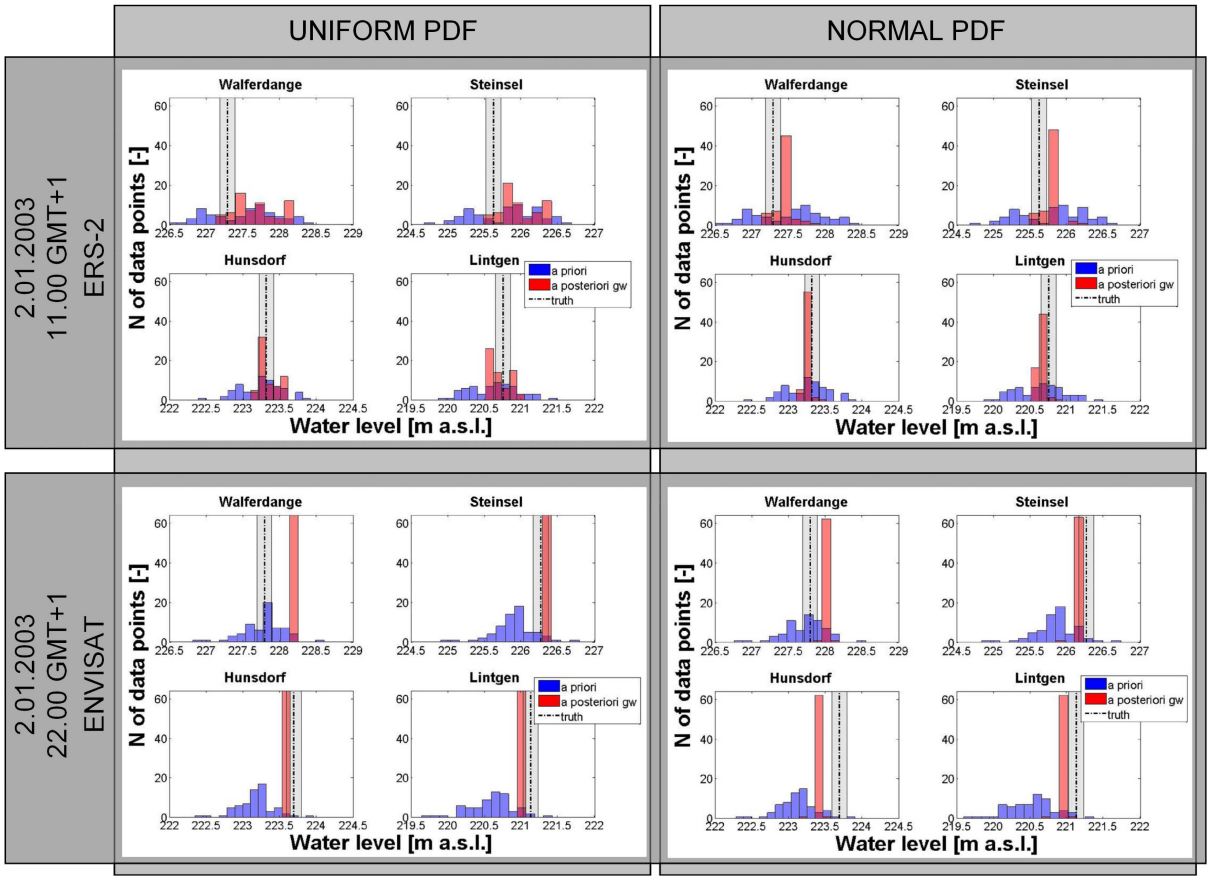

Fig. 8. Histograms of water stages at 4 intermediate cross sections, before and after the resampling step (gw: global weight). Left panels show the application of the uniform pdf on the RSD water levels, right panels the use of the normal pdf on the hydrometric station data. Top graphs refer to the first ERS-2 overpass; bottom ones to the ENVISAT overpass. Gauged level and its presumed uncertainty are also shown.

those on the bottom refer to the second assimilation time step (i.e. ENVISAT image). On the left, the results of the assimilation corresponding to the application of the uniform pdf with the RSD observed data are displayed, while on the right the reported outcome corresponds to the application of the normal pdf with the in situ data. The in situ measurements at six hydrometric stations located on the river reach also serve as validation datasets for assessing the performance of the analysis. The performance of the assimilation is evaluated through the mean error value, the change in distance between the mean of the a priori histogram and the truth compared to the distance between the mean of the a posteriori histogram and the truth. The standard deviation of the histogram both a priori and a posteriori is computed as a measure of the reduction of uncertainty in the water level at the assimilation time step.

Considering the use of the uniform pdf (panels on the left side in Fig. 8), the results obtained via the assimilation of the intervals, defined by the maxima and minima of the retrieved water stages, show a significant reduction of the spread in the a posteriori distribution of the simulated water stages. The reduction in uncertainty is evident for the first time step and becomes even more significant for the second. Moreover, at the time step of the ERS-2 image acquisition, at all the investigated cross sections the a posteriori distribution of water level estimates encompasses the truth. However, the spread reduction is most significant for cross sections in Hunsdorf and Lintgen, located in the downstream part of the river, where most of the flooding occurred (i.e. where most observations of water stage are available). As a result of the analysis there is a decrease of the mean error value, changing from -0.07 to 0.02 m for Hunsdorf cross section and from -0.14 to -0.06 m for Lintgen. The decrease in terms of standard deviation (changing from 0.29 to 0.13 m and from 0.33 to 0.14 m for the two cross sections, respectively) further outlines the positive effect that the assimilation procedure has at a local level. However, for the sections in Walferdange and Steinsel, both located in the upstream part of the river reach, we observe a tendency to overestimate the recorded stage data post assimilation. In both sections the mean error value increases, from 0.22 to 0.37 m in Walferdange and from 0.17 to 0.34 m in Steinsel. The fact that the standard

Table 1. Mean error (mev) and standand deviation (std) values computed for the two satellite acquisitions before and after the assimilation analysis step, for the four cross sections with available ground observation measurements, considering the assimilation of the RSD data with the uniform pdf and the use of the normal pdf with the hydrometric station data.

			uniform pdf				normal pdf			
			mev (m)		std (m)		mev (m)		std (m)	
			before	after	before	after	before	after	before	after
2.01.2003 11.00 GMT+1	ERS-2	Walferdange	0.22	0.37	0.46	0.28	0.22	0.17	0.46	0.10
		Steinsel	0.17	0.34	0.45	0.25	0.17	0.16	0.45	0.10
		Hunsdorf	−0.07	0.02	0.29	0.13	−0.07	−0.06	0.29	0.04
		Lintgen	−0.14	−0.06	0.33	0.14	−0.14	−0.11	0.33	0.06
2.01.2003 22.00 GMT+1	ENVISAT	Walferdange	−0.02	0.38	0.28	0.01	−0.08	0.19	0.29	0.02
		Steinsel	−0.36	0.10	0.28	0.01	−0.42	−0.16	0.29	0.02
		Hunsdorf	−0.52	−0.08	0.25	0.01	−0.58	−0.29	0.25	0.03
		Lintgen	−0.54	0.07	0.32	0.01	−0.61	−0.16	0.32	0.03

deviation is reduced merely illustrates that uncertainty, as it is defined here, only expresses model uncertainty and not truly probabilistic prediction limits of the assimilation procedure.

This limitation of the "global weighting procedure" is confirmed by the results obtained at the second assimilation time step. Overall, the assimilation of data retrieved from the ENVISAT ASAR image leads to the selection of only two particles; one is kept for the simulation and the other one is replicated 62 times. This means that only two simulations provide water surface lines that are included in the RSD intervals at all cross sections. As a matter of fact, the standard deviation values are negligible after this time step, while the mean error values are reduced to less than 10 cm for all cross sections, except Walferdange, where an overestimation remains apparent. On all other sections the a posteriori distribution includes the truth. It has to be observed that for Walferdange it was not possible to calibrate the roughness value of the hydraulic model, due to the unavailability of discharge measurements. Its Manning's coefficient was interpolated considering the values of the upstream and downstream cross sections. The poor quality of the model results at this cross section could thus be explained with a badly calibrated model. Moreover, as flooding only occurred on the downstream part of the river reach, there are no RSD observations available in the upper part of the river (i.e. upstream of the Steinsel cross section). These limitations partly explain the difficulty the global weighting procedure has to select models that perform well along the entire river reach. This result shows that one of the main assumption of the synthetic experiment, namely that input data is the only source of error in hydraulic modelling, can no longer be maintained. Table 1 summarizes the results in terms of mean error and standard deviation values for the two assimilation time steps and the two distribution functions.

Before applying and testing a procedure based on local weighting, an experiment was carried out with precise in situ measurements of water level, recorded at six cross sections along the river at the time of the two satellite overpasses. This test represents a circular way to operate, due to the fact that the same data set is used for assimilation and validation. However, the rationale behind this test is to distinguish model errors from observation errors. A good model is expected to provide results that are centred on the truth at every single cross section. In this experiment the normal pdf was used, assuming a standard deviation equal to 0.1 m to represent the uncertainty of the measurements. As can be seen from the panels on the right in Fig. 8, for the ERS-2 satellite overpass, the resampled particles show a good reduction of the spread (standard deviation ranging from 0.04 m to 0.10 m) and always encompass the truth. However, the assimilation of in situ measurements at the time step of the ENVISAT image acquisition highlights a contradictory behaviour. The reduction of the spread is very significant and only a limited number of particles are selected at any cross section. The results are surprisingly similar to those results obtained with the less accurate RSD observations. However, only in Steinsel did the assimilation methodology predict the truth, while for all other cross-sections the resampling of the particles either leads to a slight over- or underestimation. This indicates that no model run performs equally well along the entire river reach. We assume that this is due to the fact that important sources of errors are not sufficiently well represented by the ensemble of model runs.

Table 1 summarises the information in terms of performance and standard deviation values for the two satellite acquisitions and the two distribution functions. From these results we conclude that the proposed PF-based filtering approach is an efficient tool to assimilate observations described by characteristic distribution functions. However, the

observed over- and underestimations are an indication that local inconsistencies persist in the calibrated model. This can lead to a sub-optimal functioning of the PF or indeed the rejection of all models: when one particle represents the water level over the whole reach as state vector and the weights are computed according to Eq. (3), systematic model errors at a local scale heavily impact the weight that is attributed to individual particles. Rather than selecting and replicating the best particles overall, the application of the joint probability theory for independent particles penalizes particles that have low weight at some locations. As a result, the global weighting procedure favours compromise solutions that provide acceptable results at all model cross-sections. Therefore, it is important to bear in mind that the PF has been initially designed for removing noise and not systematic errors. A pre-requisite for the application of the PF is thus to reduce systematic errors in the model prior to any data assimilation experiment.

4.1.2 Forecasting step

Following the analysis step, the model is propagated in time: to do so, the hydrodynamic model is first re-initialized with updated water stages and then run with the updated upstream inflow data until a new observation becomes available. Figure 9 shows the stage hydrographs corresponding to the cross-section at Lintgen, when using the uniform pdf to assimilate the RSD observations. The performance of the forecast is illustrated considering the RMSE of the ensemble mean water stage, $\overline{h_{\mathrm{ass}}}$, with respect to the recorded water stage h_{truth}:

$$\mathrm{RMSE}(t) = \sqrt{\frac{\sum_{p=t_{\mathrm{ass}}+dt}^{t} \left(\overline{h_{\mathrm{ass}}}(p) - h_{\mathrm{truth}}(p)\right)^2}{t-(t_{\mathrm{ass}}+dt)+1\cdot dt}} \quad t \geq t_{\mathrm{ass}}+dt \quad (7)$$

which is computed over different time windows, starting from the first time step after the satellite overpass, $t_{\mathrm{ass}}+dt$, and stopping at $t-(t_{\mathrm{ass}}+dt)+1$, where dt is the time step of the simulation, in order to evaluate the usefulness of the assimilation as a function of the number of time steps following the analysis step.

As it can be seen from Fig. 9, after the ERS-2 satellite overpass, when the analysis step efficiently drags the simulated water level towards the observed water level, the RMSE is first close to zero before gradually increasing at subsequent time steps due to the predominant effect of the inflow condition. Although the relative error term was correctly inferred from satellite observations, it becomes obvious from Fig. 9 that the proposed inflow correction model (Eq. 6) underpredicts simulation errors in the time window between the two satellite acquisitions. However, the forecasts with filter are consistently better than the open loop predictions for the first time steps. After the second acquisition the RMSE approaches zero and the error terms in Eq. (6) leads to correct

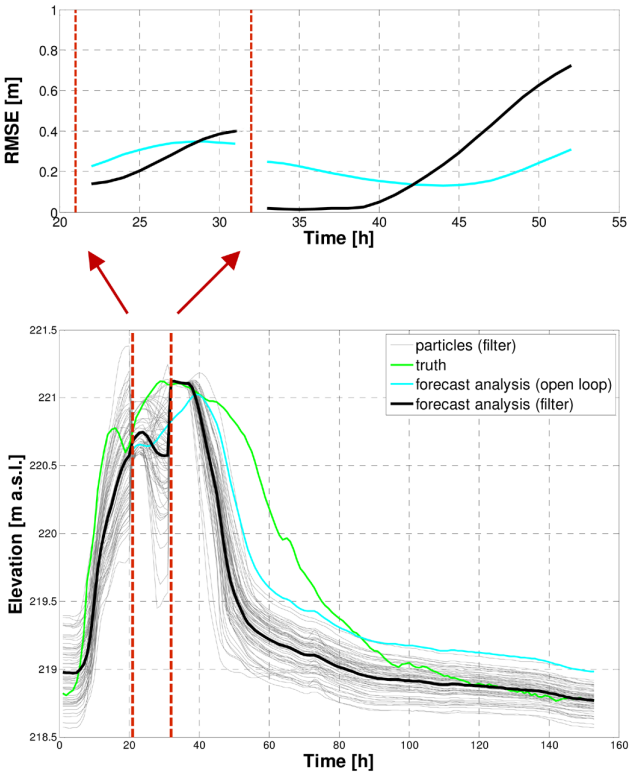

Fig. 9. Stage hydrographs at the cross section Lintgen with the 2 assimilation time steps (bottom panel) considering the RSD water level intervals assimilated through a uniform distribution: the forecasting performance is illustrated with the RMSE evolution in time (top panel). The cyan line represents the RMSE before assimilation and the black line displays the RMSE after assimilation.

predictions for more than 5 h after the assimilation, as the error remains constant for some time steps. Nevertheless, later on the application of a constant error prediction term for the inflow leads to wrong predictions, with an underestimation of the receding limb of the hydrograph. Hence, the analysis step is of fundamental importance in order to carry out an efficient inflow correction. Errors in the analysis propagate through the inflow correction model and this can significantly decrease model performance at later time steps.

4.2 Local weighting procedure (lw)

4.2.1 Analysis step

As an alternative to the global weighting procedure, an approach based on local weighting has been developed and tested. In this procedure, each cross section has its own particle set, with as state vector the water levels at the cross section itself (i.e. the state vector is a scalar). Each particle has its own weight, as required for the PF. This procedure is different from global weighting, where one particle has as state vector the water level over the whole reach.

Table 2. Idem Table 1, but considering the local weighting variant of the PF.

			uniform pdf				normal pdf			
			mev (m)		std (m)		mev (m)		std (m)	
			before	after	before	after	before	after	before	after
2.01.2003 11.00 GMT+1 ERS-2		Walferdange	0.22	0.42	0.46	0.33	0.22	−0.01	0.46	0.13
		Steinsel	0.17	0.36	0.45	0.31	0.17	0.00	0.45	0.14
		Hunsdorf	−0.07	−0.02	0.29	0.12	−0.07	0.00	0.29	0.08
		Lintgen	−0.14	−0.17	0.33	0.24	−0.14	−0.01	0.33	0.10
2.01.2003 22.00 GMT+1 ENVISAT		Walferdange	−0.02	0.04	0.28	0.16	−0.08	−0.01	0.29	0.08
		Steinsel	−0.36	−0.28	0.28	0.19	−0.42	−0.06	0.29	0.10
		Hunsdorf	−0.52	−0.40	0.25	0.17	−0.58	−0.08	0.25	0.15
		Lintgen	−0.49	−0.41	0.31	0.24	−0.61	−0.07	0.32	0.13

Once again, the uniform distribution was used in the assimilation algorithm. We expect a local weighting based method to yield better results when model structural and parameterization errors are present. However, this method will be rather sensitive to local observational errors. The results are given in Fig. 10. The histograms were obtained at four representative cross sections.

Using the uniform distribution together with the local weighting procedure, the reduction of uncertainty is less evident than with the global weighting method. At each cross section all particles that provide water stage estimates included in the RSD intervals are retained and equally weighted. As a result, the standard deviation values are generally higher than before. While the global weighting procedure applied to the ENVISAT-derived data led to the selection of only one particle, the application of a local weighting procedure causes many simulations to be retained at each cross section. For instance, in Lintgen after the second assimilation step the standard deviation is reduced to 0.00 using a global weight but only to 0.24 using local weights. All the a posteriori distributions include the truth, even if in Walferdange a tendency to overestimate the truth persists. With respect to the mean error values, the two weighting approaches give comparable results at the first assimilation step. For the second satellite overpass an improvement can be observed for the upper part of the river, whereas for Hunsdorf and Lintgen, both located in the lower part of the study area, the tendency to slightly underestimate the truth is further enhanced.

Finally, the assimilation was carried out using in situ water level measurements at six cross sections at the time of the two satellite overpasses (Fig. 10). Here we apply the local weighting procedure to compute the a posteriori histograms. As expected, this is the easiest setup for the assimilation algorithm to recognise the truth. For both time steps and in all the cross sections, the resampled particles encompass the truth. This experiment shows that if observations are of high quality, the local weighting procedure yields very satisfactory results. Adopting a local weighting procedure significantly reduced model uncertainty, as demonstrated by the means of the global weighting experiment. However, as we suspect other sources of error than inflows (e.g. spatially varying friction parameters, intermediate inflows and/or errors in geometry) to be responsible for contradicting results obtained in sub-reaches of the model domain, it has to be expected that these improvements cannot be maintained over many time steps. It is therefore recommended to use the results of the analysis to find the reasons for regionally conflicting results and to make use of such a diagnosis for improving the model in a more persistent way than through a mere reinitialization and inflow correction.

Considering the local weighting variant of the PF, Table 2 summarises the results in terms of mean error and standard deviation for the two time satellite acquisitions and for the two distribution functions.

4.2.2 Forecasting step

Figure 11 illustrates the performance of the forecasts considering the local weighting procedure to assimilate the ground measurements recorded at six hydrometric stations. It shows that when the analysis step gives good results (i.e. when the error term at the time of the observation is correctly estimated), the short-term forecasts with assimilation are improved. However, the limitation of a possible overcorrection of inflow persists as the inflow-corrected mid-term to long-term forecasts seem to have less skill than the open loop predictions. A possible explanation is that the two satellite observations were acquired during the hydrograph's rising limb when model errors are known to be only weakly correlated in time. This is due to the fact that during the rising limb, errors are difficult to predict as precipitation errors continuously add to model parameter and model structural errors. This conclusion is in line with the findings of Matgen et al. (2010) who stated that because of the underlying

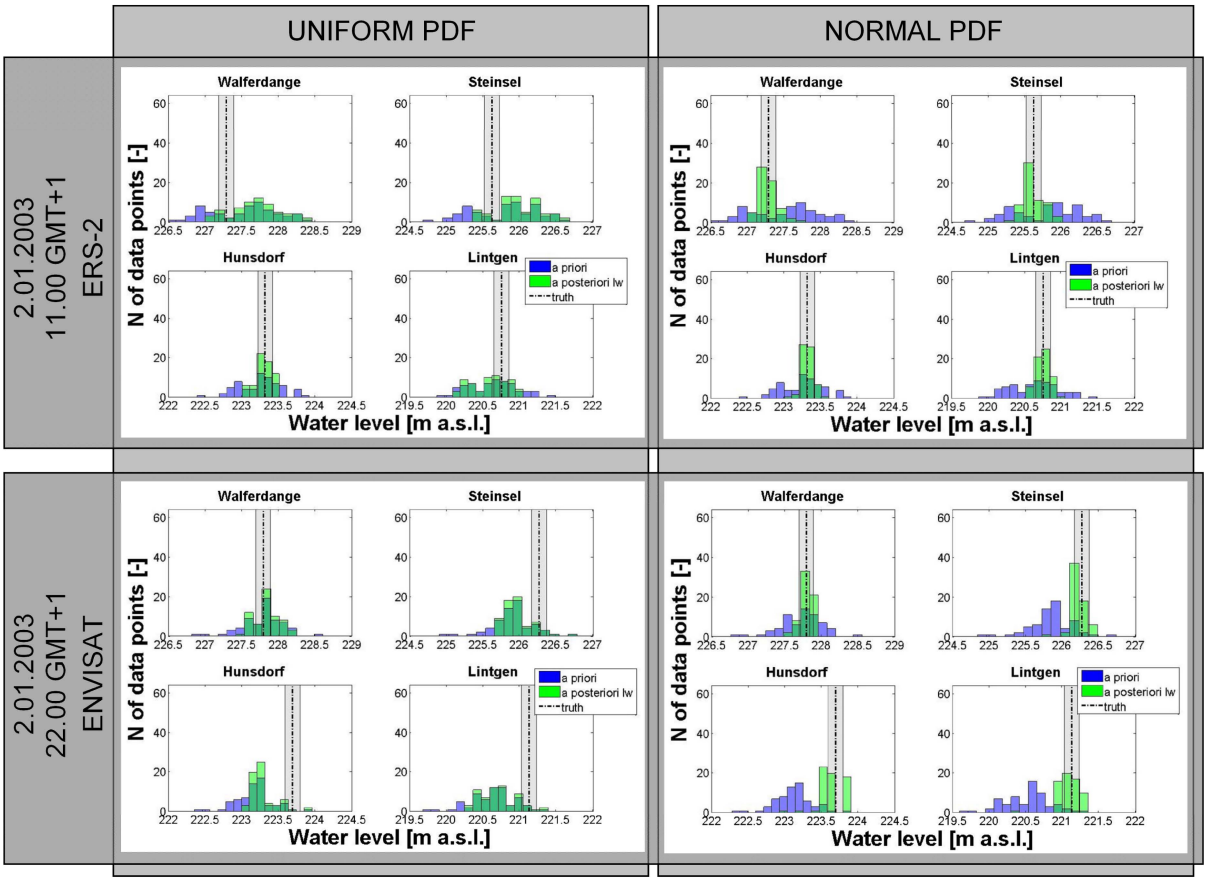

Fig. 10. Idem Fig. 8, but applying the local weighting approach for every location along the river (lw: local weight).

assumption of constant relative errors, the inflow correction model is reliable only during flow recession periods.

5 Conclusions

Our case study illustrates advantages and drawbacks related to the application, in a quasi-operational context, of a PF-based assimilation of RSD water levels into a hydraulic model. Two variants of the PF, based respectively on local weighting and global weighting procedures, are proposed. In the global weighting procedure, a single particle contains water levels at all cross sections as state vector. Hence, the likelihood for each particle is derived from its ability to correctly predict water levels along the entire river reach. The local weighting procedure attributes a separate particle set to each cross section (i.e. a single particle has the water level from one cross section as state vector) and thus associates likelihoods to each particle according to its ability to correctly predict water stage at a given cross section. The experiment concludes with the following findings.

1. Matgen et al. (2010) demonstrated through a series of synthetic experiments with unbiased model forecasts and observations that a PF-based assimilation scheme enables the sequentially updating of flood forecasting models. The filter helps to correct for errors in the forcings and guides the recovery of the correct water depth over a modelled river reach. In our real-event case study, even according to the best-case scenario when precise in situ measurements are assimilated into a hydraulic model, difficulties arise from the fact that model accuracy varies in space. This makes it difficult for a global weighting procedure to identify a model run that performs equally well at all cross sections. In fact, input errors are not the only source of model uncertainty. Parameter uncertainty and geometry errors, as well as intermediate inflow errors, lead to locally biased model results. Therefore, an assimilation scheme that is based on a local weighting procedure seems to be the preferred solution when dealing with a model that cannot be well calibrated and when observations with a very low uncertainty are to be assimilated.

2. Before any assimilation of data, the set-up and calibration of the hydraulic model are of paramount importance. It is important to bear in mind that the Particle

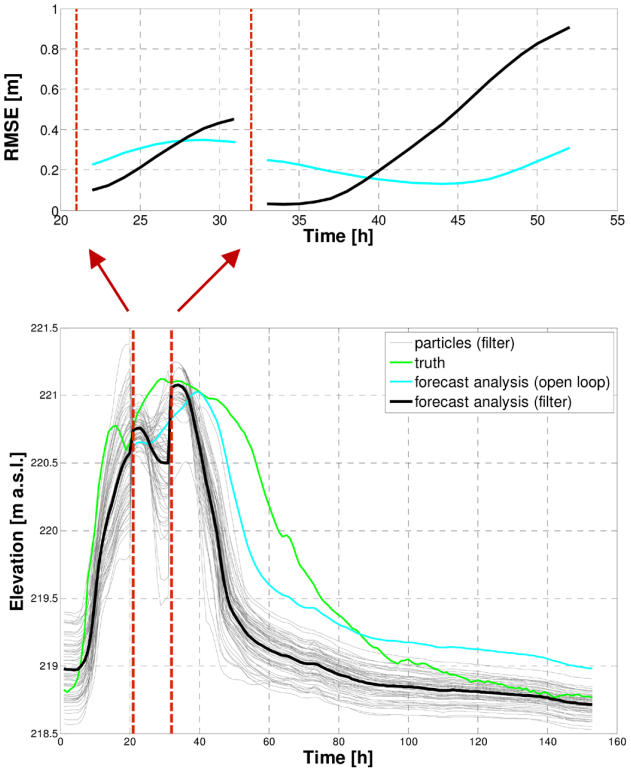

Fig. 11. Idem Fig. 9, but for the local weighting procedure and the assimilation of the ground measurements.

Filter (and also the Kalman Filter) is a method designed to filter noise, not systematic errors. Our results show that this is particularly important when in situ measurements are assimilated, because there is a significant risk that the performance of a model at a local level is not truly representative for its behaviour at a regional level. In this case, the assimilation can potentially lead to a deterioration of model performance.

3. The quality of the observation data is the second factor that largely determines the effectiveness of the filter. In instrumented basins with well-calibrated models, the hydrodynamic model uncertainty appears low compared to currently available remote sensing observation uncertainty. Nevertheless, our experiment shows that forecast improvements are achievable with currently existing SAR data. However, there is a need to take into account the possibility of bias in the observation data. A PF that is based on a local weighting procedure is the preferred solution when assimilating unbiased and/or very precise observations as it helps to identify the true water surface line at the time of data acquisition. In ungauged basins where RSD water levels are the only available data source, the PF with a global weighting procedure is to be recommended. Certainly, methodologies for retrieving water levels from remote sensing observations need to be improved. The availability of VHR SAR satellites and the global DEMs with increased accuracy can be used to further reduce uncertainty and bias of such data sets. The hydraulic coherence concept that was applied in this study is another step forward. We show that observational uncertainty can be significantly reduced by using hydraulic rules governing overland flow in a floodplain to correct unrealistic water levels.

4. Our results further show the added value of RSD water levels when compared to in situ measurements. Both data sets appear to be complementary. In situ measurements are precise and provide time-continuous data. However, the data sets are only available as point measurements, which can lead to the over- or under-correction of models. The RSD information provides distributed water level information over many cross sections. The uncertainty of water stage estimates inferred from currently operating sensors, as well as sampling rates of 24 h and less, represent serious limitations. The combination of both data sets likely yields the best assimilation results but more research on this topic is required.

5. For operational applications, it is important to achieve a persistent improvement of the forecasts as a result of a PF-based assimilation of water stage data. Due to the dominant effect of the upstream boundary condition, this means that the results of the analysis need to be used to correct erroneous inflow data. Although this study focused mainly on an improvement of the analysis step, two limitations of the initially proposed inflow correction model are highlighted. First, it becomes obvious that the analysis step is of paramount importance for carrying out an efficient inflow correction: errors in the analysis propagate through the inflow correction model, thereby potentially degrading the skill of the forecasts. Second, the error prediction model itself needs to be reviewed as it is clearly shown that the underlying assumption of constant relative errors is not valid, especially during the rising limb of the hydrograph. Hence, we advocate the development of enhanced error prediction models.

Moreover, future research should consider the application of the proposed assimilation scheme to longer river reaches. We believe that the approach we introduced in this paper has the highest potential for model improvements in large river systems that are poorly gauged but which could benefit from the use of globally and freely available remote sensing data (see also Schumann et al., 2010). In fact, when the ultimate objective is the use of updated levels for flood forecasting applications, we hypothesize that in larger river systems the dominating effect of the boundary condition is reduced and this would indeed favor more persistent model improvements

through data assimilation procedures. Moreover, the application of the proposed assimilation scheme to other case studies will lead to a better understanding of the scaling issue linking the length of the river reach to the model forecast performance.

Acknowledgements. This study was part of the HYDRASENS project, financed by the National Research Fund (FNR) of the Grand Duchy of Luxembourg and the Belgian Federal Science Policy Office in the framework of the STEREO II research programme (Contract nr. SR/00/100). Renaud Hostache was funded by the FLOODTRACKER project, financed by the National Research Fund (FNR) of the Grand Duchy of Luxembourg in the framework of the CORE research programme. Gabriëlle De Lannoy is a postdoctoral research fellow of the Research Foundation Flanders (FWO) and a visiting scientist at NASA/GSFC. The authors wish to thank the Reviewers G. Di Baldassarre, D. Yamazaki and J. Neal as well as the Editor A. Weerts for their valuable suggestions and comments.

Edited by: A. Weerts

References

Alsdorf, D. E., Rodriguez, E., and Lettenmaier, D. P.: Measuring surface water from space, Rev. Geophys., 45, RG2002, doi:10.1029/2006RG000197, 2007.

Andreadis, K. M., Clark, E. A., Lettenmaier, D. P., and Alsdorf, D. E.: Prospects for river discharge and depth estimation through assimilation of swath-altimetry into a raster-based hydrodynamics model, Geophys. Res. Lett., 34, L10403, doi:10.1029/2007GL029721, 2007.

Bates, P. D. and De Roo, A. P. J.: A simple raster-based model for floodplain inundation, J. Hydrol., 236, 57–77, doi:10.1016/S0022-1694(00)00278-X, 2000.

Biancamaria, S., Durand, M., Andreadis, K. M., Bates, P. D., Booneg, A., Mognard, N. M., Rodriguez, E., lsdorf, D. E., Lettenmaier, D. P., and Clark, E. A.: Assimilation of virtual wide swath altimetry to improve Arctic river modeling, Remote Sense. Environ., 115(2), 373–381, doi:10.1016/j.rse.2010.09.008, 2010.

Burgers, G., Leeuwen, P. J. V., and Evensen, G.: Analysis scheme in the ensemble Kalman filter, Mon. Weather Rev., 126, 1719–1724, 1998.

Dai, Y., Zeng, X., Dickinson, R. E., Baker, I., Bonan, G., Bosilovich, M., Denning, S., Dirmeyer, P., Houser, P., Niu, G., Oleson, K., Schlosser, C. A., and Yang, Z.-L.: The common land model (CLM), B. Am. Meteorol. Soc., 84, 1013–1023, 2003.

De Lannoy, G. J. M., Houser, P. R., Pauwels, V. R. N., and Verhoest, N. E. C.: Assessment of model uncertainty for soil moisture through ensemble verification, J. Geophys. Res., 111, D10101, doi:10.1029/2005JD006367, 2006.

De Lannoy, G. J. M., Houser, P. R., Pauwels, V. R. N., and Verhoest, N. E. C.: State and bias estimation for soil moisture profiles by an ensemble Kalman filter: Effect of assimilation depth and frequency, Water Resour. Res., 43(6), W06401, doi:10.1029/2006WR005100, 2007.

Di Baldassarre, G., Schumann, G., and Bates, P. D.: Near real time satellite imagery to support and verify timely flood modeling, Hydrol. Process., 23, 799–803, doi:10.1002/hyp.7229, 2009.

Durand, M., Andreadis, K. M., Alsdorf, D. E., Lettenmaier, D. P., Moller, D., and Wilson, M. D.: Estimation of bathymetric depth and slope from data assimilation of swath altimetry into a hydrodynamic model, Geophys. Res. Lett., 35, L20401, doi:10.1029/2008GL034150, 2008.

Evensen, G.: Sequential data assimilation with a nonlinear quasi-geostrophic model using Monte Carlo methods to forecast error statistics, J. Geophys. Res., 99(C5), 10143–10162, 1994.

Fearnhead, P.: Markov chain Monte Carlo, sufficient statistics, and particle filters, J.Comput. Graph. Stat., 11, 848–862, 2002.

Gordon, N., Salmond, D., and Smith, A. F. M.: Novel approach to nonlinear and non-Gaussian Bayesian state estimation, in: Proceedings of the Institute of Electrical Engineering, Part F, 140, 107–113, 1993.

HEC-RAS 4.0: online available at: http://www.hec.usace.army.mil/software/hec-ras/index.html, last access: 20 July 2011.

Hostache, R., Matgen, P., Schumann, G., Puech, C., Hoffmann, L., and Pfister, L.: Water level estimation and reduction of hydraulic model calibration uncertainties using satellite SAR images of floods, IEEE T. Geosci. Remote, 47, 431–441, 2009.

Lee, H., Durand, M., Jung, H., Alsdorf, D., Shum, C. K., and Sheng, Y.: Characterization of surface water storage changes in Arctic lakes using simulated SWOT measurements, Int. J. Remote Sens., 31(14), 3931–3953, 2010.

Madsen, H. and Skotner, C.: Adaptive state updating in real-time river flow forecasting a combined filtering and error forecasting procedure, J. Hydrol., 308, 302–312, 2005.

Martinis, S., Twele, A., and Voigt, S.: Towards operational near real-time flood detection using a split-based automatic thresholding procedure on high resolution TerraSAR-X data, Nat. Hazard Earth Sys. Sci., 9, 303–314, 2009.

Mason, D. C., Devereux, B., Schumann, G. J.-P., Neal, J. C., and Bates, P. D.: Flood detection in urban areas using TerraSAR-X, IEEE T. Geosci. Remote, 48(2), 882–894, 2010.

Matgen, P., Schumann, G., Pappenberger, F., and Pfister, L.: Sequential assimilation of remotely sensed water stages in flood inundation models, in: Remote Sensing for Environmental Monitoring and Change Detection (Proceedings of Symposium HS3007 at IUGG2007, Perugia, July 2007), IAHS Publ. 316, 2007, 78–88, 2007.

Matgen, P., Montanari, M., Hostache, R., Pfister, L., Hoffmann, L., Plaza, D., Pauwels, V. R. N., De Lannoy, G. J. M., De Keyser, R., and Savenije, H. H. G.: Towards the sequential assimilation of SAR-derived water stages into hydraulic models using the Particle Filter: proof of concept, Hydrol. Earth Syst. Sci., 14, 1773–1785, doi:10.5194/hess-14-1773-2010, 2010.

Matgen, P., Hostache, R., Schumann, G., Pfister, L., Hoffmann, L., and Savenije, H. H. G.: Towards an automated SAR-based flood monitoring system, Lessons learned from two case studies, Phys. Chem. Earth, 36(7–8), 241–252, doi:10.1016/j.pce.2010.12.009, 2011.

Montanari, M., Hostache, R., Matgen, P., Schumann, G., Pfister, L., and Hoffmann, L.: Calibration and sequential updating of a coupled hydrologic-hydraulic model using remote sensing-derived water stages, Hydrol. Earth Syst. Sci., 13, 367–380, doi:10.5194/hess-13-367-2009, 2009.

Moradkhani, H., Hsu, K.-L., Gupta, H., and Sorooshian, S.: Uncertainty assessment of hydrologic model states and parameters: Sequential data assimilation using the particle filter, Water Resour.

Res., 41, W05012, doi:10.1029/2004WR003604, 2005.
Moradkhani, H.: Hydrologic Remote Sensing and Land Surface Data Assimilation, Sensors, 8, 2986–3004, doi:10.3390/s8052986, 2008.
Neal, J. C., Atkinson, P. M., and Hutton, C. W.: Flood inundation model updating using an ensemble Kalman filter and spatially distributed measurements, J. Hydrol., 336, 401–415, 2007.
Neal, J., Schumann, G., Bates, P. D., Buytaert, W., Matgen, P., and Pappenberger, F.: A data assimilation approach to discharge from space, Hydrol. Process., 23, 3641–3649, 2009.
Pauwels, V. R. N. and De Lannoy, G. J. M.: Ensemble-based assimilation of discharge into rainfall-runoff models: A comparison of approaches to mapping observational information to state space, Water Resour. Res., 45, W08428, doi:10.1029/2008WR007590, 2009.
Raclot, D.: Remote sensing of water levels on floodplains: a spatial approach guided by hydraulic functioning, Int. J. Remote Sens., 27, 2553–2574, 2006.
Schumann, G., Matgen, P., Pappenberger, F., Hostache, R., and Pfister, L.: Deriving distributed roughness values from satellite radar data for flood inundation modeling, J. Hydrol., 344, 96–111, 2007.
Schumann, G., Matgen, P., Pappenberg, F.: Conditioning water stages from satellite imagery on uncertain data points, IEEE T. Geosci. Remote, 4, 81-813, 2008.
Schumann, G., Bates, P. D., Horritt, M. S., Matgen, P., and Pappenberger, F.: Progress in integration of remote sensing-derived flood extent and stage data and hydraulic models, Rev. Geophys., 47, RG4001, doi:10.1029/2008RG000274, 2009.
Schumann, G., Di Baldassarre, G., Alsdorf, D, and Bates, P. D.: Near real time flood wave approximation on large rivers from space: application to the River Po, Northern Italy, Water Resour. Res., 46, W05601, doi:10.1029/2008WR007672, 2010.
Smith, P. J., Beven, K. J., and Tawn, J. A.: Detection of structural inadequacy in process-based hydrological models: A particle-filtering approach, Water Resour. Res., 44, W09403, doi:10.1029/2005WR004093, 2008.
Zwenzner, H. and Voigt, S.: Improved estimation of flood parameters by combining space based SAR data with very high resolution digital elevation data, Hydrol. Earth Syst. Sci., 13, 567–576, doi:10.5194/hess-13-567-2009, 2009.

5. SYNTHESIS

5.1. Conclusions

This thesis offered a number of insights into the progresses towards the implementation of an end-to-end processing chain that integrates remote sensing information into hydraulic models.

A first step in this direction concerns the development of an algorithm that is capable of providing satisfactory results in mapping, in a completely unsupervised way, flood extents in both rural and urban areas. The latter is the most challenging environment, due to man-made features, but it also represents the area where flooding is a major hazard, as a consequence of the increased risks to life and property in such a region. Build-up environments are therefore at the centre of the interest of stakeholders in flood management and civil protection agencies.

A fully automated SAR mapping algorithm was here developed to enable the automated, objective, and reliable flood extent extraction from SAR data (Giustarini et al., 2013), both in rural and urban areas. It is a hybrid methodology that integrates statistical modelling of backscatter values attributed to water bodies with backscatter thresholding, region growing and change detection. This combination of different image treatment techniques aims to combine their respective strengths, limiting at the same time their own shortcomings, if considered individually.

The main advantage of the proposed algorithm lies in the fact that no manual and subjective user input is required from the user, enabling therefore automated flood detection. The flood mapping procedure of Giustarini et al. (2013) automatically optimizes all its parameters, overcoming one of the limitations of Matgen et al. (2010), i.e. the presence of a parameter with a fixed a-priori value. Building on the conclusion of the same paper, the developed algorithm include an "all-at-once" calibration that optimizes all algorithms' parameters, including the region growing threshold parameter. The method operates with minimum data requirements and it efficient in terms of computational time, a characteristic that is fundamental for near real time applications. The algorithm is also currently hosted in the Grid Processing On Demand (G-POD) platform of the European Space Agency (https://gpod.eo.esa.int/).

The use of a couple flood/reference images enables the creation of a mask of permanent surface-like radar response areas (tarmac, paved roads, parking lots) and of shadow-affected regions. These areas, not visible to the satellite, are then removed from the final flood map. The merit of this approach is that, other than the flood image, it only requires one additional input, which is the reference image, to produce such a mask of "undetectable" areas. On the other hand, the algorithm of Mason et al. (2010) necessitates of two additional inputs, i.e. a high-resolution DEM and a SAR simulator. A potential issue of the method of Giustarini et al. (2011) concerns the number of suitable candidate images, which can be (currently) limited in case of relatively new satellites. However, it is important to note that image archives are gradually being built up, which

will progressively increase the likelihood of finding adequate reference images in the online archives in the near future.

This algorithm of Giustarini et al. (2013) overcomes some limitations of previous methods. In particular, with minimum data requirements and taking advantage of change detection, it allows mapping rural and urban flooding, in a completely unsupervised way, providing accurate and reliable results. The challenging test case of flooding in the city of Twekesbury (UK) proved that the algorithm is capable of mapping urban flooding with good accuracy. Nevertheless, further technological and methodological improvements are still necessary for SAR-based flood detection algorithm in urban areas to match the mapping capability of high-quality aerial photography.

Some of the difficulties of mapping flood in urban environment were addressed by the use of a reference image. Concerning the issue of shadow areas, some progresses were possible through the use of change detection. Its strength lies in the fact that it allows the region growing to extend further into the high percentiles of the gamma distribution, as it efficiently removes part of the resulting overdetection. Here, it was assumed that the resulting overdetection might be addressed through change detection, since urban shadow areas do not change between two images acquired with the same imaging characteristics. The main part of the misclassification can be imputed to limitations of the SAR imaging techniques. On the other hand, one of the remaining limitations is the detection of flooding in layover regions.

A second drawback of the algorithm of Giustarini et al. (2013) is the assumption of bimodality in the image histogram. In the proposed method, an appropriate option is already available in case of non-bimodal histogram. It consists in the option, for the user, to manually set a range of plausible backscatter values, inside which the algorithm tests different modes searching for the optimal one. However, this violates the assumption of a complete level of automation, introducing subjectivity and reducing traceability and reproducibility.

Further research is still needed to improve the algorithm's performances and to do so it is also hypothesize that ancillary data (topography, land use, …) could play a significant role and should be included in all cases where higher classification accuracy is needed.

A rapid access to the archive of images is also of paramount importance for an algorithm based on change detection. Moreover, in a crisis management context, it is well known that the value of remote sensing information rapidly decreases (Matgen et al., 2007). The time delay between image acquisition and distribution of flood information needs thus to be substantially shortened, if current and future SAR satellite missions are to be routinely used for flood observations.

Moving to the analysis of flood mapping uncertainty, the paper of Giustarini et al. (2015a) investigated the influence of speckle on both the image histogram and the resulting flood map. To investigate the propagation of this component of uncertainty, from the SAR image to the final map, the algorithm of Giustarini et al. (2013) was applied.

From the original SAR image, several synthetic images were generated by bootstrapping the image pixels. Visual inspection of the different histograms of the synthetic images showed minimal differences. This outcome was confirmed by similar values, in terms of the flood

mapping algorithm's parameters, when the synthetic images were provided as input to the code of Giustarini et al. (2013). From this it was concluded that speckle uncertainty could be considered as a negligible component of the total uncertainty. Additionally, flood maps obtained from the synthetically generated images were compared against validation data, concluding that also in terms of classification accuracy the influence of speckle uncertainty can be regarded as minor.

Next key tasks will be the analysis of other uncertainty components, such as other imaging characteristics (e.g. imaging modes, resolution) and/or ground perturbations (e.g. wind, trees, buildings masking water, terrain geometry).

A further conclusion of this paper concerned the identification of the smallest number of synthetic images needed to adequately describe uncertainty due to speckle. From the initial number of 1000 images, it was found that an ensemble of 200 would still be correctly representative of speckle uncertainty. Nevertheless, for near real time applications such a number is still too high, particularly w.r.t. the fact that only one component of the total uncertainty is addressed.

The final step of the proposed end-to-end processing chain is the actual integration of remote sensing information into hydraulic models. This was performed through data assimilation, using a PF to weigh the different ensemble members.

Real event water elevations were assimilated into a properly adapted version of the PF of Matgen et al. (2010), modified to deal with non-Gaussian distribution of observations. The flexibility of the assimilation filter was tested considering uniform distribution of observations, envisaging also the exploitation of the full empirical distribution of water elevations. Unfortunately, for the specific test case, the uncertainty of the full empirical distribution in SAR-derived water elevations was too high to prove useful in the specific assimilation study.

To deal with model structure error and, at the same time, possibly biased observations, a global and a local weight variant of the PF were tested. The variant to be preferred depends on the level of confidence that is attributed to the observations or to the model. It was found that an assimilation scheme based on a local weighting procedure seems to be the preferred solution when dealing with a model that cannot be well calibrated and also when unbiased and/or very precise observations are to be assimilated. In ungauged basins, where remote sensing derived water elevations are the only available data source, the PF with a global weighting procedure is to be recommended.

The availability of two subsequent satellite observations allowed testing the capability of error prediction model to correctly update the input discharge to the model. It was found that the underlying assumption of constant relative errors is not valid in a real case study, especially during the rising limb of the hydrograph. Therefore, future research will deal with the revision of the error prediction model.

The study of Giustarini et al. (2011) also highlighted the complementarity of remote sensing derived and in-situ data sets. In-situ measurements are precise and provide time-continuous data but they are only available as point measurements, which can lead to the over- or undercorrection

of models. On the other hand, the remote sensing derived information provides distributed water level information over many cross sections but only at times of satellite overpasses.

A major limitation of the proposed method is the fact that the step of water elevations extraction, intersecting a DEM and a mapped flood extent, tend to be a rather time consuming task, which hampers the application of this approach in near real time.

5.2. Further applications

In addition to the material presented in this thesis, some recent developments have been proposed to deal with several limitations of the presented approach.

5.2.1. Further improvements in flood mapping

One of the limitations of the algorithm of Giustarini et al. (2013) is the assumption of bimodality in the image histogram. As anticipated, in case the image histogram is not bimodal, the optimization of the theoretical curve describing the water pixels has to be manually constrained in a user-defined range. This violates the assumption of a complete level of automation. To overcome this shortcoming, Lu et al. (2014) proposed an alternative procedure for core water body identification, in case of non-bimodal image histogram. In their method, the statistical distribution of the "open water" backscatter is derived through a difference image obtained from the flood and the reference ones. After a mask of core water bodies is identified in the difference image, the mask itself is applied on the flood image to extract the pixels located in the core water bodies and estimate on the histogram obtained with only those pixels the statistical distribution of the "open water" backscatter. Experimental results with two pairs of SAR images showed accurate classification accuracy, for images characterized by non-bimodal histograms. With respect to the algorithm of Giustarini et al. (2013), the method of Lu et al. (2014) is characterized by an increased robustness in detecting floods in SAR images is its robustness, obtained without losing accuracy and efficiency.

A remaining limitations of the algorithm of Giustarini et al. (2013) was the detection of flooding in layover regions. The more recent paper of Mason et al. (2014) investigated the use of double scattering to detect urban flooding in layover regions, where flooding may not normally be apparent. In this paper, urban flooding was successfully detected in layover regions using double scattering between the (possibly flooded) ground surface and the walls of adjacent buildings. The authors tested their approach, both including and excluding a change detection step between flood and reference image, obtaining similar results.

In spite of the progress in the development of flood mapping procedures, the detection of inundation in vegetated and urban areas still represents a critical issue. The presence of water is rarely detectable in an unambiguous way with intensity SAR data alone (i.e., the backscattering coefficient sigma nought) because, especially in urban environments, multiple effects influence the radar response. To fully exploit available SAR data, SAR interferometric coherence represents a potentially valuable technique. While the usefulness of the coherence for detecting water in

open space has been demonstrated in several studies (Marinelli et al., 1997; Nico et al., 2000; Refice et al., 2014), first insights on how this feature can be used to detect water in urban areas have been reported only recently. For example, Chini et al. (2012) analysed the use of COSMO-SkyMed data for the floods caused by the 2011 tsunami in Japan. Franceschetti et al. (2002) showed that the double bounce effect in urban areas is typically represented in SAR images by a very bright line that appears on the side of the wall that is illuminated by the radar. However, using the model developed by Ferro et al. (2011), which assumes for simplicity an isolated building, Pulvirenti et al. (under review) found that even in an ideal situation of an isolated building surrounded by a homogenous ground surface, the increase of the double bounce due to the presence of floodwater is not very high, if buildings are not aligned parallel to the SAR flight direction. This increase can hardly be detected through an intensity change detection approach in a complex urban environment, where the assumption of isolated buildings is often unrealistic. Hence, an idea would be to integrate intensity data with other features extracted from SAR data, such as the coherence. The interferometric coherence is basically a measurement of the degree of correlation between two complex (phase and amplitude) SAR images. It is defined as the normalized cross correlation between the images (Zebker and Villasenor, 1992). It is particularly related to the change in the spatial arrangement of the scatterers within a SAR image pixel (Chini et al., 2015), and thus to geometric changes in the scene. An interferometric pair can be built using two images taken before the flood (hereafter denoted as pre-event pair), after the flood (post-event pair) or one image before and another after the flood (co-event pair). It is expected that flooded areas will exhibit low coherence, which helps distinguishing them from non-flooded regions (especially over targets such as urban areas) where this feature is expected to be high. These considerations suggest that a coherence change detection approach could effectively complement one that is solely based on intensity change detection.

An additional improvement in terms of flood mapping and its uncertainty would be the generation of flood probabilistic maps. All the previously mentioned mapping algorithms provide flood extent estimates in the form of binary maps. In other words, each pixel is classified either as flooded or as non-flooded, without any uncertainty to characterize its status. As an alternative, flood extent estimates could be expressed in the form of probabilistic maps, where the estimated condition of any given pixel is represented by a continuous probability in the range [0, 1]: with 0 indicating pixels that are certainly dry, 1 indicating pixels that are certainly flooded, and intermediate values indicating an intermediate probability of a pixel being flooded. A map displaying uncertainty in the prediction of each pixels' status would represent a precious source of information, in the sense that it would show pixel by pixel the level of confidence of the output map. For example, pixels with a value of 1 (flooded) or of 0 (non-flooded) are characterized by no uncertainty: they are located in the core of the water bodies, either permanent or temporary, or considerably far away from the river network and/or on regions raised about the river network, respectively. This lack of uncertainty will make these pixels the less problematic areas in terms of decision making. On the other hands, pixels with a probabilistic value of ~0.5 will be the most uncertain, requiring to be treated with caution by decision makers. They are presumably located in the transition area between the core of water bodies and the non-flooded regions around them.

In literature, some attempts to characterise uncertainties in flood extent maps have been proposed, based on random realisations of potential sources of uncertainty (e.g. Hostache et al. 2006; 2009; Schumann et al., 2008a; Di Baldassarre et al., 2009; Giustarini et al., 2015a), but these studies tend to be rather time consuming and do not characterise uncertainty from a statistical point of view, necessary for assimilation purposes.

A possibility to explore is an approach inspired by the algorithms of Giustarini et al. (2013) and based on a Bayesian framework. The idea is to use the first part of the flood mapping algorithm to decompose the image histogram in its two components and then to estimate the probability of a pixel to be flooded, conditioned on its backscatter value, with a Bayesian approach (Giustarini et al., 2015b). The method is composed of two steps. First, the statistical distribution of open water backscatter in the flood image is estimated. Assuming that the image histogram is composed of two populations (flooded and non-flooded), subtracting the statistical distribution of open water from the total image histogram, the statistical distribution of non-flooded pixels can be obtained. Second, in the framework of a Bayesian approach, the probability of being flooded of each pixel is derived based on its backscatter value, using two sets of probabilities: the already computed two probability distributions of the two populations and two prior probabilities of pixels status, which have to be estimated.

5.2.2. Data Assimilation in a broader context

In a broader context, it is interesting to report two more applications of the same data assimilation algorithm of Giustarini et al. (2011). The first study, still concerning the field of hydrology, uses the same PF assimilation scheme and assimilates the same type of satellite derived observations, i.e. water elevations, of Giustarini et al. (2011). However, here the aim is the retrieval of riverbed bathymetry. A second study moves to the research field of crop growth modelling and presents an adaption of the PF assimilation scheme of Giustarini et al. (2011). In this case, also the assimilated observations are different, being derived from multi spectral satellite data. These studies show the flexibility of such an assimilation scheme based on the PF and its usefulness for different research and application fields.

The study by Hostache et al. (2015) used the same PF developed in Giustarini et al. (2011) to assimilate synthetic observations of water elevations, similar to those that can be expected to be measured by a drifting buoy floating along a river reach. The idea is to evaluate the potentiality of Global Navigation Satellite System (GNSS), like for instance Global Positioning System (GPS), for measuring such data. These observations of water elevations would be extremely beneficial if assimilated into hydraulic models to retrieve riverbed bathymetry, which is generally rarely available but mandatory for accurate hydrodynamic modelling. Synthetic observations of a drifting buoy were generated assuming a 30 cm average error of water surface elevation measurements. By assimilating the synthetic observation into a 1D hydrodynamic model, it was shown that the riverbed bathymetry can be retrieved with an accuracy of 36 cm. Moreover, the water surface elevations simulated by the hydro dynamic model using the retrieved bathymetry were found to be in good agreement with the synthetic "truth", exhibiting an RMSE of 27 cm.

In the paper of Machwitz et al. (2014), a second application of the developed PF assimilation scheme was tested in a the research field of crop growth modelling. The coupling of a crop growth model (CGM) with a radiative transfer (RTM) model offers the possibility to assimilate remote sensing data and to overcome uncertainties in input parameters and settings. The particle filter of Giustarini et al. (2011) was adapted to assimilate spectra observations and later used to assimilate multi spectral satellite data into the CGM APSIM, coupled with the RTM PROSAIL. As the PF does not require Gaussian distribution of the parameters and is capable of dealing with non-linear models, it provides a flexible method to integrate any remote sensing data into a coupled CGM-RTM. The method was applied for maize fields in Luxembourg. First, to test the applicability and the robustness of the algorithm, a synthetic experiment in a completely controlled environment was setup. The suitability of synthetically generated RapidEye and Sentinel-2 data was tested. The spectral resolution of both sensors proved to be capable of improving model forecasts after assimilation. A major outcome of the synthetic experiment was highlighting the importance of the remote sensing acquisition time. Only assimilations performed in a limited time window of 20 days between Day Of the Year 175 and 195 was found to provide a significant improvement in model forecast. The real case study with observed RapidEye data from 2010 confirmed these findings. In the optimal time window determined through the synthetic experiment, data assimilation lead to a significant increase of accuracy (up to 36%) in model forecast. In some of the case studies, accuracy did not vary (1-2%) and this happened mainly for situations where biomass prediction in the open-loop was already quite accurate. It is important to mention that a CGP like APSIM provides only one value (at each time stamp) for an entire test site area. This mean that the entire polygonal region will be attributed the same unique value modelled in APSIM. The added value of data assimilation, through the coupling with spatially distributed remote sensing observations, is that assimilation can be performed pixel by pixel, obtaining after assimilation a spatial distribution of different forecasted values inside the given polygon. This is a move beyond point information, as generally provided by models, towards spatially distributed predictions.

6. PERSPECTIVES

Before the proposed end-to-end processing chain can be turned into practice, several improvements are needed. In terms of user access to satellite data, efforts should be made towards a reduction of the latency time, i.e. time between the acquisition of an image and the moment it is available to the user. It goes without saying that a rapid access to images would increase the efficiency of the proposed method. Concerning the issue of time, while the described flood mapping algorithm has been proved of having time-efficient performances, the bottleneck of the procedure remains in the accessibility to the SAR images.

Nevertheless, faster and automated procedures are still needed to extract water elevations from detected flood extents. Moving towards an approach purely based on satellite observations, the availability of global DEM with high resolution, such as the WorldDEM DTM, would be welcome. This would render the processing chain independent from the existence of a local LiDAR DEM.

This remains valid as long as the variable assimilated into hydraulic model is water elevation. In fact, assimilation of flood extent could be envisaged for the first time if observations in terms of probabilistic maps could be obtained, replacing the currently used binary maps (flooded/nonflooded).

Such a probabilistic map (Giustarini et al., 2015b) would offer exciting opportunities for reducing the number of inputs and steps required before data assimilation can be performed. For example, the need of a DEM to derive water elevation would be relieved and, with this, the corresponding and generally time-consuming, step of water elevation computation. For a reliable assessment of flood mapping uncertainty and a subsequent successful data assimilation, a probabilistic map would need to take into account all other uncertainty components, rather than the simple speckle effect (Giustarini et al., 2015a).

Eventually, for flood mapping applications, systematic and more frequent acquisition would be of paramount importance to improve model forecast. The upcoming Sentinel 1 mission offer a unique opportunity to observe the Earth with a short revisit interval, essential to capture highlydynamic basin-scale hydrological processes, coupled with high-spatial resolution imaging characteristics.

6.1. Flood hazard mapping

A move beyond pure mapping of flood from satellite would be the assignment of a non-exceedance probability (and corresponding return period) to the retrieved pattern of an inundation. Flood risk mapping from space would be then achieved, combining several imaged inundations with their attributed return periods.

Traditional approaches for flood risk mapping are based on a cascade of process-based models. A hydraulic model is set up for the region of interest and design flood hydrographs of a given return period are routed through it (Alfieri et al., 2014). The general assumption is that the return period of the design hydrograph is attributed to the flood extent so obtained. While this procedure is commonly accepted as best practice, it is well known that this assumption is not always valid, particularly in situations where long river reaches are considered and long travel times and possible interactions between different tributaries play a significant role (Neal et al., 2013). That is why, in the framework of a comprehensive and standardized flood risk management at global scale, the development of a remote sensing-based flood hazard mapping method is of primary interest.

A flood hazard mapping approach purely based on satellite observations would be welcome by the scientific community, as it would have the merit of being accurate, robust and applicable throughout the world, particularly in regions where ground observations are not available. However, this approach is currently limited by the fact that collected time series of images are discontinuous and the time periods covered are not long enough to provide an estimate of flood inundation probability distributions.

Because of the aforementioned limitations of existing methods, a step change in large scale flood hazard mapping could be achieved by combining discontinuous (and typically short) series of remote sensing-derived flood inundation maps with a time-continuous (long) series of hydrological data. The assumption behind this approach is that observed inundations of the discontinuous series show a good correlation with the synchronous value of the hydrological variable in the continuous series. This has been proven true for the relationship between inundation and river discharge (Frazier and Page, 2009) and for the relationship between inundation and water height (Jung et al., 2011).

Huang et al. (2014) combined remotely sensed data obtained with Moderate Resolution Imaging Spectroradiometer (MODIS) and gauge observations of discharge, to derive a flood probability map over the Murray-Darling basin in Australia. The first step of the procedure is the selection of a point measurement, i.e. a stream gauge, which is assumed to be representative of a predefined floodable area. The choice is based on the understanding of the hydrology of the region in response to floods, with constrains related to the length and completeness of available data records, for reasons of statistical significance. An inherent limitation of this approach is therefore the type of hydrological variable used. Considering that river gauge networks tend to be poorly distributed and in decline, a global scale application of this method remains problematic.

As an alternative, a recent work (Giustarini et al., submitted) combines the global water information provided by the PDWC2012 (Pappenberger et al., 2012) model at high temporal (daily) and relatively coarse spatial (1 km) resolution with discontinuous but comparatively high spatial-resolution flood maps, derived from microwave remote sensing observations. The novelty of this study relies on the use of modelled time-continuous series of flood extent or volume that cover, on a global scale and with consistent quality, a period that is adequate for enabling statistical analysis. The study site is the Severn basin (UK), a data-rich catchment that allows for a comprehensive validation of the proposed procedure.

A first objective of this study is the analysis of correlation between satellite-derived flood extent and synchronous modelled variables, i.e. modelled flood extent and volume. Secondly, the aim is to explore the possibility of using variables derived from a global scale hydrodynamic model to attribute probabilities to satellite-derived flood maps. The idea behind such an approach is to highlight the complementarity of remote sensing-derived inundation maps and time-continuous modelled series for flood hazard mapping, building upon the availability for all regions of the world of a modelled time series of flood inundation map, both complete and of sufficient length for statistical analysis.

6.2. Assimilation of flood extent

The probabilistic map of Giustarini et al. (2015b) would be beneficial also for data assimilation studies.

Assimilation of hydraulic variables derived from remote sensing has gained momentum in recent years with several proof-of-concept studies, demonstrating the ability of these data to improve model predictions (Matgen et al., 2010; Hostache et al., 2010; Giustarini et al., 2011; Mason et al., 2012b). The observation most commonly assimilated is represented by water elevation data, at various points along the modelled reach. The above mentioned methods all make use of water elevations, which may be estimated indirectly along the flood extents in SAR images by intersecting flood extent and floodplain topography. This procedure cannot generally be performed in a real-time scenario, as it tends to be rather time-consuming.

The direct assimilation of flood extents into models would then be extremely beneficial, eliminating the intermediate step of water levels extraction. New data assimilation method will need to be developed to assimilate a 2D product such a probabilistic map. In fact, in a flood probabilistic map each pixel value represents the uncertainty associated with its status of being flooded. For example, pixels with a value of 1 (flooded) or of 0 (non-flooded) are characterized by no uncertainty and they will not be taken into account in the assimilation algorithm. On the other hands, pixels with a probabilistic value of ~0.5 will be the most uncertain and also crucial for assimilation applications. While the pixel value represents its uncertainty, the variable of interest, i.e. the pixel status, remains a binary one (flooded/non-flooded). A binary pdf can therefore be envisaged to assimilate into hydraulic models this type of observation as provided by a flood probabilistic map.

REFERENCES

Alfieri, L., Salamon, P., Bianchi, A., Neal, J., Bates, P., Feyen, L. (2014). Advance in pan-European flood hazard mapping. Hydrological Processes, 28, 4067-4077.

Aubert, D., Loumagne, C., Oudin, L. (2003). Sequential assimilation of soil moisture and streamflow data in a conceptual rainfall–runoff model. Journal of Hydrology, 280(1-4), 145-161.

Alsdorf, D.E., Rodríguez, E., Lettenmaier, D.P. (2007). Measuring surface water from space. Reviews of Geophysics, 45.

Andreadis, K.M., Clark, E.A., Lettenmaier, D.P., Alsdorf, D.E. (2007). Prospects for river discharge and depth estimation through assimilation of swath-altimetry into a rasterbased hydrodynamics model. Geophysical Research Letters, 34, L10403.

Bates, P.D., Horritt, M.S., Smith, C.N., Mason, D.C. (1997). Integrating remote sensing observations of flood hydrology and hydraulic modelling. Hydrological Processes, 11, 1777-1795.

Bates, P.D., Wilson, M., Horritt, M.S., Mason, D.C., Holden, N., Currie, A. (2006). Reach scale floodplain inundation dynamics observed using airborne SAR imagery. Journal of Hydrology, 328(1-2), 306-318.

Bates, P.D., Neal, J.C., Alsdorf, D., Schumann, G.J. (2013).Observing Global Surface Water Flood Dynamics. Surveys in Geophysics, 1-14.

Bazi, Y., Bruzzone, L., Melgani, F. (2005). An Unsupervised Approach Based on the Generalized Gaussian Model to Automatic Change Detection in Multitemporal SAR Images. IEEE Transactions on Geoscience and Remote Sensing, 43(4), 874-887.

Biancamaria, S., Durand, M., Andreadis, K., Bates, P., Boone, A., Mognard, N., Rodriguez, E., Alsdorf, D., Lettenmaier, D.P., Clark, E. (2011). Assimilation of virtual wide swath altimetry to improve Arctic river modeling. Remote Sensing of Environment, 115 (2), 373-381.

Brakenridge, G.R., Anderson, E., Nghiem, S.V., Caquard, S., Shabaneh, T. (2002). Flood warnings,flood disaster assessments, and flood hazard reduction: the roles of orbital remote sensing. Proceedings of the 30th International Symposium on Remote Sensing of the Environment, Honolulu, Hawaii, November 10-14, 4 p.

CEOS Disaster Risk Management Observation Strategy, Issue 2.1, CEOS ad hoc Disasters Team November 1 (2013).

Chini, M., Pulvirenti, L., Pierdicca, N. (2012). Analysis and Interpretation of the COSMO-SkyMed Observations of the 2011 Japan Tsunami. IEEE Geosciences and Remote Sensing Letters, 9(3).

Chini, M., Albano, M., Saroli, M., Pulvirenti, L., Moro, M., Bignami, C., Falcucci, E., Gori, S., Modoni, G., Pierdicca, N., Stramondo, S. (2015). Coseismic liquefaction phenomenon analysis by COSMO-SkyMed: 2012 Emilia (Italy) earthquake. International Journal of Applied Earth Observation and Geoinformation, 39, 65-78.

Di Baldassarre, G., Schumann, G., Bates, P.D. (2009). A technique for the calibration of hydraulic models using uncertain satellite observations of flood extent. Journal of Hydrology, 367(3–4), 276-282.

De Roo, A.P.J., Van Der Knijff, J., Horritt, M., Schmuck, G., De Jong, S.M. (1999). Assessing flood damages of the 1997 Oder flood and the 1995 Meuse flood. In: Proceedings of the Second International ITC Symposium on Operationalization of Remote Sensing, Enschede. The Netherlands, 16-20 August 1999, 8 pp (Published on CD-ROM).

Directive 2007/60/EC of the European Parliament and of the Council on the assessment and management of flood risks, published online: http://eur-lex.europa.eu/legalcontent/EN/TXT/PDF/?uri=CELEX:32007L0060&from=EN

Evensen, G. (1994). Sequential data assimilation with a nonlinear quasi-geostrophic model using Monte Carlo methods to forecast error statistics. Journal of Geophysical Research, 99(C5), 10143-10162.

Ferro, A., Brunner, D., Bruzzone, L., Lemoine, G. (2011). On the relationship between double bounce and the orientation of buildings in VHR SAR images. IEEE Geoscience and Remote Sensing Letters, 8, 612-616.

Franceschetti, G., Iodice, A., Riccio, D. (2002). A canonical problem in electromagnetic backscattering from buildings. IEEE Transanctions on Geoscience and Remote Sensing, 40(8), 1787-1801.

García-Pintado, J., Neal, J.C., Mason, D.C., Dance, S.L., Bates, P.D. (2013). Scheduling satellite-based SAR acquisition for sequential assimilation of water level observations into flood modelling. Journal of Hydrology, 495, 252-266.

García-Pintado, J., Mason, D., Dance, S.L., Cloke, H., Neal, J.C., Freer, J., Bates, P.D. (2015). Satellite-supported flood forecasting in river networks: a real case study. Journal of Hydrology, 523, 706-724.

Giustarini, L., Matgen, P., Hostache, R., Plaza, D., Pauwels, V.R.N., Lannoy, G.J., Keyser, R.D., Pfister, L., Hoffmann, L., Savenije, H.H.G. (2011). Assimilating SAR-derived water level data into a flood model: A case study. Hydrology and Earth System Sciences, 15, 2349-2365.

Giustarini, L., Hostache, R., Matgen, P., Schumann, G., Bates, P.D., Mason, D.C. (2013). A change detection approach to flood mapping in urban areas using TerraSAR-X. IEEE Transactions on Geoscience and Remote Sensing, 51(4), 2417-2430.

Giustarini, L., Viernieuwe, J., Verwaeren, J., Chini, M., Hostache, R., Matgen, P., Verhoest N.E.C., De Baets, B. (2015a). Accounting for image uncertainty in SAR-based flood

mapping. International Journal of Applied Earth Observation and Geoinformation, 34, 70-77.

Giustarini, L., Hostache, R., Chini, M., Matgen, P. (2015b). A probabilistic framework to characterize uncertainties in SAR-based flood mapping. Oral presentation at Mapping Water Bodies from Space 2015 ESA Conference (http://due.esrin.esa.int/mwbs2015/files/4_Giustarini_MWBS2015.pdf)

Giustarini, L., Chini, M., Hostache, R., Pappenberger, F., Matgen, P. (submitted to Remote Sensing of Environment) Flood hazard mapping combining hydrodynamic modelling and multi annual remote sensing data.

Hallegatte, S., Green, C., Nicholls, R.J., Corfee-Morlot, J. (2013). Future flood losses in major coastal cities. Nature Climate Change, 3, 802-806.

Heathman, G.C., Starks, P.J., Ahuja, L.R., Jackson, T.J. (2003). Assimilation of surface soil moisture to estimate profile soil water content. Journal of Hydrology, 279, 1-17.

Henderson, F.M., Lewis, A.J., eds. Principles and Applications of Imaging Radar , Manual of Remote Sensing, 3rd ed., v. 2. NY: John Wiley & Sons.

Hirabayashi, Y., Mahendran, R., Koirala, S., Konoshima, L., Yamazaki, D., Watanabe, S., Kim, H., Kanae, S. (2013). Global flood risk under climate change. Nature Climate Change, 3, 816-821.

Horritt, M.S. (1999). A statistical active contour model for SAR image segmentation. Image and Vision Computing, 17(3), 213-224.

Hostache, R., Puech, C., Schumann, G., Matgen, P. (2006). Estimation de niveaux d'eau en plaine inondée à partir d'images satellites radar et de données topographiques fines (estimation of water levels in a floodplain using satellite radar images and high resolution topographic data). Revue Télédétection (Remote Sensing Journal), 6(4), 325-343.

Hostache, R., Matgen, P., Schumann, G., Puech, C., Hoffmann, L., Pfister, L. (2009). Water level estimation and reduction of hydraulic model calibration uncertainties using satellite SAR images of floods. IEEE Transactions on Geoscience and Remote Sensing, 47, 431-441.

Hostache, R., Lai, X., Monnier, J., Puech, C. (2010). Assimilation of spatially distributed water levels into a shallow-water flood model. Part II: Use of a remote sensing image of Mosel River. Journal of Hydrology, 390(3-4), 257-268.

Hostache, R., Matgen, P., Giustarini, L., Teferle, F.N., Tailliez, C., Iffly, J.-F., Corato, G. (2015). A drifting GPS buoy for retrieving efficient riverbed bathymetry. Journal of Hydrology, 520, 397-406.

Jongman, B., Ward P.J., Aerts J.C.J.H. (2012). Global exposure to river and coastal flooding: Long term trends and changes. Global Environmental Change 22, 823-835.

Lai, X., Monnier, J. (2009). Assimilation of spatially distributed water levels into a shallow-water flood model. Part I: Mathematical method and test case. Journal of Hydrology 377(1-2), 1-11.

Lu, J., Giustarini, L., Xiong, B., Zhao, L., Jiang, Y., Kuang, G. (2014). Automated flood detection with improved robustness and efficiency using multi-temporal SAR data. Remote Sensing Letters, 5(3), 240-248.

Machwitz, M., Giustarini, L., Bossung, C., Frantz, D., Schlerf, M., Lilienthal, H., Wandera, L., Matgen, P., Hoffmann, L., Udelhoven, T. (2014). Enhanced biomass prediction by assimilating satellite data into a crop growth model. Environmental Modelling & Software, 62, 437-453.

Madsen, H., Skotner, C. (2005). Adaptive state updating in real-time river flow forecasting—a combined filtering and error forecasting procedure. Journal of Hydrology, 308(1), 302- 312.

Marinelli, L., Michel, R., Beaudoin, A., Astier, J. (1997). Flood mapping using ERS tandem coherence image: A case in southern France. 3rd ERS symposium on space at the service of our environment - ESA special publications, 4, 531-536.

Martinis, S., Twele, A., Voigt, S. (2009). Towards operational near real-time flood detection using a split-based automatic thresholding procedure on high resolution TerraSAR-X data. Natural Hazards and Earth System Sciences, 9(2), 303-314.

Mason, D.C., Speck, R., Devereux, B., Schumann, G.J.-P., Neal, J.C., Bates, P.D. (2010). Flood Detection in Urban Areas Using TerraSAR-X. IEEE Transactions on Geoscience and Remote Sensing, 48(2).

Mason, D.C., Davenport, I.J., Neal, J.C., Schumann, G.J-P., Bates, P.D. (2012a). Near real-time flood detection in urban and rural areas using high resolution Synthetic Aperture Radar images. IEEE Transactions on Geoscience and Remote Sensing, 50(8), 3041-3052.

Mason, D.C., Schumann, G.J.-P., Neal, J.C., Garcia-Pintado, J., Bates, P.D. (2012b). Automatic near real-time selection of flood water levels from high resolution Synthetic Aperture Radar images for assimilation into hydraulic models: a case study. Remote Sensing of Environment, 124, 705-716.

Mason, D.C, Giustarini, L., García-Pintado, J., Cloke, H.L. (2014). Detection of flooded urban areas in high resolution Synthetic Aperture Radar images using double scattering. International Journal of Applied Earth Observation and Geoinformation, 28, 150-159.

Matgen, P., Schumann, G., Pappenberger, F., Pfister, L. (2007). Sequential assimilation of remotely sensed water stages in flood inundation models. Remote Sensing for Environmental Monitoring and Change Detection (Proceedings of Symposium HS3007 at IUGG2007, Perugia, July 2007). IAHS Publ. 316, 78-88.

Matgen, P., Montanari, M., Hostache, R., Pfister, L., Hoffmann, L., Plaza, D., Pauwels, V.R.N., De Lannoy, G.J.M., Keyser, R.D., Savenije, H.H.G. (2010). Towards the sequential assimilation of SAR-derived water stages into hydraulic models using the particle filter: Proof of concept. Hydrology and Earth System Sciences, 14 (9), 1773-1785.

Matgen, P., Hostache, R., Schumann, G., Pfister, L., Hoffmann, L., Savenjie, H.H.G. (2011). Towards an automated SAR-based flood monitoring system: Lessons learned from two case studies. Physics and Chemistry of the Earth, 36 (7-8), 241-252.

Montanari, M., Hostache, R., Matgen, P., Schumann, G., Pfister, L., Hoffmann, L. (2009). Calibration and sequential updating of a coupled hydrologic-hydraulic model using remote-sensing derived water stages. Hydrology and Earth System Sciences, 13, 367-380.

Moradkhani, H. (2008). Hydrologic Remote Sensing and Land Surface Data Assimilation. Sensors, 8(5), 2986-3004.

Munich RE, Natural catastrophes first half of 2013, published online: http://www.munichre.com/site/corporate/get/documents_E-

2004907462/mr/assetpool.shared/Documents/0_Corporate%20Website/6_Media%20

Relations/Press%20Releases/2013/2013_07_09_natcat_en.pdf (2013).

Nico, G., Pappalepore, M., Pasquariello, G., Refice, A., Samarelli, S. (2000). Comparison of SAR amplitude vs. coherence flood detection methods- a GIS application. International Journal of Remote Sensing, 21, 1619-1631.

Neal, J.C., Atkinson, P.M., Hutton, C.W. (2007). Flood inundation model updating using an ensemble Kalman filter and spatially distributed measurements. Journal of Hydrology, 336, 401-415.

Neal, J.C., Schumann, G., Bates, P., Buytaert, W., Matgen, P., Pappenberger, F. (2009). A data assimilation approach to discharge estimation from space. Hydrological Processes, 23(25), 3641-3649.

Neal, J.C., Keef, C., Bates, P., Beven, K., Leedal, D. (2013). Probabilistic flood mapping including spatial dependency. Hydrological Processing, 27(9), 1349-1363.

Oberstadler, R., Hoensch, H., Huth, D. (1997). Assessment of the mapping capabilities of ERS-1 SAR data for flood mapping: a case study in Germany. Hydrological Processes, 10, 1415-25.

Pappenberger, F., Beven, K.J., Hunter, N.M., Bates, P.D. Gouweleeuw, B.T., Thielen, J., De Roo, A.P.J. (2005). Cascading model uncertainty from medium range weather forecasts (10 days) through a rainfall-runoff model to flood inundation predictions within the European Flood Forecasting System (EFFS). Hydrology and Earth System Sciences, 9, 381-393.

Pappenberger, F., Frodsham, K., Beven, K., Romanowicz, R., Matgen, P. (2006). Fuzzy set approach to calibrating distributed flood inundation models using remote sensing observations, Hydrology and Earth System Sciences Discussions, 23(4), 2243-2277.

Pellenq, J., Boulet, G. (2004). A methodology to test the pertinence of remote-sensing data assimilation into vegetation models for water and energy exchange at the land surface. Agronomie, 24(4), 197-204.

Pierdicca, N., Chini, M., Pulvirenti, L., Macina, F. (2008). Integrating Physical and Topographic Information into a fuzzy scheme to Map Flooded Area by SAR. Sensors, 8, 4151-4164.

Pringent, C., Papa, F., Aires, F., Rossow, W.B., Matthews, E. (2007). Global inundation dynamics inferred from multiple satellite observations, 1993-2000. Journal of Geophysical Research, 112.

Pulvirenti, L., Chini, M., Pierdicca, N., Guerriero, L., Ferrazzoli, P. (2011a). An algorithm for operational flood mapping from Synthetic Aperture Radar (SAR) data based on the fuzzy logic. Natural Hazards and Earth System Sciences, 11, 529-540.

Pulvirenti, L., Chini, M., Pierdicca, N., Guerriero, L., Ferrazzoli, P. (2011b). Flood monitoring using multi-temporal COSMO-SkyMed data: Image segmentation and signature interpretation. Remote Sensing of Environment, 115(4), 990-1002.

Pulvirenti, L., Chini, M., Pierdicca, N., Boni, G. (Under Review). Use of SAR data for detecting floodwater in urban and suburban areas: the role of the interferometric coherence. IEEE Transactions on Geoscience and Remote Sensing.

Raclot, D. (2006). Remote sensing of water levels on floodplains: a spatial approach guided by hydraulic functioning. International Journal of Remote Sensing, 27, 2553-2574.

Refice, A., Capolongo, D., Pasquariello, G., D'Addabbo, A., Bovenga, F., Nutricato, R., Lovergine, F.P., Pietranera, L. (2014). SAR and InSAR for flood monitoring: examples with COSMO-SkyMed data. IEEE Selected Topics in Applied Earth Observations and Remote Sensing, 7, 2711-2722.

Schlaffer, S., Matgen, P., Hollaus, M., Wagner, W. (2015). Flood detection from multi-temporal SAR data using harmonic analysis and change detection. International Journal of Applied Earth Observation and Geoinformation, 38, 15-24.

Schumann, G., Matgen, P., Hoffmann, L., Hostache, R., Pappenberger, F., Pfister, L. (2007). Deriving distributed roughness values from satellite radar data for flood inundation modelling. Journal of Hydrology, 344, 96-111.

Schumann, G., Matgen, P., Pappenberger, F. (2008a). Conditioning Water Stages From Satellite Imagery on Uncertain Data Points. IEEE Geoscience and Remote Sensing Letters, 5(4), 810-813.

Schumann, G., Pappenberger, F., Matgen, P. (2008b). Estimating uncertainty associated with water stages from a single SAR image. Advances in Water Resources, 31(8), 1038-1047.

Schumann, G., Di Baldassarre, G., Alsdorf, D., Bates P.D. (2010). Near real-time flood wave approximation on large rivers from space: Application to the River Po, Italy. Water Resources Research, 46, W05601.

Smith, P.J., Hughes, D., Beven, K.J., Cross, Ph., Tych, W., Coulson, G., Blair, G. (2009). Towards the provision of site specific flood warnings using wireless sensor networks. Meteorological Applications, 16, 57-64

Soergel, U., Thoennessen, U, Stilla, U. (2003). Visibility analysis of man-made objects in SAR images. 2nd GRSS/ISPRS Joint Workshop on "Data Fusion and Remote Sensing over Urban Areas", Berlin, 22-23.

Townsend, P.A. (2002). Relationships between forest structure and the detection of flood inundation in forested wetlands using C-band SAR. International Journal of Remote Sensing, 23, 443 -460.

Ulaby, F.T., Bare, J.E. (1979). Look direction modulation function of the radar backscattering coefficient of agricultural fields. Photogrammetric Engineering and Remote Sensing, 45 (11), 1495-1506.

Vörösmarty, C.J., Willmott, C.J., Choudhury, B.J., Schloss, A.L., Stearns, T.K., Robeson, S.M., Dorman, T.J. (1996). Analyzing the discharge regime of a large tropical river through remote sensing, ground-based climatic data, and modelling. Water Resources Research, 32, 3137-3150.

Vörösmarty, C.J., Green, P., Salisbury, J., Lammers, R.B. (2000). Global water resources: vulnerability from climate change and population growth. Science, 14(289), 284-288.

Wagner, W., Fröhlich, J., Wotawa, G., Stowasser, R., Staudinger, M., Hoffmann, C., Walli, A., Federspiel, C., Aspetsberger, M., Atzberger, C., Briese, C., Notarnicola, C., Zebisch, M., Boresch, A., Enenkel, M., Kidd, R., von Beringe, A., Hasenauer, S., Naeimi, V., Mücke, W. (2014). Addressing grand challenges in earth observation science: The Earth Observation Data Centre for Water Resources Monitoring, ISPRS Annals of the Photogrammetry, Remote Sensing and Spatial Information Sciences (ISPRS Annals), ISPRS Commission VII Mid-term Symposium, Istanbul, Turkey, 29 September-2 October 2014, in press.

Wood, E.F., Roundy, J.K., Troy, T.J., van Beek, L.P.H., Bierkens, M.F.P., Blyth, E., de Roo, A., Döll, P., Ek, M., Famiglietti, J., Gochis, D., van de Giesen, N., Houser, P., Jaffé, P.R., Kollet, S., Lehner, B., Lettenmaier, D.P., Peters-Lidard, C., Sivapalan, M., Sheffield, J., Wade, A., Whitehead, P. (2011). Hyperresolution global land surface modeling: Meeting a grand challenge for monitoring Earth's terrestrial water. Water Resources Research 47, W05301.

World Health Organization, FLOODS - Technical Hazard Sheet - Natural Disaster Profile published online: http://www.who.int/hac/techguidance/ems/floods/en/ (2015).

Zebker, H.A., Villasenor, J. (1992). Decorrelation in interferometric radar echoes. IEEE Transactions on Geoscience and Remote Sensing, 30(5), 950-959.

PERMISSIONS

Giustarini, L., Hostache, R., Matgen, P., Schumann, G., Bates, P.D., Mason, D.C. (2013). A change detection approach to flood mapping in urban areas using TerraSAR-X. IEEE Transactions on Geoscience and Remote Sensing, 51(4), 2417-2430.

Thesis / Dissertation Reuse

The IEEE does not require individuals working on a thesis to obtain a formal reuse license, however, you may print out this statement to be used as a permission grant:

Requirements to be followed when using any portion (e.g., figure, graph, table, or textual material) of an IEEE copyrighted paper in a thesis:

1) In the case of textual material (e.g., using short quotes or referring to the work within these papers) users must give full credit to the original source (author, paper, publication) followed by the IEEE copyright line © 2011 IEEE.
2) In the case of illustrations or tabular material, we require that the copyright line © [Year of original publication] IEEE appear prominently with each reprinted figure and/or table.
3) If a substantial portion of the original paper is to be used, and if you are not the senior author, also obtain the senior author's approval.

Requirements to be followed when using an entire IEEE copyrighted paper in a thesis:

1) The following IEEE copyright/ credit notice should be placed prominently in the references: © [year of original publication] IEEE. Reprinted, with permission, from [author names, paper title, IEEE publication title, and month/year of publication]
2) Only the accepted version of an IEEE copyrighted paper can be used when posting the paper or your thesis on-line.
3) In placing the thesis on the author's university website, please display the following message in a prominent place on the website: In reference to IEEE copyrighted material which is used with permission in this thesis, the IEEE does not endorse any of [university/educational entity's name goes here]'s products or services. Internal or personal use of this material is permitted. If interested in reprinting/republishing IEEE copyrighted material for advertising or promotional purposes or for creating new collective works for resale or redistribution, please go to http://www.ieee.org/publications_standards/publications/rights/rights_link.html to learn how to obtain a License from RightsLink.

If applicable, University Microfilms and/or ProQuest Library, or the Archives of Canada may supply single copies of the dissertation.

Giustarini, L., Viernieuwe, J., Verwaeren, J., Chini, M., Hostache, R., Matgen, P., Verhoest N.E.C., De Baets, B. (2015). Accounting for image uncertainty in SAR-based flood mapping. International Journal of Applied Earth Observation and Geoinformation, 34, 70-77.

https://s100.copyright.com/CustomerAdmin/PLF.jsp?ref=42e53c6a-7420-4a9f-b12d-a99a6dac645d

ELSEVIER LICENSE
TERMS AND CONDITIONS
Dec 08, 2015

This is a License Agreement between Laura Giustarini ("You") and Elsevier ("Elsevier") provided by Copyright Clearance Center ("CCC"). The license consists of your order details, the terms and conditions provided by Elsevier, and the payment terms and conditions.

All payments must be made in full to CCC. For payment instructions, please see information listed at the bottom of this form.

Supplier	Elsevier Limited The Boulevard,Langford Lane Kidlington,Oxford,OX5 1GB,UK
Registered Company Number	1982084
Customer name	Laura Giustarini
Customer address	19, rue de Beggen Luxembourg, Luxembourg 1221
License number	3723010147223
License date	Oct 06, 2015
Licensed content publisher	Elsevier
Licensed content publication	International Journal of Applied Earth Observation and Geoinformation
Licensed content title	Accounting for image uncertainty in SAR-based flood mapping
Licensed content author	L. Giustarini,H. Vernieuwe,J. Verwaeren,M. Chini,R. Hostache,P. Matgen,N.E.C. Verhoest,B. De Baets
Licensed content date	February 2015
Licensed content volume number	34
Licensed content issue number	n/a
Number of pages	8
Start Page	70
End Page	77
Type of Use	reuse in a thesis/dissertation
Portion	full article
Format	both print and electronic
Are you the author of this Elsevier article?	Yes
Will you be translating?	No
Title of your thesis/dissertation	Integrating remote sensing information from SAR sensors and hydraulic modelling
Expected completion date	Nov 2015
Estimated size (number of pages)	70
Elsevier VAT number	GB 494 6272 12
Permissions price	0.00 EUR
VAT/Local Sales Tax	0.00 EUR / 0.00 GBP
Total	0.00 EUR

Terms and Conditions

INTRODUCTION

1. The publisher for this copyrighted material is Elsevier. By clicking "accept" in connection with completing this licensing transaction, you agree that the following terms and conditions apply to this transaction (along with the Billing and Payment terms and conditions established by Copyright Clearance Center, Inc. ("CCC"), at the time that you opened your Rightslink account and that are available at any time at http://myaccount.copyright.com).

GENERAL TERMS

2. Elsevier hereby grants you permission to reproduce the aforementioned material subject to the terms and conditions indicated.

3. Acknowledgement: If any part of the material to be used (for example, figures) has appeared in our publication with credit or acknowledgement to another source, permission must also be sought from that source. If such permission is not obtained then that material may not be included in your publication/copies. Suitable acknowledgement to the source must be made, either as a footnote or in a reference list at the end of your publication, as follows:

"Reprinted from Publication title, Vol /edition number, Author(s), Title of article / title of chapter, Pages No., Copyright (Year), with permission from Elsevier [OR APPLICABLE SOCIETY COPYRIGHT OWNER]." Also Lancet special credit - "Reprinted from The Lancet, Vol. number, Author(s), Title of article, Pages No., Copyright (Year), with permission from Elsevier."

4. Reproduction of this material is confined to the purpose and/or media for which permission is hereby given.

5. Altering/Modifying Material: Not Permitted. However figures and illustrations may be altered/adapted minimally to serve your work. Any other abbreviations, additions, deletions and/or any other alterations shall be made only with prior written authorization of Elsevier Ltd. (Please contact Elsevier at permissions@elsevier.com)

6. If the permission fee for the requested use of our material is waived in this instance, please be advised that your future requests for Elsevier materials may attract a fee.

7. Reservation of Rights: Publisher reserves all rights not specifically granted in the combination of (i) the license details provided by you and accepted in the course of this licensing transaction, (ii) these terms and conditions and (iii) CCC's Billing and Payment terms and conditions.

8. License Contingent Upon Payment: While you may exercise the rights licensed immediately upon issuance of the license at the end of the licensing process for the transaction, provided that you have disclosed complete and accurate details of your proposed use, no license is finally effective unless and until full payment is received from you (either by publisher or by CCC) as provided in CCC's Billing and Payment terms and conditions. If full payment is not received on a timely basis, then any license preliminarily granted shall be deemed automatically revoked and shall be void as if never granted. Further, in the event that you breach any of these terms and conditions or any of CCC's Billing and Payment terms and conditions, the license is automatically revoked and shall be void as if never granted. Use of materials as described in a revoked license, as well as any use of the materials beyond the scope of an unrevoked license, may constitute copyright infringement and publisher reserves the right to take any and all action to protect its copyright in the materials.

9. Warranties: Publisher makes no representations or warranties with respect to the licensed material.

10. Indemnity: You hereby indemnify and agree to hold harmless publisher and CCC, and their respective officers, directors, employees and agents, from and against any and all claims arising out of your use of the licensed material other than as specifically authorized pursuant to this license.

11. No Transfer of License: This license is personal to you and may not be sublicensed, assigned, or transferred by you to any other person without publisher's written permission.

12. No Amendment Except in Writing: This license may not be amended except in a writing signed by both parties (or, in the case of publisher, by CCC on publisher's behalf).

13. Objection to Contrary Terms: Publisher hereby objects to any terms contained in any purchase order, acknowledgment, check endorsement or other writing prepared by you, which terms are inconsistent with these terms and conditions or CCC's Billing and Payment terms and conditions. These terms and conditions, together with CCC's Billing and Payment terms and conditions (which are incorporated herein), comprise the entire agreement between you and publisher (and CCC) concerning this licensing transaction. In the event of any conflict between your obligations established by these terms and conditions and those established by CCC's Billing and Payment terms and conditions, these terms and conditions shall control.

14. Revocation: Elsevier or Copyright Clearance Center may deny the permissions described in this License at their sole discretion, for any reason or no reason, with a full refund payable to you. Notice of such denial will be made using the contact information provided by you. Failure to receive such notice will not alter or invalidate the denial. In no event will Elsevier or Copyright Clearance Center be responsible or liable for any costs, expenses or damage incurred by you as a result of a denial of your permission request, other than a refund of the amount(s) paid by you to Elsevier and/or Copyright Clearance Center for denied permissions.

LIMITED LICENSE

The following terms and conditions apply only to specific license types:

15. **Translation**: This permission is granted for non-exclusive world **English** rights only unless your license was granted for translation rights. If you licensed translation rights you may only translate this content into the languages you requested. A professional translator must perform all translations and reproduce the content word for word preserving the integrity of the article.

16. **Posting licensed content on any Website**: The following terms and conditions apply as follows: Licensing material from an Elsevier journal: All content posted to the web site must maintain the copyright information line on the bottom of each image; A hyper-text must be included to the Homepage of the journal from which you are licensing at http://www.sciencedirect.com/science/journal/xxxxx or the Elsevier homepage for books at http://www.elsevier.com; Central Storage: This license does not include permission for a scanned version of the material to be stored in a central repository such as that provided by Heron/XanEdu.

Licensing material from an Elsevier book: A hyper-text link must be included to the Elsevier homepage at http://www.elsevier.com . All content posted to the web site must maintain the copyright information line on the bottom of each image.

Posting licensed content on Electronic reserve: In addition to the above the following clauses are applicable: The web site must be password-protected and made available only to bona fide students registered on a relevant course. This permission is granted for 1 year only. You may obtain a new license for future website posting.

17. **For journal authors:** the following clauses are applicable in addition to the above:

Preprints:

A preprint is an author's own write-up of research results and analysis, it has not been peer-reviewed, nor has it had any other value added to it by a publisher (such as formatting, copyright, technical enhancement etc.).

Authors can share their preprints anywhere at any time. Preprints should not be added to or enhanced in any way in order to appear more like, or to substitute for, the final versions of articles however authors can update their preprints on arXiv or RePEc with their Accepted Author Manuscript (see below).

If accepted for publication, we encourage authors to link from the preprint to their formal publication via its DOI. Millions of researchers have access to the formal publications on ScienceDirect, and so links will help users to find, access, cite and use the best available version. Please note that Cell Press, The Lancet and some society-owned have different preprint policies. Information on these policies is available on the journal homepage.

Accepted Author Manuscripts: An accepted author manuscript is the manuscript of an article that has been accepted for publication and which typically includes author-incorporated changes suggested during submission, peer review and editor-author communications.

Authors can share their accepted author manuscript:

- – immediately
    - via their non-commercial person homepage or blog
    - by updating a preprint in arXiv or RePEc with the accepted manuscript
    - via their research institute or institutional repository for internal institutional uses or as part of an invitation-only research collaboration work-group
    - directly by providing copies to their students or to research collaborators for their personal use
    - for private scholarly sharing as part of an invitation-only work group on commercial sites with which Elsevier has an agreement
- – after the embargo period
    - via non-commercial hosting platforms such as their institutional repository
    - via commercial sites with which Elsevier has an agreement

In all cases accepted manuscripts should:

- – link to the formal publication via its DOI
- – bear a CC-BY-NC-ND license - this is easy to do
- – if aggregated with other manuscripts, for example in a repository or other site, be shared in alignment with our hosting policy not be added to or enhanced in any way to appear more like, or to substitute for, the published journal article.

Published journal article (JPA): A published journal article (PJA) is the definitive final record of published research that appears or will appear in the journal and embodies all value-adding publishing activities including peer review co-ordination, copy-editing, formatting, (if relevant) pagination and online enrichment.

Policies for sharing publishing journal articles differ for subscription and gold open access articles:

Subscription Articles: If you are an author, please share a link to your article rather than the full-text. Millions of researchers have access to the formal publications on ScienceDirect, and so links will help your users to find, access, cite, and use the best available version.

Theses and dissertations which contain embedded PJAs as part of the formal submission can be posted publicly by the awarding institution with DOI links back to the formal publications on ScienceDirect.

If you are affiliated with a library that subscribes to ScienceDirect you have additional private sharing rights for others' research accessed under that agreement. This includes use for classroom teaching and internal training at the institution (including use in course packs and courseware programs), and inclusion of the article for grant funding purposes.

Gold Open Access Articles: May be shared according to the author-selected end-user license and should contain a CrossMark logo, the end user license, and a DOI link to the formal publication on ScienceDirect.

Please refer to Elsevier's posting policy for further information.

18. **For book authors** the following clauses are applicable in addition to the above: Authors are permitted to place a brief summary of their work online only. You are not allowed to download and post the published electronic version of your chapter, nor may you scan the printed edition to create an electronic version. **Posting to a repository:** Authors are permitted to post a summary of their chapter only in their institution's repository.

19. **Thesis/Dissertation**: If your license is for use in a thesis/dissertation your thesis may be submitted to your institution in either print or electronic form. Should your thesis be published commercially, please reapply for permission. These requirements include permission for the Library and Archives of Canada to supply single copies, on demand, of the complete thesis and include permission for Proquest/UMI to supply single copies, on demand, of the complete thesis. Should your thesis be published commercially, please reapply for permission. Theses and dissertations which contain embedded PJAs as part of the formal submission can be posted publicly by the awarding institution with DOI links back to the formal publications on ScienceDirect.

Elsevier Open Access Terms and Conditions

You can publish open access with Elsevier in hundreds of open access journals or in nearly 2000 established subscription journals that support open access publishing. Permitted third party re-use of these open access articles is defined by the author's choice of Creative Commons user license. See our open access license policy for more information.

Terms & Conditions applicable to all Open Access articles published with Elsevier:

Any reuse of the article must not represent the author as endorsing the adaptation of the article nor should the article be modified in such a way as to damage the author's honour or reputation. If any changes have been made, such changes must be clearly indicated.

The author(s) must be appropriately credited and we ask that you include the end user license and a DOI link to the formal publication on ScienceDirect.

If any part of the material to be used (for example, figures) has appeared in our publication with credit or acknowledgement to another source it is the responsibility of the user to ensure their reuse complies with the terms and conditions determined by the rights holder.

Additional Terms & Conditions applicable to each Creative Commons user license:

CC BY: The CC-BY license allows users to copy, to create extracts, abstracts and new works from the Article, to alter and revise the Article and to make commercial use of the Article (including reuse and/or resale of the Article by commercial entities), provided the user gives appropriate credit (with a link to the formal publication through the relevant DOI), provides a link to the license, indicates if changes were made and the licensor is not represented as endorsing the use made of the work. The full details of the license are available at http://creativecommons.org/licenses/by/4.0.

CC BY NC SA: The CC BY-NC-SA license allows users to copy, to create extracts, abstracts and new works from the Article, to alter and revise the Article, provided this is not done for commercial purposes, and that the user gives appropriate credit (with a link to the formal publication through the relevant DOI), provides a link to the license, indicates if changes were made and the licensor is not represented as endorsing the use made of the work. Further, any new works must be made available on the same conditions. The full details of the license are available at http://creativecommons.org/licenses/by-nc-sa/4.0.

CC BY NC ND: The CC BY-NC-ND license allows users to copy and distribute the Article, provided this is not done for

commercial purposes and further does not permit distribution of the Article if it is changed or edited in any way, and provided the user gives appropriate credit (with a link to the formal publication through the relevant DOI), provides a link to the license, and that the licensor is not represented as endorsing the use made of the work. The full details of the license are available at http://creativecommons.org/licenses/by-nc-nd/4.0. Any commercial reuse of Open Access articles published with a CC BY NC SA or CC BY NC ND license requires permission from Elsevier and will be subject to a fee.

Commercial reuse includes:

- – Associating advertising with the full text of the Article
- – Charging fees for document delivery or access
- – Article aggregation
- – Systematic distribution via e-mail lists or share buttons

Posting or linking by commercial companies for use by customers of those companies.

20. **Other Conditions**:

v1.8

Questions? customercare@copyright.com or +1-855-239-3415 (toll free in the US) or +1-978-646-2777.

As an Elsevier journal author, any author retains various rights including Inclusion of the article in a thesis or dissertation (provided that this is not to be published commercially) whether in part or *in toto*; see http://www.elsevier.com/about/company-information/policies/copyright#Author%20rights for more information. As this is a retained right, no written permission is necessary provided that proper acknowledgement is given.

This extends to the online version of your dissertation and would include any version of the article including the final published version provided that it is not available as an individual download but only embedded within the dissertation itself.

Giustarini, L., Matgen, P., Hostache, R., Plaza, D., Pauwels, V.R.N., Lannoy, G.J., Keyser, R.D., Pfister, L., Hoffmann, L., Savenije, H.H.G. (2011). Assimilating SAR-derived water level data into a flood model: A case study. Hydrology and Earth System Sciences, 15, 2349- 2365.